UNIVERSITÀ DEGLI STUDI DI PADOVA

DIPARTIMENTO DI SCIENZE CHIMICHE

CORSO DI LAUREA MAGISTRALE IN CHIMICA

TESI DI LAUREA MAGISTRALE

Tripodal receptors for the transmembrane transport of anions

Supervisor: Prof. Leonard Prins (Università degli Studi di Padova)

Co-Examiner: Prof. Antonio Toffoletti (Università degli Studi di Padova)

Supervisor: Dr. Hennie Valkenier (Université Libre de Bruxelles)

Co-Supervisor: Dr. Karolis Norvaiša (Université Libre de Bruxelles)

Student: Andrea Naccari

2120803

ACADEMIC YEAR 2024/2025

Abstract

Tripodal anion receptors can be developed as synthetic anion carriers for transmembrane transport of anions if they fulfil specific structural requirements. 1,3,5-tris(-ethyl)-phenylene (TEP) and Tris(2-aminoethyl)amine (TREN) scaffolds, functionalized with anion recognition modules, originally designed for anion recognition, where shown to be effective in promoting transport across lipid membranes. Using Large Unilamellar Vesicles (LUVs) as model systems it was further shown that they can facilitate the transport of more challenging anions, including strongly hydrated phosphate esters. The transmembrane transport activity was also evaluated for Cl^-, $PhHPO_4^-$, $SO4^{2-}$, and $H_2PO_4^-$. The efflux of anions was monitored by fluorescence and ^{31}P-NMR assays. In addition, the binding affinities were assessed via NMR titration studies obtain quantitative data regarding the interaction between the receptor and anion.

Content

1 Introduction

1.1 Ions in biology

Living organisms contain dissolved ions at varied concentrations (**Fig. 1**), which differ between intracellular and extracellular environment. These ionic concentrations play a critical role in maintaining the homeostasis of the organism, and thus the proper functioning of biological mechanisms.

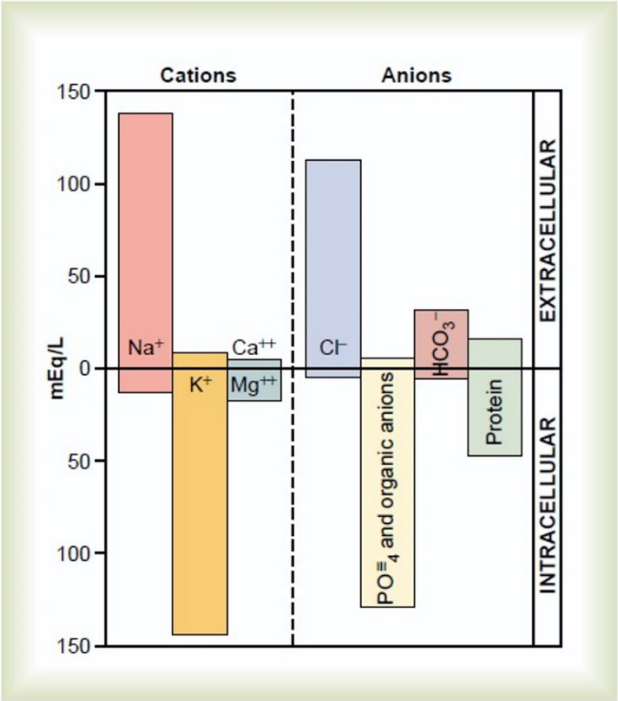

Figure 1: Ion concentration in extracellular and intracellular environment [1]

The hydrophobic interior of the lipid bilayer in the membranes acts as a barrier, preventing charged substances from diffusing through it. Thus, ions cannot freely cross cellular membranes. In nature, ion transport across the membranes has to be mediated by membrane proteins, which not only regulate ionic concentrations, but also maintain the electrochemical gradient. These transmembrane transport proteins facilitate the movement of ions across membranes through two main modalities (**Fig. 2**). In passive transport, ions move along their concentration gradient, a process often mediated by channel proteins but also possible via carriers. In contrast, active transport requires energy consumption, with carrier proteins undergoing conformational changes to pump ions against their gradient and establish new concentration differences.

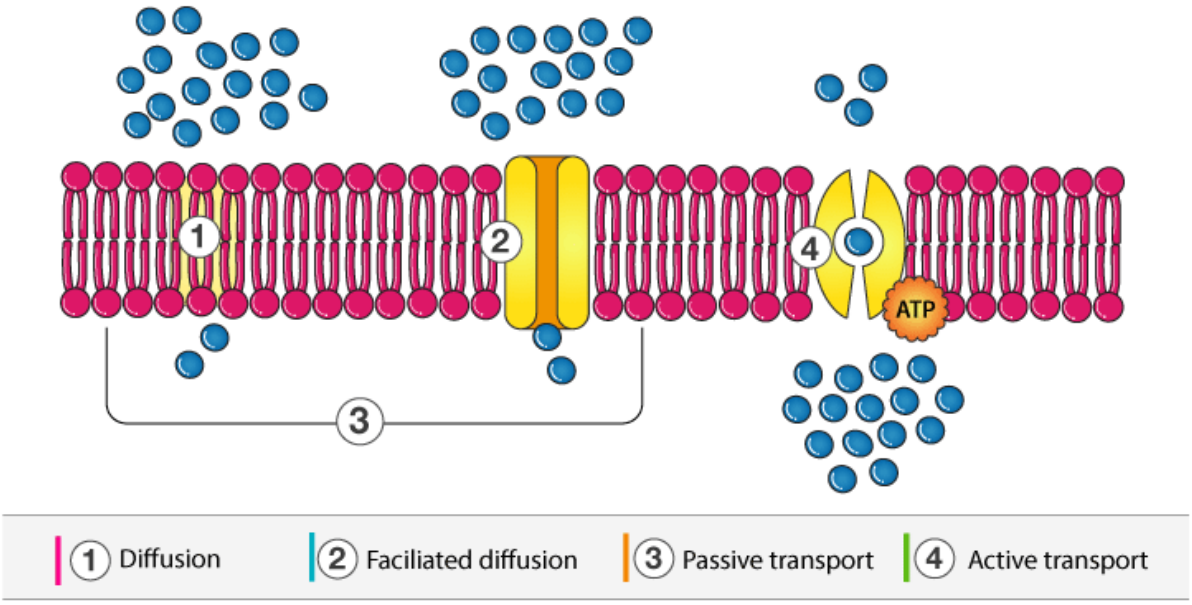

Figure 2: Visual representation of transport across membranes [2]

Transmembrane transport proteins mediate different mechanisms depending on their function: antiporters exchange two ions bearing charges of the same sign in opposite directions; symporters co-transport two ions of opposite charge in the same direction; uniporters facilitate the movement of a single ion across the membrane, contributing to the establishment or maintenance of electrochemical and concentration gradients (**Fig. 3**).

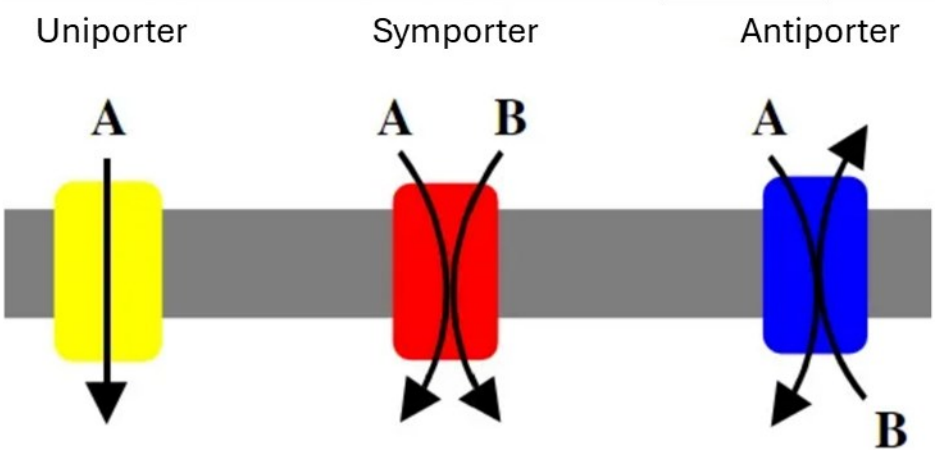

Figure 3: Uniport, symport and antiport visual representation

Genetic mutations can result in dysfunction of these proteins, causing channelopathies, that are disorders associated with ion channel malfunctions. [3] One of the most well-known channelopathies is cystic fibrosis, which is the most common autosomal recessive disease among people of Caucasian ethnicity. [3] This disease is caused by mutations in the CFTR gene, which encodes a chloride/bicarbonate channel in epithelial cells. Loss of CFTR function impairs chloride and bicarbonate secretion into the airway surface liquid. Reduced chloride and water transport leads to dehydrated, more viscous mucus, while defective bicarbonate secretion lowers the pH of the airway surface liquid, further aggravating mucus dehydration and

impairing clearance.[4] Cystic fibrosis is among the most prevalent life-shortening genetic disorders, with a mean life expectancy of 47.7 years. [5] Despite its clinical importance and the drastic progress made in therapies over the past 20 years, no general cure currently exists. Available medications have been developed only recently and are effective for specific mutations, making a universal treatment for all patients still unattainable. The numerous genetic mutations (about 2000) responsible for this disease also make gene therapy extremely challenging.

1.2 Synthetic ion carriers

A potential strategy to combat cystic fibrosis is the use of synthetic ion carriers, that can be used to help counteract the effects of channelopathies by compensating for defective proteins and directly transporting the desired ions across membranes. This approach is called 'channel replacement therapy'. [6] The use of this approach is not yet well established, but it appears promising. Synthetic ion carriers have also been developed and are currently being studied with the aim of becoming therapeutic drugs. [7]

A synthetic ion carrier is a small molecule that is able to transport ions across the membrane, mimicking the action of natural ion channels. A synthetic ion carrier is a receptor for the ion of interest that is soluble in the lipophilic domain of the membrane, [8] and it can extract the ion from the aqueous phase, shuttle it across the membrane, and then release it on the other side (**Fig. 4a**).

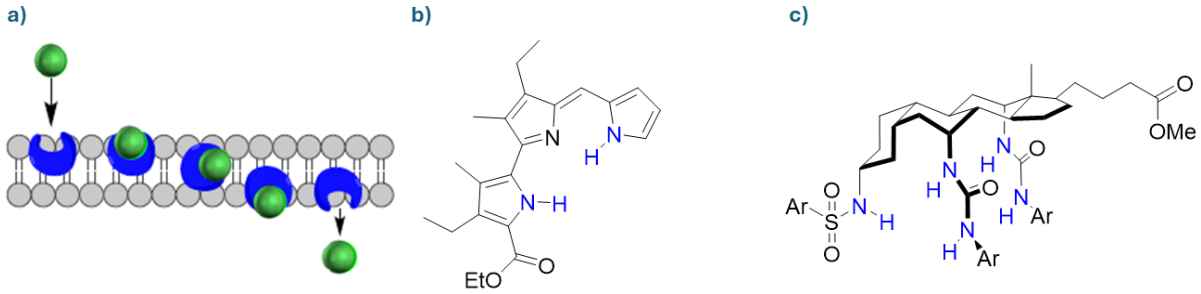

Figure 4**: **a) Schematic representation of the operating mechanism of a synthetic ion carrier. ***b)*** [9] and ***c)*** [10] Examples of synthetic anion carriers.

1.3 Model System: Liposomes

Studying the efficiency in cells is generally difficult due to multiple factors including reproducibility, additional variables influencing carrier behaviour, cost, and the complexity of monitoring ion transport. One simpler way to test the functioning of a synthetic anion carrier is by using liposomes as model systems. In aqueous solution, lipids spontaneously self-assemble into spherical vesicles known as liposomes. Each liposome is formed by a bilayer of natural or synthetic lipids, with polar head groups exposed to the surrounding aqueous environment and hydrophobic tails forming the interior of the membrane, thereby encapsulating an aqueous compartment. One of the advantages of using liposomes as model system is the possibility to prepare lipid films together with the synthetic anion carrier. The so-called pre-incorporation method allows to test also poorly deliverable synthetic anion carriers. In this study, large unilamellar vesicles (LUVs) with diameters ranging from 100 to 200

nm were employed. These vesicles are below the resolution limit of optical microscopy and smaller than most biological cells; for comparison, a typical human epithelial cell measures approximately 10 µm. [11] LUVs were preferred over larger vesicles, such as Giant Unilamellar Vesicles (GUVs diameter > 1 µm), due to their relative ease of preparation in the laboratory without requiring specific machinery. The liposomes were composed of POPC (1-palmitoyl-2-oleoyl-sn-glycero-3-phosphocholine) as the constituent lipid (**Fig. 5**). Since research on synthetic anion carriers ultimately aims at therapeutic applications in human medicine, the lipid composition of model liposomes should resemble mammalian cells. For this reason, POPC is widely employed in anion transport studies, as it closely mimics epithelial membranes. Moreover, it forms stable vesicles, is chemically robust, commercially available, and, being a well-established standard lipid, enables reliable comparison of data across different laboratories.

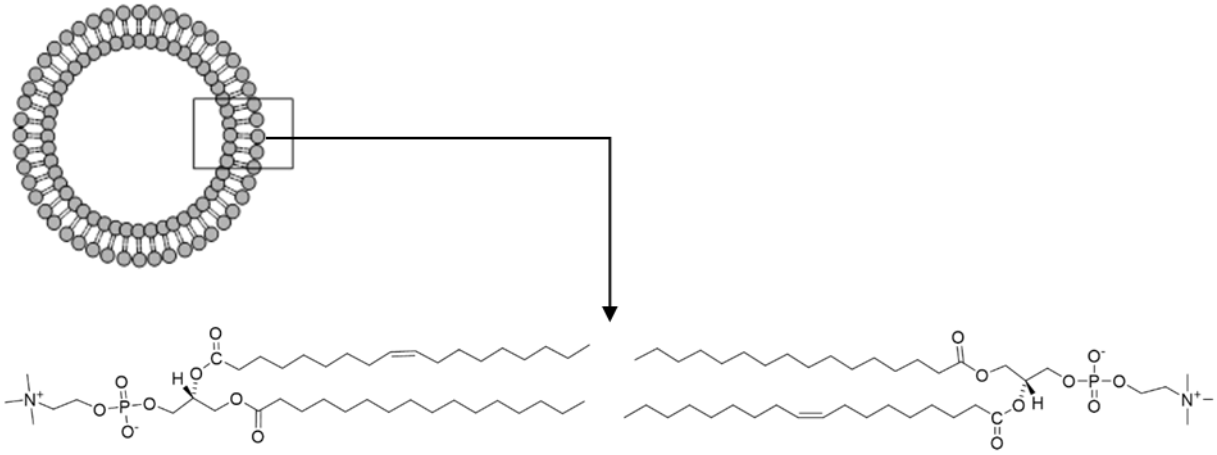

***Figure 5**:* Visual representation of liposomes and bilayer made of POPC

1.4 Liposomes preparation

LUVs are prepared following an established method. [12] Minor modifications to the procedure may be applied depending on the specific assay requirements and the target anion.

A lipid solution in organic solvents such as chloroform, optionally supplemented with the synthetic anion carrier, is prepared and subjected to solvent evaporation to form a thin lipid film. The lipid film is then hydrated by adding an aqueous solution containing: a salt having an anion different from the one investigated, to allow for antiport; the pH buffer; an emissive probe for transport monitoring when required. The hydration step results in vesicles with broad size distribution, as well as the presence of multilamellar vesicles, containing multiple concentric lipid bilayers, and multivesicular vesicles, which consist of numerous smaller vesicles encapsulated within a larger one (**Fig. 6**). To obtain unilamellar vesicles, the lipid suspension is subjected to freeze-thaw cycles. This process involves rapid freezing at low temperatures followed by thawing at mild temperatures, effectively disrupting multilamellar and multivesicular vesicles and reforming as unilamellar. To achieve a narrow size distribution, the lipid suspension is repeatedly extruded through a porous membrane. During this process, larger liposomes break apart under the applied force, and their lipids are redistributed into smaller vesicles, resulting in a more homogeneous size distribution. Finally, if the method

requires the liposomes to contain an internal probe, it is necessary to remove the external probe added during the hydration step. This is achieved by size exclusion chromatography, facilitating effective separation of liposomes from unencapsulated probe molecules.

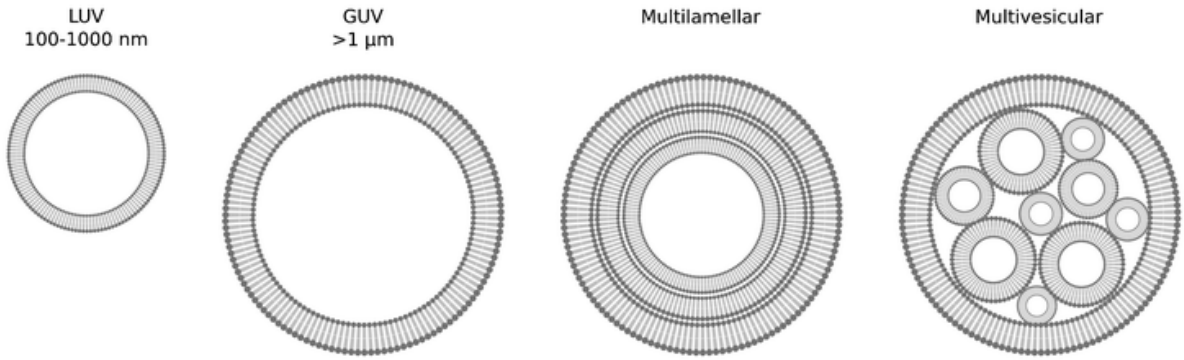

Figure 6: Visual representation of different types of vesicles. [13]

1.5 Design of a synthetic anion carrier

1.5.1 Synthetic anion carriers as receptors

Because this master thesis project focuses only on anion transport, an overview is provided regarding the requirements for synthetic anion carriers. The carrier has to be a lipophilic receptor for the desired anion, non-covalent, reversible interactions for anion binding. Mainly hydrogen bonds but also halogen bonds can be employed. Some of the most common recognition motifs used as H-bond donors are ureas, thioureas, amides, squaramides and others.

The affinity between the synthetic anion carrier (host) and the anion (guest) can be measured by the binding constant K_a, that for a 1:1 complex is defined as:

$$H + G \rightleftharpoons HG \quad (1)$$

$$K_a(M^{-1}) = \frac{[HG]}{[H][G]} \qquad (2)$$

To determine the K_a, several methods can be employed. In this thesis, a ^{1}H-NMR titration was used. In a ^{1}H-NMR titration, aliquots of the guest were added to a solution of the host at a known concentration, if complexation occurs between host and guest, this interaction can be detected in the ^{1}H-NMR spectrum. In ^{1}H-NMR binding studies, the observed behaviour depends on the relative speed of complex formation and dissociation compared to the NMR timescale, which reflects the characteristic time over which NMR can detect changes in the chemical environment of nuclei. In ^{1}H-NMR titrations, two typical cases can be observed:

-**slow exchange regime**, the formation and dissociation of the complex are slow on the ^{1}H-NMR timescale, and consequently, both the free and bound species are observed as distinct signals in the spectrum. The K_a can be obtained from the integrals of the peaks corresponding to the free and complexed species and calculating their relative ratios at each titration point, using the appropriate binding model;

-**fast exchange regime**, the formation and dissociation of the complex is fast on than the ^{1}H-NMR timescale, the observed signals correspond to a weighted average between the free and bound states. The K_a is determined by fitting the difference of the chemical shift as a function of the guest concentration, using the appropriate binding model.

The ^{1}H-NMR titration is a technique that can be applied to measure K_a in the range from 10 to 10^4 M^{-1} for a 1:1 complex.

An excessively high K_a can limit the functionality of synthetic anion carriers, as overly strong binding may prevent efficient release of the anion, reducing transport efficiency across the membrane, although only a handful of cases exhibiting this issue have been reported. [14] For a series of closely related compounds, stronger binding generally leads to better transport.

To increase H-bond strength, electron-withdrawing substituents are typically introduced in the receptors. By adding electron-withdrawing groups, the acidity of groups such as urea or thiourea is increased, making the receptor a better H-bond donor. [14] Some examples of the most common electron-withdrawing groups used are 3,5-bis(trifluoromethyl)phenyl, 4-trifluoromethylphenyl, pentafluorophenyl, 4-nitrophenyl and 4-trifluoromethylthiophenyl (**Fig. 7**).

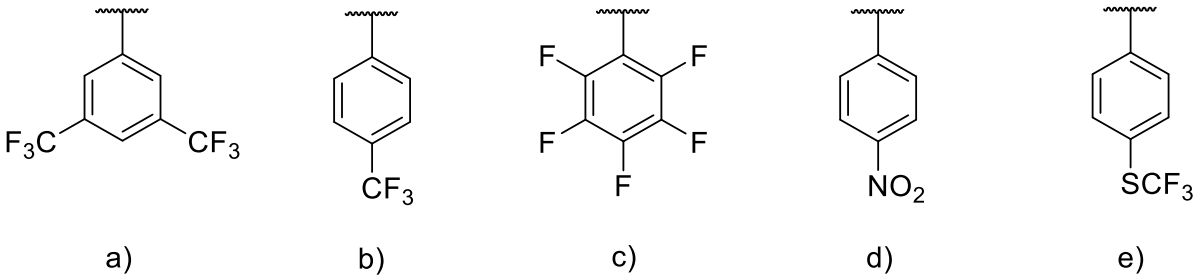

Figure 7: a) 3,5-bis(trifluoromethyl)phenyl, ***b)*** 4-trifluoromethylphenyl, ***c)*** pentafluorophenyl, ***d)*** 4-nitrophenyl, ***e)*** 4-trifluoromethylthiophenyl.

As previously mentioned, ureas and thioureas are commonly used hydrogen bond donor groups. Despite their similar chemical properties and geometry, thioureas are usually preferred over ureas. The oxygen atom in the urea functional group is highly electronegative and can act as a hydrogen bond acceptor, which enhances the carrier's affinity for the water at the water-membrane interface (**Fig. 8**). [15] The interaction with water molecules hampers the carrier's ability to cross the membrane, consequently reducing its lipophilicity and leading to a decrease in anion transport efficiency.

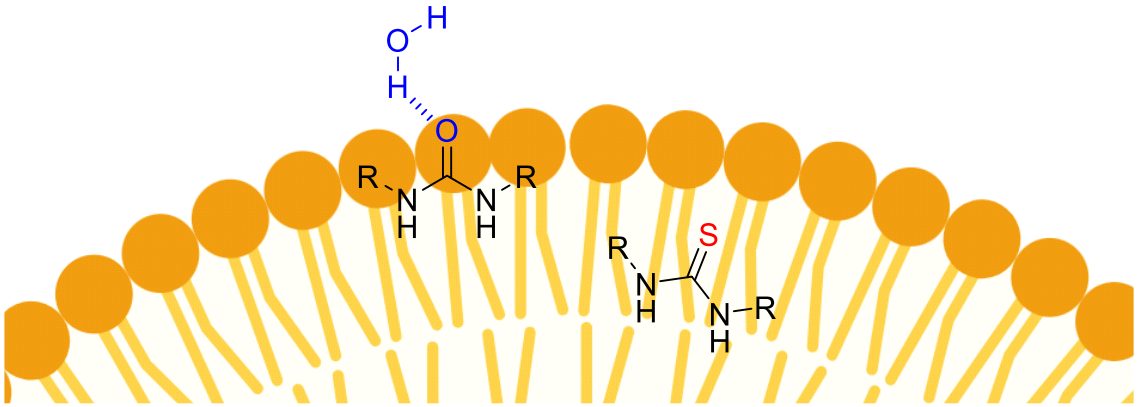

Figure 8: Visual representation of H-bond acceptor property of urea and thiourea.

1.5.2 Synthetic anion carrier deliverability to liposomes

As mentioned previously, a synthetic anion carrier has to be lipophilic. [8] For this reason most of the reported synthetic anion carriers are neutral molecules. [16] Ensuring the deliverability of a synthetic anion carrier is a major challenge in developing functional transporters for biological applications, since a carrier cannot be pre-incorporated into cellular membranes. Thus, it is advantageous to be able to incorporate the carrier into the membranes even after the formation of liposomes. [17] In liposomes, various strategies exist to incorporate synthetic carriers into the lipid bilayer, such as membrane fusion. [18] A simpler approach involves post-inserting the carrier into an already prepared liposome suspension by adding a small volume of a water-miscible organic solvent containing the carrier. For effective integration, the carrier must exhibit sufficient lipophilicity to partition into and remain in the membranes, without leaking out. At the same time, the transporter should not be too hydrophobic, which could lead to immediate precipitation upon addition to the aqueous liposome suspension.

The clogP parameter is commonly employed to quantify the lipophilicity of a compound. It is defined as the logarithm of the octanol–water partition coefficient, reflecting the relative distribution of the molecule between the two phases:

$$clogP = log_{10}\left(\frac{c_{octanol}}{c_{water}}\right) \qquad (3)$$

The clogP value used in this thesis was not experimentally measured but it was predicted based on the molecular structure and its functional groups using ChemDraw 23.1.2. Although not an absolute rule, empirical observations suggest that synthetic anion carriers require a clogP value greater than 5 to prevent leakage from liposomes, and lower than 12 to enable effective post-insertion into liposomes. [15,16]

1.6 Transport differences among anions

Research groups engaged in anion transport focus on different anions, and their research interest varies depending on the functional roles these anions may play. Although the fundamental principles that govern the function of synthetic anion carriers remain unchanged, the choice of structural features often depends on the specific anion to be transported. Each anion presents distinct characteristics, such as size, geometry, and charge

distribution, which must be considered when designing the binding site. For instance, halides share a simple spherical symmetry, yet their ionic radii vary considerably (**Table 1**), requiring carriers with binding cavities appropriately matched to ensure efficient recognition and transport.

Table 1: Ionic radii of halides [19]

Halide	Ionic radius (Å)
F^-	1.33
Cl^-	1.81
Br^-	1.96
I^-	2.20

Oxoanions represent a significant class of anions the field of anion transport; they can have various symmetry and sizes depending on the elements, and behaviour that depends on the protonation state. A critical factor influencing the difficulty of anion transport is the hydration enthalpy $\Delta H°_{hyd}$, defined as is the enthalpy change when one mole of gaseous ions becomes surrounded by water molecules. $\Delta H°_{hyd}$ is a measure that quantifies the interaction strength between an anion and surrounding water molecules. [20] Successful translocation across membranes necessitates the extraction of anions from the aqueous environment. Consequently, less hydrated anions, such as nitrate, are generally easier to transport compared to more strongly hydrated anions like sulphate or phosphate (**Table 2**) which require receptors equipped with multiple hydrogen bond donor groups in order to effectively extract the anion from aqueous environment. It is important to underline that the lower $\Delta H°_{hyd}$ of the anion is, the stronger the hydrogen bonds it forms with the receptors.

Table 2: $\Delta H°_{hyd}$ of anions [21]

Anions	$\Delta H°_{hyd}$ (kJ/mol)
F^-	−505
Cl^-	−367
Br^-	−335
I^-	−298
NO_3^-	−312
$H_2PO_4^-$	−522
SO_4^{2-}	−1145

The importance of the hydration enthalpy is further highlighted by the experimental conditions used to evaluate synthetic anion carriers. For moderately hydrated anions, as chloride, the carrier-to-lipid molar ratio can reach values as small as 1:1000 000. [14] In contrast,

for more strongly hydrated anions, such as phosphate esters, a thousand-fold higher carrier concentrations is required to achieve detectable transport. [22]

1.7 Transport experiments

A variety of anions are of interest for transmembrane transport, and the selection of appropriate assays depends both on the specific anion and on the experimental conditions under which it is evaluated. This requirement represents a challenge in developing synthetic anion carriers, as it necessitates not only designing and synthesizing the carriers themselves but also establishing reliable methods to evaluate their performance.

Transport assays are designed to provide a measurable readout that reflects the concentration and movement of anions across the membranes, while also allowing a clear distinction between those located inside and outside the liposomes. Different approaches are possible, fluorescence-based techniques were chosen as the main experimental strategy in this thesis. These methods combine ease of use with high sensitivity, enabling the detection of anion transport even at low concentrations, and can be performed without the need for highly specialized instrumentation.

In a typical transport experiment, the process relies on establishing a concentration gradient between the interior and exterior of the liposomes. This gradient represents the driving force for transport, which, however, can only take place if a synthetic anion carrier is present to facilitate the passage of anions across the lipid membrane.

In general, when performing a transport experiment aimed at studying an anion via an antiport mechanism, the exchanged anion in the antiport process is chosen to have a less negative $\Delta H°_{hyd}$ than the target anion. This ensures, in most cases, that it does not represent the rate-limiting step of the transport process.

For post-insertion measurements, the carrier is added to the lipid suspension after liposomes preparation and before the pulse, and then the lipid suspension is stirred for a few minutes to ensure its uniform distribution within the membranes. When performing transport experiments in post-insertion mode, a blank measurement can be recorded by adding an anion pulse in the absence of the carrier; this control verifies that the liposomes are not leaking and that no passive diffusion of the probe occurs in the absence of the carrier.

In this introduction, only the assays employed are described in detail; other assays exist that, although not employed in this work, are important to mention due to their relevance in related studies: the ion-selective electrode (ISE) technique, which detects ions released by transporters; and selective probes such as $[Eu.pBOH_2]^+$, a fluorescent probe developed by J. Butler et al. can be employed to monitor selective anion transport, including inorganic phosphate transport. [23]

1.8 SPBA assay

Bis(3-sulfopropyl)-9,9’-biacridine (SPBA) is a fluorescent molecule soluble in water that can be used to study anion transport processes. This compound was first synthesized by Werner et al. as a derivative of lucigenin (**Fig. 9**). [24, 25]

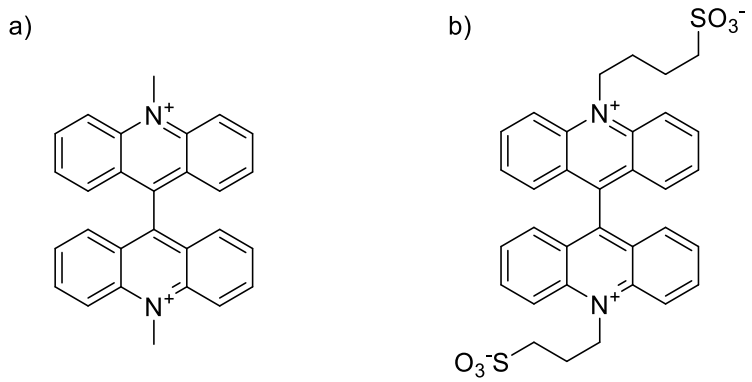

Figure 9: a) Lucigenin and ***b)*** SPBA structure

SPBA serves as a probe in certain anion transport studies due to its fluorescence being quenched by various anions. The quenching mechanism proposed involves charge transfer from SPBA to the anion:

$$(P)^* + X^- \rightarrow P^{\cdot} + X^{\cdot} \rightarrow P + X^-$$

Where P is the probe and X^- is the quencher anion.
Quenching can be described by the Stern–Volmer equation:

$$\frac{F_0}{F} = 1 + K_{sv}[X^-] \qquad (4)$$

where F_0 is the fluorescence intensity without the quencher, F is the fluorescence intensity in the presence of a quencher, K_{SV} is the Stern–Volmer constant and $[X^-]$ is the quencher concentration. SPBA is quenched only by certain anions, depending on the specific K_{SV} value of each species (**Table 3**). Moreover, some phosphate esters like $PhHPO_4^-$ or $Ph_2PO_4^-$ are able to quench SPBA fluorescence. [12]

Table 3: K_{SV} values for anions [25]

Anion	K_{SV} (M^{-1})
Cl^-	129
Br^-	181
I^-	333
NO_3^-	3
SO_4^{2-}	4
CH_3COO^-	19
HCO_3^-	13
OH^-	80

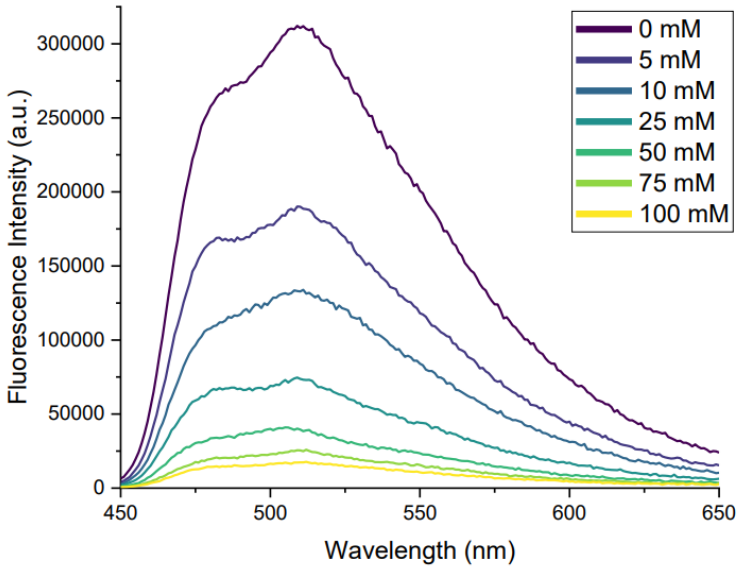

Figure 10: Emission spectrum (λ_{exc}=435 nm) of SPBA in water in the presence of NaCl [12]

Anions such as NO_3^- or SO_4^{2-} have very low K_{SV} values, meaning that they produce almost no quenching of the SPBA fluorescence. This property makes them particularly suitable for use in antiport experiments with chloride. For example, the exchange between external Cl^- and internal NO_3^- can be effectively monitored by SPBA, since the entry of chloride into the liposomes decreases the fluorescence intensity.

In a standard SPBA transport assay, liposomes are prepared with an internal concentration of the probe and an anion that does not quench it, such as nitrate, in the presence of a synthetic anion carrier embedded in the membrane (either pre-incorporated or post-inserted). Fluorescence is recorded, and after 30 s a sample of the target anion is added to the solution (pulse), which upon crossing the membrane aided by the transporter quenches the probe. After 600 s from the sample addiction, the addition of a surfactant agent (typically Triton-X) induces lipid membrane lysis, showing the lowest possible fluorescence intensity given the external anion concentration. [12]

It should be noted that SPBA is a temperature-sensitive fluorophore, so the temperature must be carefully controlled during experiments.

SPBA can also be employed for indirect measurements of anions that do not directly quench its fluorescence. For example, the transport of SO_4^{2-} can be studied via Cl^-/SO_4^{2-} antiport, since chloride has a lower $\Delta H°_{hyd}$, the rate-limiting step of the transport is unlikely to be chloride transport. If the synthetic anion carrier is active, the exchange alters the internal chloride concentration, which in turn produces a detectable change in fluorescence emission.

SPBA has only recently gained attention as a superior alternative to the traditional lucigenin assay in transport studies that is still more commonly used in this field. Lucigenin has higher lipophilicity, compared to SPBA, which promotes membrane partitioning and subsequent leakage, limiting assay stability over longer periods of time. Liposomes loaded with lucigenin must be used within hours of preparation and requires cholesterol (usually 7:3 lipid to cholesterol ratio) to reduce the leakage. In contrast, SPBA-loaded liposomes retain integrity

for at least a day without detectable leakage, representing a significant improvement in assay reliability and amount of liposomes solution that can be tested in one batch.

1.9 HPTS assay

8-Hydroxypyrene-1,3,6-trisulfonic acid (HPTS) is a water-soluble, pH-sensitive fluorophore that can be used as a probe to monitor anion transport processes. [26]

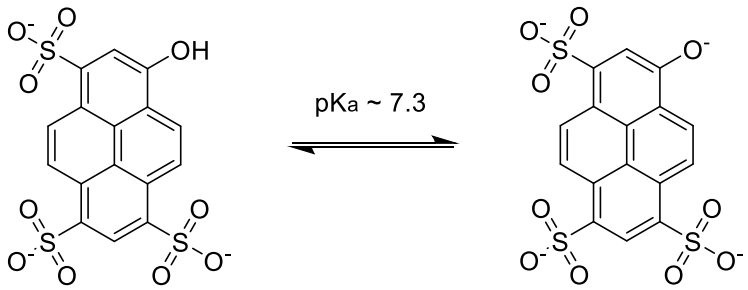

Figure 11: HPTS protonated and de-protonated structure

HPTS has a hydroxyl group with a pK_a ~7.3, close to physiological pH, which makes it a useful probe for monitoring pH variations in systems that mimic biological environments. The protonated and deprotonated species of HPTS exhibit distinct absorption and emission spectra (**Fig. 12**).

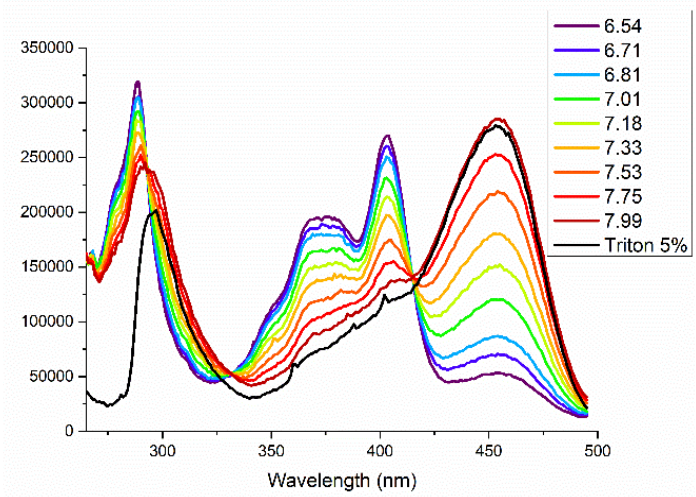

Figure 12: Excitation spectra of HPTS at different pH $\lambda_{emission}$ = 511 nm [27]

By exciting the molecule at two different wavelengths, 403 nm for the protonated form and 455 nm for the deprotonated form, and recording the emission intensity at 511 nm, it is possible to monitor internal pH in real time using ratiometric analysis with a single probe. Since, unlike the SPBA assay, we do not monitor a single fluorescence intensity, the transport curve is obtained from the time-dependent ratio of normalized fluorescence intensities.

$$R = \frac{F_{455}}{F_{403}} \qquad (5)$$

$$Normalised\ curves = \frac{R_t - R_0}{R_f - R_0} \qquad (6)$$

In which R is the ratio of fluorescence intensity from two different excitation wavelengths: λ_{exc}=455 nm and λ_{exc}=403 nm. R_t is the fluorescent ratio at time t, R_0 is the fluorescent ratio at time t=0, and R_f is the fluorescent ratio measured after the lysis of the liposomes.
The ratiometric analysis minimizes errors associated with probe concentration, instrumental variability, and photobleaching.
The experiment relies on establishing a pH gradient, with a more acidic internal environment and a more basic external one, this gradient is generated by applying a basic pulse. This gradient can be dissipated by a synthetic anion carrier capable of performing OH^-/X^- antiport or H^+/X^- symport. To ensure that OH^- and H^+ transport are not the rate-limiting steps, carbonyl cyanide m-chlorophenyl hydrazone (CCCP) is added to the liposomes at a 1:1000 CCCP-to-lipid ratio. By facilitating proton transport across the membrane, CCCP enables the experiment to study the carrier's anion transport activity without potential limitation arising form OH^- and H^+ transport. The protocol for this assay is similar to that previously described for SPBA, consisting of a baseline measurement for 30 s before the base pulse is applied, followed by 10 min of transport monitoring, and finally liposome lysis using Triton-X.

1.10 ^{31}P-NMR assay

The ^{31}P-NMR assay does not require the use of an internal fluorescent probe, instead, the experimental setup can be designed to differentiate phosphorus nuclei located inside the vesicles from those outside. Other protocols that use heteronuclear NMR spectroscopy exist to monitor anion transport, such as ^{35}Cl, ^{33}S, and ^{13}C, [10, 28, 29] given the growing interest in inorganic phosphate transport; this assay was also developed by the EMNS group. [30]
This assay is particularly valuable as it enables the investigation of species that cannot be directly measured using the SPBA assay or as additional method to confirm transport activity, and can be used to study transport of inorganic phosphate.
Liposomes are prepared with an internal buffer containing chloride ions and incorporate the synthetic anion carrier. To differentiate between the phosphate located outside and inside the liposomes, a Mn(II) salt is added to the liposome suspension. The Mn(II) ions, present only in the external solution, are paramagnetic species capable of inducing relaxation of the phosphorus nuclei, resulting in broadening of the peaks in the ^{31}P-NMR spectrum. As a result, the external phosphate signal is not detected. If the synthetic carrier is active, phosphate is transported into the liposomes, where Mn(II) is absent. The internal phosphate is therefore not subject to paramagnetic relaxation and can be observed in the ^{31}P-NMR spectrum. To ensure a quantitative measurement of the transport, the NMR tube has a coaxial tube containing a solution of a known concentration of a reference phosphate species, usually trimethylphosphate.
The ^{31}P-NMR signal of phospholipid headgroups in liposomes is broad due to restricted, anisotropic motions within the bilayer and slow overall tumbling of large vesicles, which cause incomplete averaging of magnetic interactions. [31] Since inorganic phosphate is a strongly hydrated anion (**Tab. 2**), these experiments took longer times, often multiple hours.

An alternative assay to monitor inorganic phosphate transport is by using an europium(III)-based phosphate-sensitive probe, which exhibits enhanced fluorescence in the presence of phosphate species. [17, 24]

2 Aim

This thesis focuses on the use of tripodal receptors as synthetic carriers for transmembrane anion transport, with a particular attention to phosphate esters.

The transport of phosphate and phosphate esters is particularly challenging, as these species possess a considerable hydration energy, especially in the case of inorganic phosphate. Therefore, the receptors employed should provide multiple binding sites capable of interacting with the several oxygen atoms that can act as hydrogen-bond acceptors.

Tripodal receptors constitute a class of acyclic ligands characterized by a C_{3v} symmetry and possess 3 arms that can be employed to bind the anion. Tripodal receptors are utilized in various fields due to their ability to sense both anions and cations. [32] Importantly, tripodal receptors are especially suitable for the recognition and transport of oxoanions such as phosphate esters, since they provide multiple binding sites that can simultaneously engage the substrate through hydrogen bonding from different directions (**Fig. 13**); this makes them effective receptors and synthetic carriers for this class of anions.

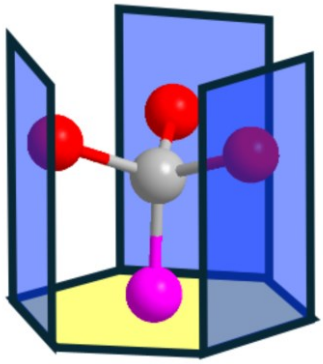

Figure 13: Visual representation of the binding between a tripodal receptor and an oxoanion such as HPO_4^{2-}

Tripodal receptors have already been investigated as synthetic anion carriers, and their ability to mediate transmembrane transport has been demonstrated. They are effective not only for anions with moderate hydration energies, such as chloride, but also for more demanding substrates like phosphate esters, including phenylphosphate and bisphenylphosphate. [22] Given their proven functionality, this thesis aims to investigate how specific structural modifications could improve both the transport efficiency and the deliverability of these receptors.

An important advantage of this class of receptors is their relative ease of synthesis, especially when compared to other receptors often employed in anion transport, such as cholapods and diureidodecalins [15]. A potential risk of a synthetic anion carrier that has multiple binding sites is that if one binding arm is not used to bind the anion during transport, it may interact with the polar head group of membrane lipids. Such an interaction can prevent the carrier from successfully transporting the anion across the membrane. [33]

Among the most notable scaffolds for tripodal receptors, tris(2-aminoethyl)amine (TREN)-based receptors (**Fig. 14**) are among the most widely utilized. [34] A TREN-based receptor

features a flexible core capable of forming a cavity, and binding moieties are present on the three arms, also, in this class of receptor, intramolecular H-bond is often possible. The TREN scaffold allows the introduction of multiple binding moieties, enabling the construction of receptors with several potential anion binding sites.

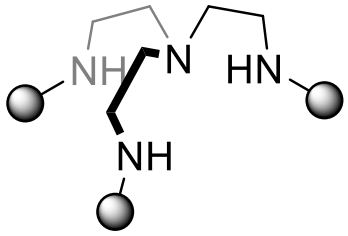

Figure 14: **TREN** scaffold

To date, no hexa-urea-based compound has been reported as synthetic anion carrier in liposomes. In this thesis, we decided to investigate a hexa-urea receptor to evaluate whether increasing the number of hydrogen-bond donors could enhance anion binding. Our interest is particularly focused on oxoanions, which possess multiple potential hydrogen-bond acceptor sites. We turned our attention to a reported tripodal receptor for SO_4^{2-} based on six urea groups and a TREN scaffold **Fig. 15**. developed by Biao Wu and co-authors, [35] This research group has developed a variety of hexa-urea receptors, which have been primarily employed in the field of ion recognition. This receptor was chosen because it fulfils the structural requirements for a synthetic anion carrier: it is a neutral anion receptor bearing multiple binding sites, incorporates an electron-withdrawing group, and is based on a TREN scaffold that has already proven effective in other synthetic anion carriers. By increasing the number of hydrogen-bond donors, we aim to strengthen the interaction between the receptor and the anion and retain its functionality as synthetic anion carrier.

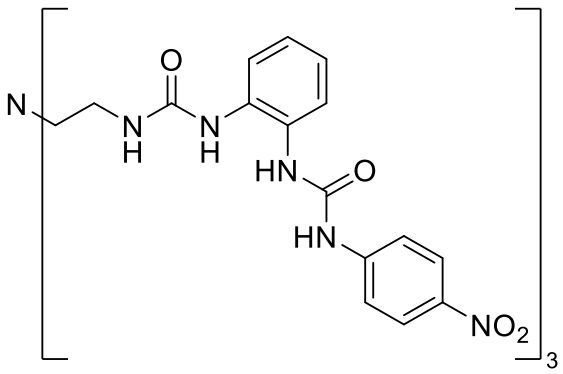

Figure 15: **Tren-Hex-U**

In **Fig. 15**, the electron-withdrawing group in **TREN-Hex-U** is a nitro substituent. However, alternative electron-withdrawing groups such as -CF_3 could be employed. It is therefore of interest to compare the performance of structurally related hexa-ureas, particularly those bearing *para*-CF_3 and *meta*-CF_3 substituents. [22] Since hexa-ureas have not yet been

investigated as anion transporters, one of the aims of this thesis is to explore their potential as synthetic carriers for different anions (**Table 4**).

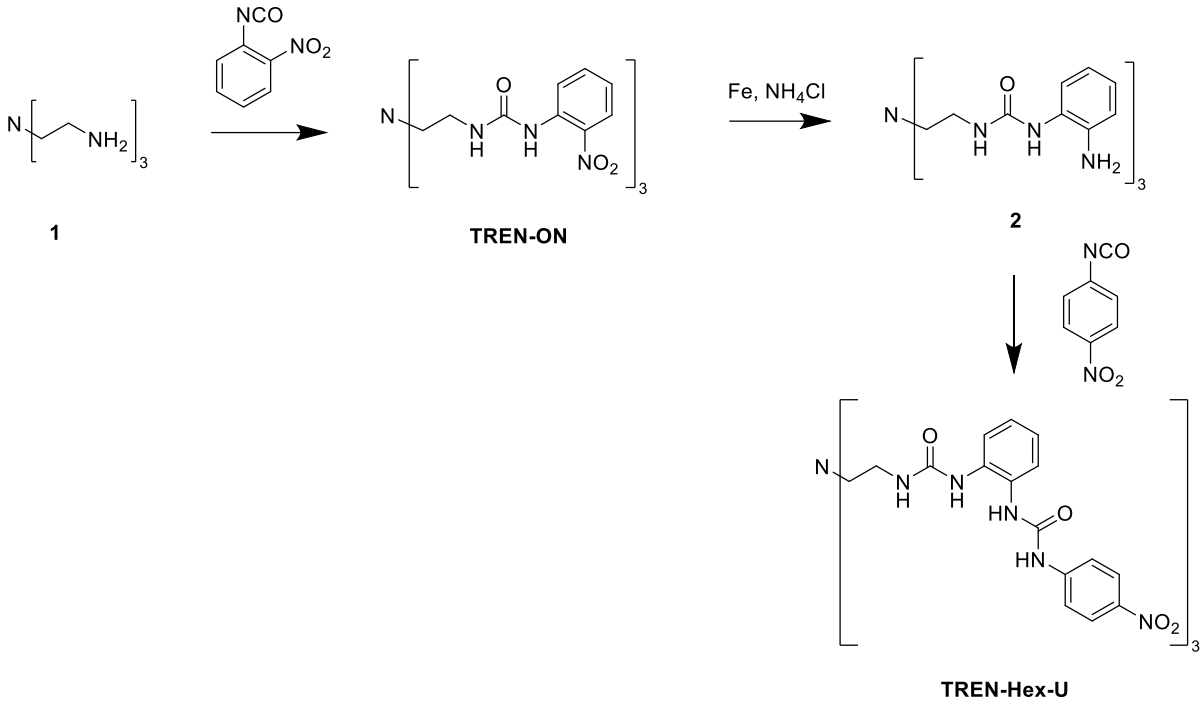

General Reaction Scheme 1

Table 4

	Investigated anion			
TREN-Hex-U	Cl^-	$PhHPO_4^-$	SO_4^{2-}	$H_2PO_4^-$
assay	SPBA, HPTS	SPBA	SPBA	^{31}P-NMR

The 1,3,5-trisphenylene scaffold can also be employed to synthesize tripodal receptors that function as synthetic anion carriers. These receptors feature three substituents on the aromatic rings that serve as binding sites (**Fig. 16**). [36, 37]

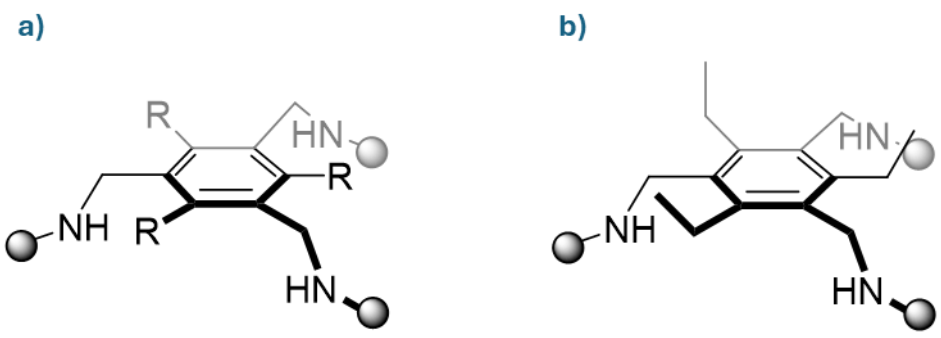

Figure 16: a) 1,3,5-trisphenylene-based scaffold and ***b)*** 1,3,5-tris(-ethyl)-phenylen-based scaffold

The nature of the three R substituents may vary; however, they are frequently ethyl groups. Tris(-ethyl)-phenylene (TEP)-based receptors are extensively employed due to the role of the ethyl substituents, especially the $–CH_2–$ units, controlling pre-organization.

The alternating spatial arrangement ("up/down") of the ethyl groups and binding sites effectively positions all binding moieties on the same side of the molecule, creating a cone-shaped cavity that favours the cooperative binding of an anion by the tree arms[36].

It could be possible to achieve this type of pre-organization through other groups as well. There are examples of receptors that remain pre-organized even without –Et groups, thanks to intramolecular interactions. [37] Other substituents, such as methoxy and methyl groups, have also been reported as viable alternatives, although it is generally more difficult for these to reproduce the same effect of pre-organization as ethyl groups.[37], [38]

Tripodal receptors have already been employed as synthetic anion carriers using both TREN and TEP scaffolds, proving to be highly effective chloride carriers. Comparative studies among various designs indicate that the optimal performance is achieved using thiourea functionalities (S) rather than ureas, coupled with the presence of *meta*-CF_3-phenyl (F2) groups as electron-withdrawing substituents:

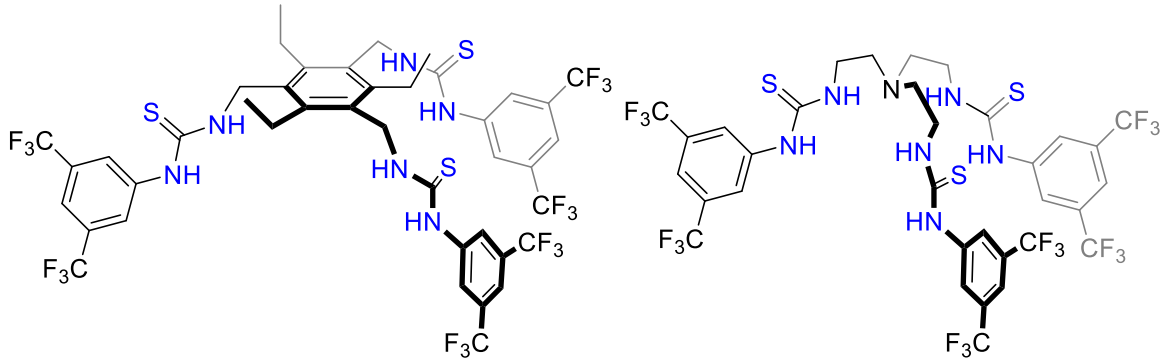

Figure 17: **TEP-SF2** [36] (left) and **TREN-SF2** [39] (right)

The presence of multiple binding sites within these receptors can enhances their ability to transport oxoanions. The synthetic anion carriers shown in **Fig. 17** are also able to transport phosphate esters such as phenylphosphate and bisphenylphosphate across membranes. [22]

TEP-SF2 is an effective synthetic anion carrier, ranking among the best tripodal receptor for transport both Cl^- and organic phosphates such as phenyl phosphate. [28, 32] However, its clogP value may be too high to allow efficient post-insertion into liposomes (**Fig. 18a**). Thus, another aim of this thesis is study and modulate the deliverability of **TEP-SF2** by lowering the clogP values, while maintaining its promising transport properties for phosphate esters. To reduce its lipophilicity, we designed an analogue compound lacking the ethyl groups, (1,3,5-tris(3-(3,5-bis(trifluoromethyl)phenyl)thioureidomethyl)-benzene) **THP-SF2** (**Fig. 18b**).

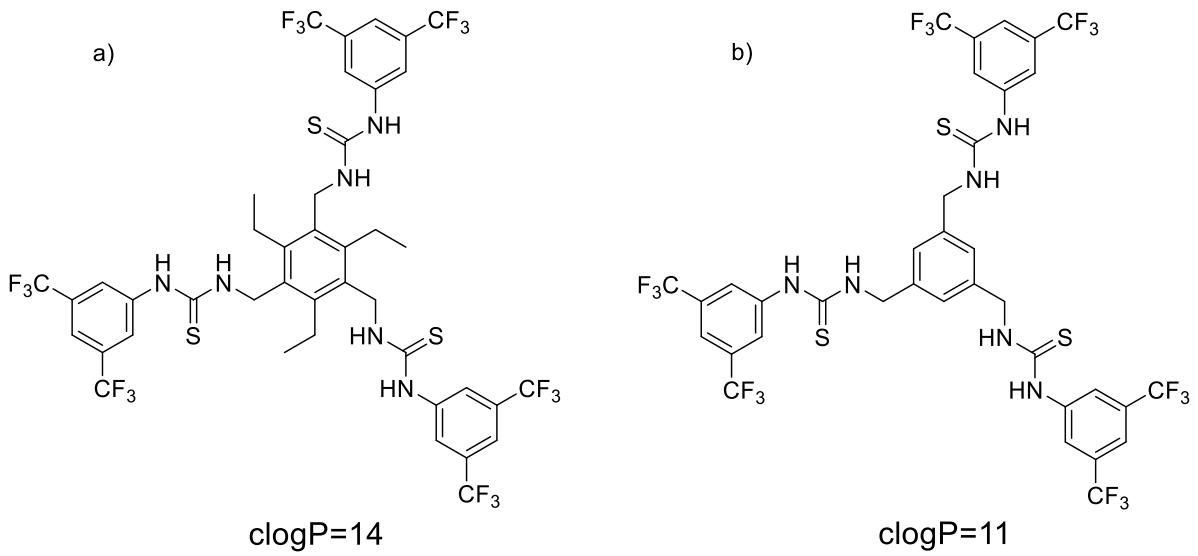

Figure 18: a) **TEP-SF2** structure and ***b)*** **THP-SF2** structure

The role of ethyl groups in receptor pre-organization and their influence on binding and transport is difficult to predict. Examples of THP-based receptors that undergo pre-organization are reported, and even without pre-organization, **THP-SF2** may still represent a valid synthetic anion carrier.

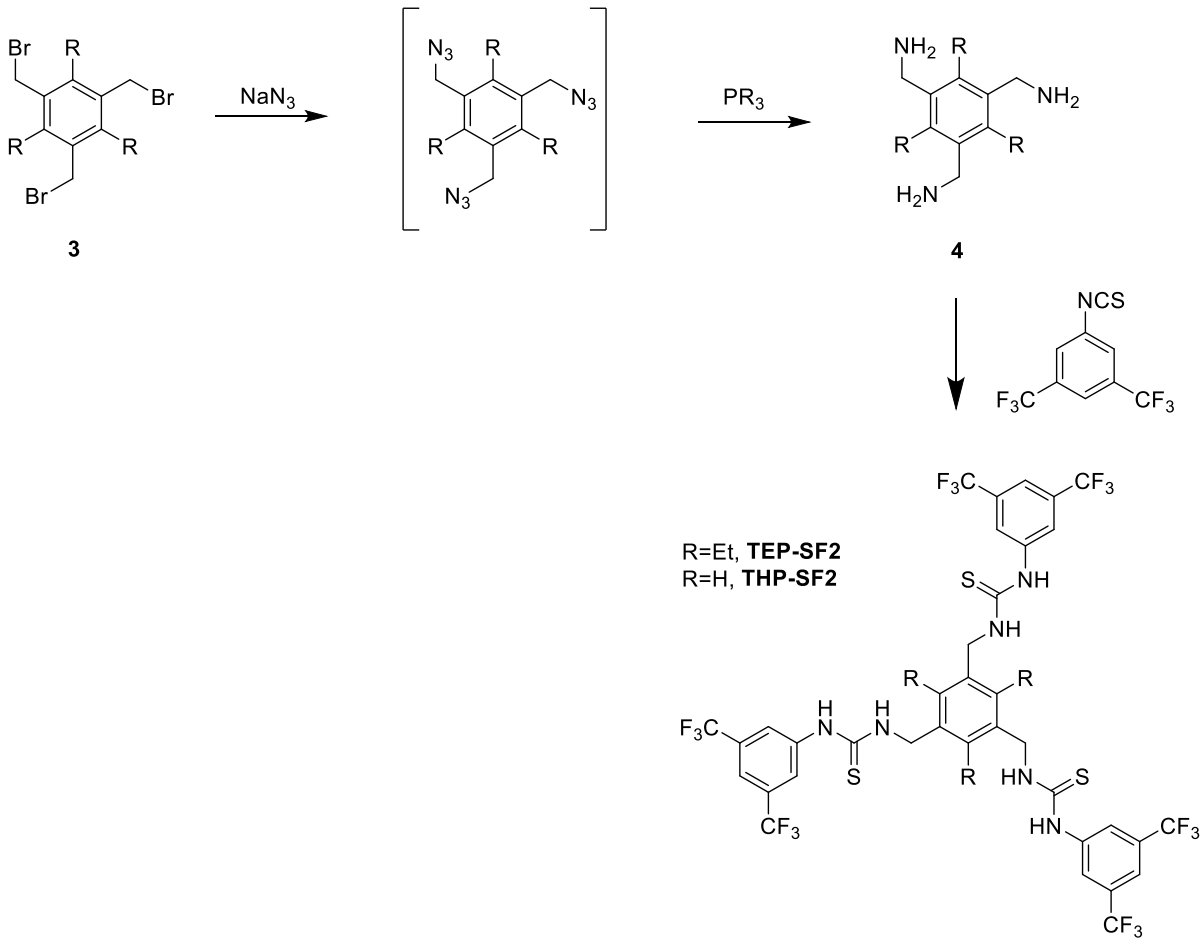

General Reaction Scheme 2

We will test and compare the two analogues, TEP-SF2 and THP-SF2 for anion transport, in both pre-incorporation and post-insertion, in order to evaluate the influence of the ethyl groups on transport and their effect on the deliverability of the synthetic anion carrier in membranes (**Table 5**).

Table 5

Synthetic anion carrier	Transport activity (pre-incorporated)	Transport activity (post inserted)
TEP-SF2	Cl^-	Cl^-
THP-SF2	Cl^-	Cl^-

All transport experiments will be performed using liposomes as the reference model, specifically LUVs composed of 100% POPC as the constituent lipid. Experimental conditions varied depending on the assay employed and are detailed in the experimental section. Whenever possible, we will simplify reported synthetic procedures to make them more feasible in our laboratory setting and to reduce costs by employing more affordable reagents.

3 Results and discussion

3.1 TREN-Hex-U synthesis

To synthesize the desired **TREN-Hex-U**, we started from commercially available tris(2-aminoethyl)amine **1**. Reaction with the corresponding isocyanate afforded **TREN-ON** (**Reaction Scheme 1**). Upon mixing, a yellow precipitate formed, which was isolated by filtration and obtained as a yellow solid in excellent yield (94%).

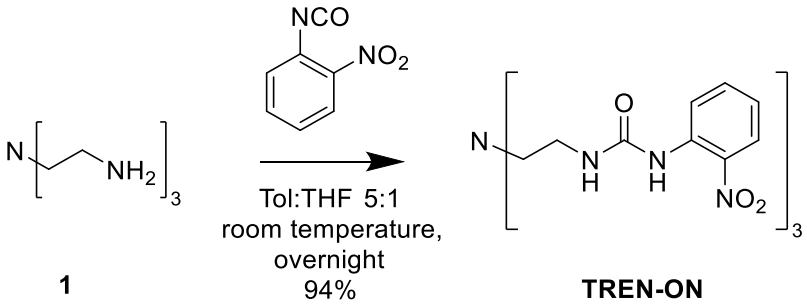

1 **TREN-ON**

Reaction Scheme 1

The subsequent step involves the reduction of the nitro group to an amine. Literature procedures employ hydrazine (N_2H_4) as the reducing agent and palladium on carbon (Pd/C) as catalyst (**Reaction Scheme 2a**). [35] To avoid using such a large amount (10 mol%) of relative expensive catalyst, alternative reactions were explored.

An initial attempt employing $SnCl_2$, a reported reducing agent for nitro groups in similar compounds, [40] resulted in partial reduction accompanied by the formation of side products (**Reaction Scheme 2b**). For this reason, we tested an alternative reduction using iron powder, which is also reported as an effective reagent for nitro group reduction in nitrophenyl derivatives (**Reaction Scheme 2c**). [41] The reaction, carried out under reflux in ethanol (EtOH)/H_2O, led to the formation of a dark suspension, which was filtered and after solvent removal, the desired product was isolated.

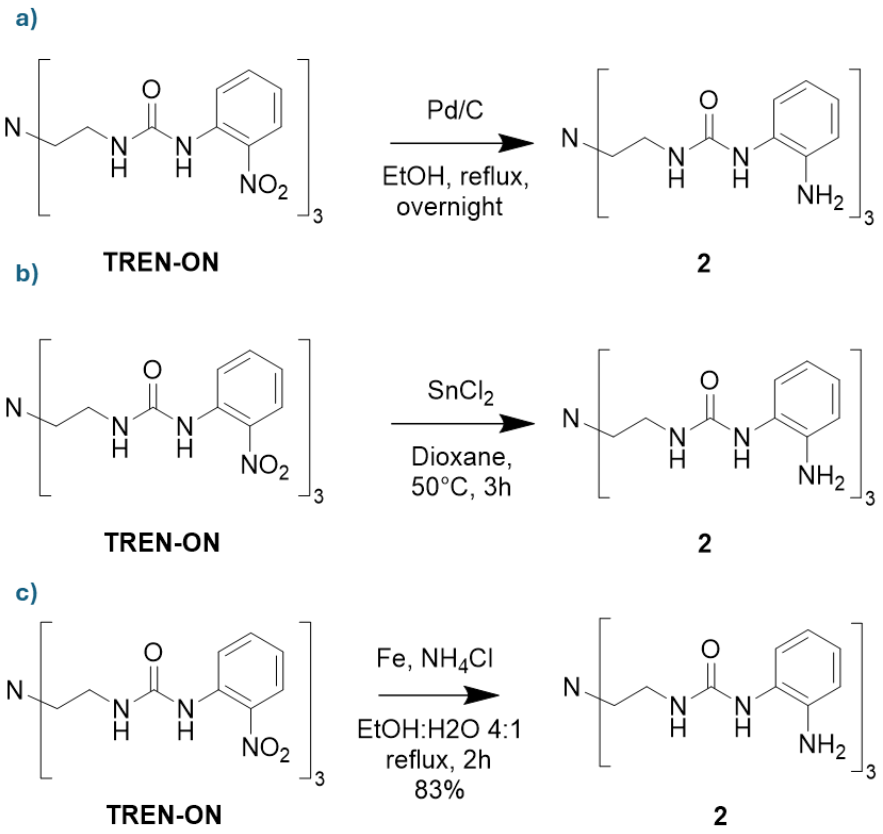

Reaction Scheme 2

The reduction was successfully carried out without Pd/C, used in the original procedure, yielding the product efficiently and without requiring column chromatography during work-up. Although, as previously discussed (Section 1.5.1), thiourea moieties generally outperform ureas as binding units in synthetic anion carriers, the thiourea analogue of this molecule was not pursued, because, in an analogous synthetic route, the resulting intermediate would contain both an amine and a thiourea group in the *ortho* position. This configuration of functional groups would likely promote an intramolecular reaction, thereby preventing the successful synthesis of the hexa-thiourea (**Reaction Scheme 3**).

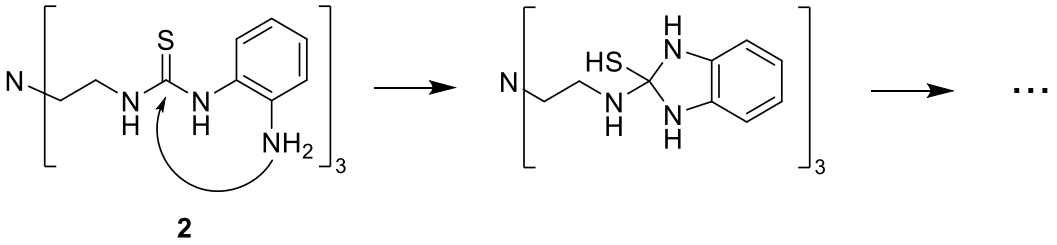

Reaction Scheme 3

TREN-Hex-U was obtained by reacting the resulting amine **2** with the corresponding isocyanate (**Reaction Scheme 5**). After refluxing the mixture, a yellow precipitate was formed, which was collected by filtration and washed. The crude product was subsequently purified by flash column chromatography, affording **TREN-Hex-U** as a yellow powder in moderate yield.

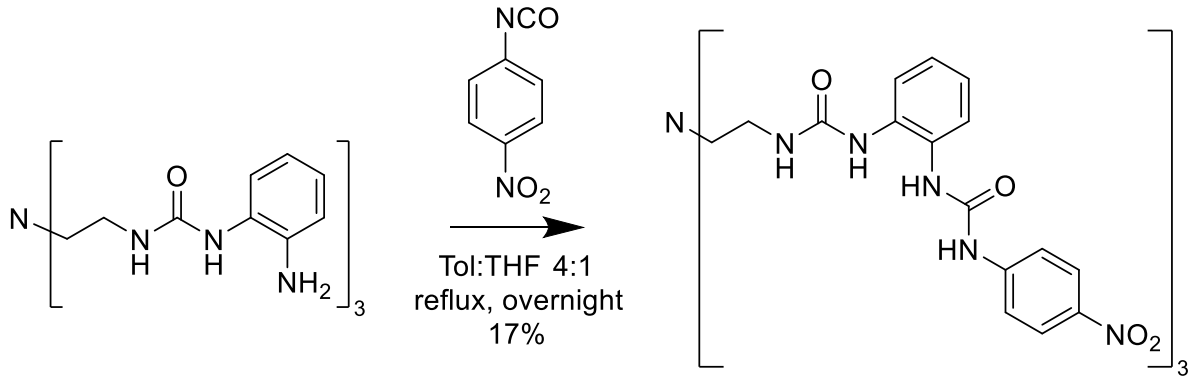

2 **TREN-Hex-U**

Reaction Scheme 4

We tested other isocyanates to obtain different hexa-ureas, but none of the reactions succeeded, despite several attempts and variations in reaction conditions including solvent, temperature, equivalent of isocyanate, and even in the presence of a template (tetrabutylammonium sulfate). **Table 6** summarizes the explored conditions.

Table 6

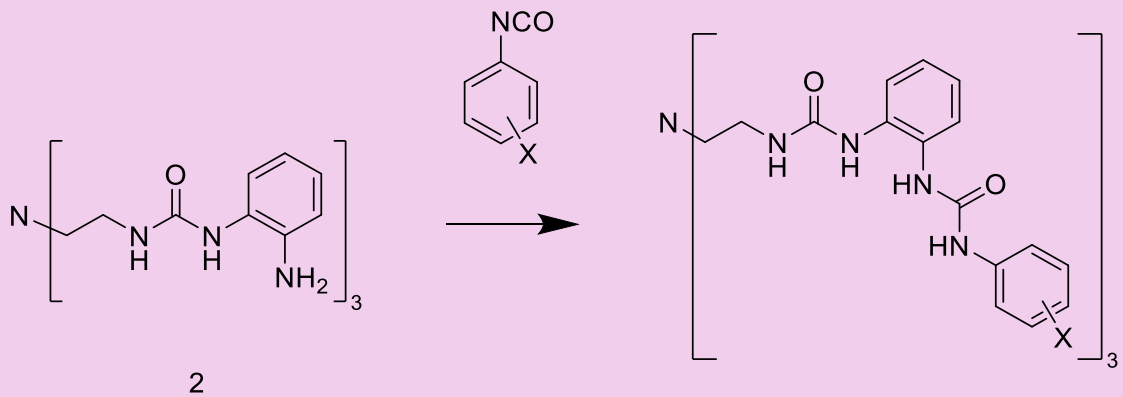

2

Isocyanate	Reaction solvent	Eq. of isocyanate	Temperature	Template
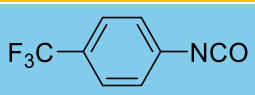 (*a*)	THF:Tol = 1:4	3,5	Reflux	no
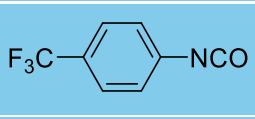	THF:Tol = 1:4	3,5	Room temperature	no
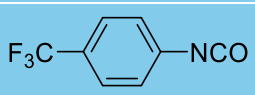 (*b*)	ACN	3,5	Room temperature	no
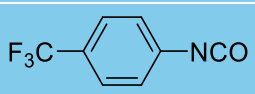 (*c*)	ACN	6	60°C	no
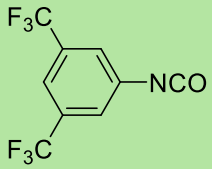	THF:Tol = 1:4	3,5	Reflux	no
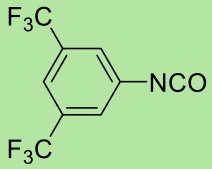	THF:Tol = 1:4	7	Room temperature	no
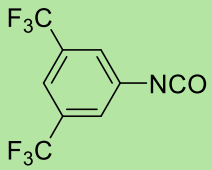	THF:Tol = 1:4	5,5	Room temperature	Tetrabutylammonium sulfate
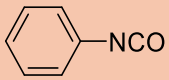	THF:Tol = 1:4	3,5	Room temperature	no

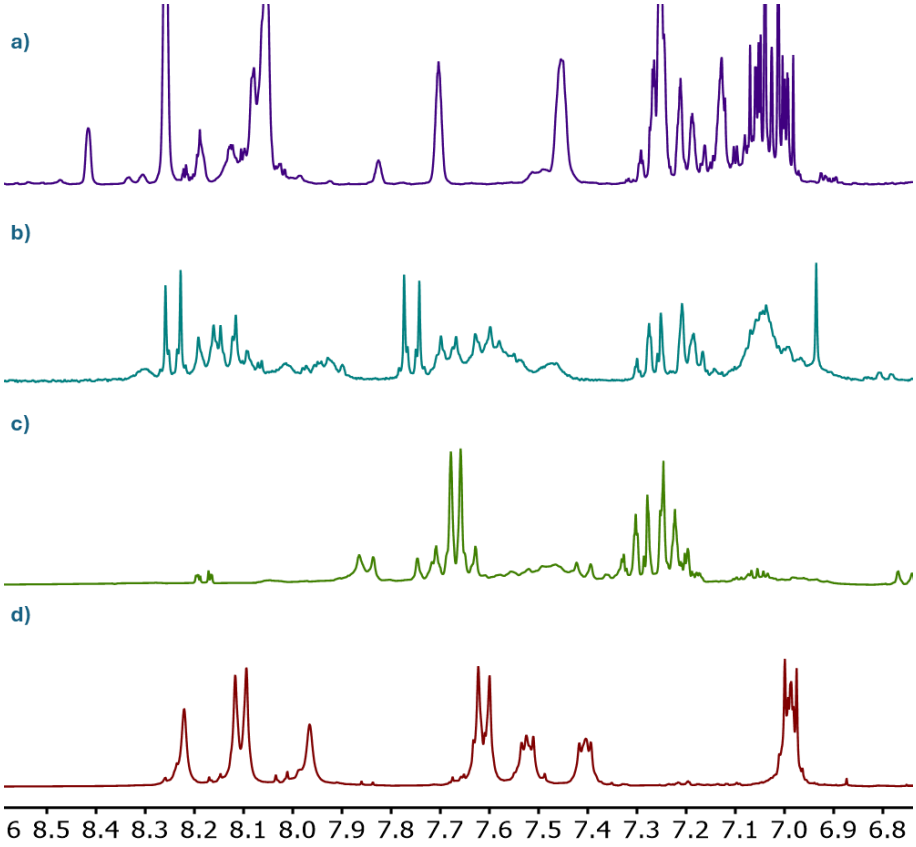

Figure 19: Aromatic region of ^{1}H-NMR spectra of failed attempts of Table 6 (a, b, c) and TREN-Hex-U (d) in DMSO-d_6

Thin-layer chromatography (TLC) analysis revealed the presence of multiple species. The aromatic region of the ^{1}H-NMR spectrum indicated the formation of several different products. In the case of reagents bearing *p*-CF_3 substituents, no aromatic signals matching the expected similar pattern of **TREN-Hex-U** (**Fig. 19**). The ethyl signals of the TREN scaffold in the ^{1}H-NMR spectrum were also examined as potential indicators of the desired product, as they are easily recognizable and generally little affected by electron-withdrawing substituents. Their disappearance provides additional evidence that the reaction did not proceed as intended. Mass spectrometry was also employed to analyze the products of reactions (b) and (c); in both cases, no signals corresponding to the target compound were found.

3.2 Transport experiment for hexa-urea

We evaluated the transport properties of **TREN-Hex-U** through a series of experiments involving different assays and anions, aiming to assess its potential as a synthetic anion carrier. In the SPBA assay, we tested Cl^-/NO_3^- and $PhHPO_4^-/NO_3^-$ antiport mechanisms (**Fig. 20**).

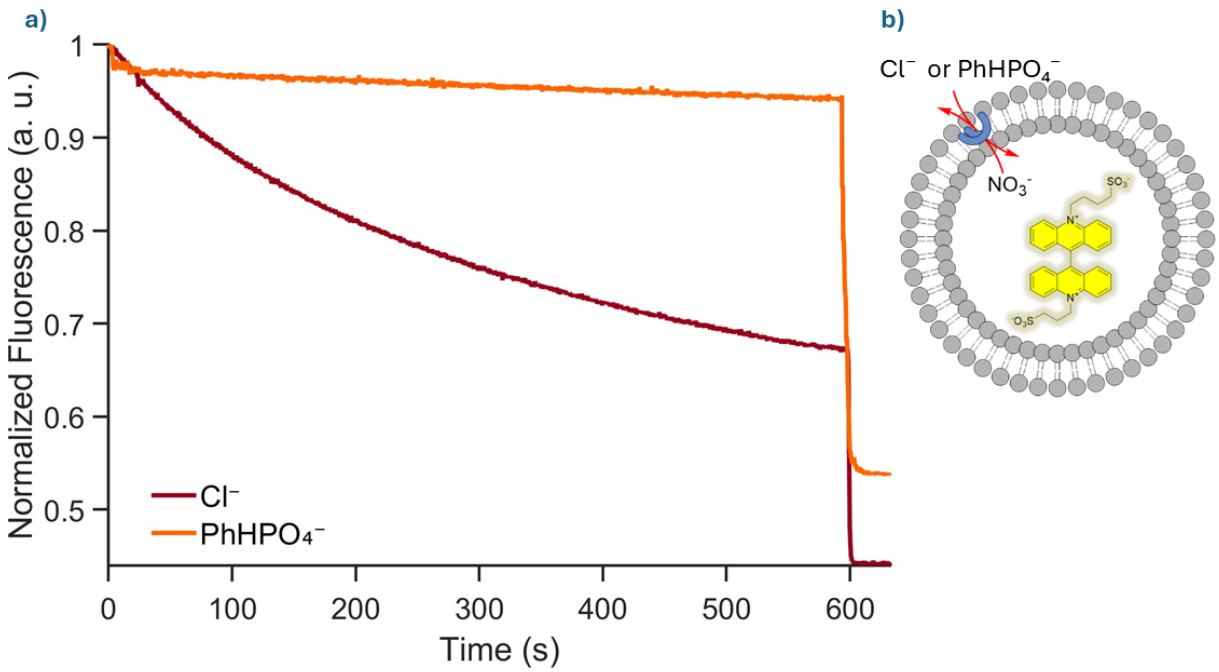

Figure 20: a) Transport activity of TREN-Hex-U (1 mol% carrier/lipid ratio) in the SPBA assay monitoring Cl^-/NO_3^- (brown curve) and $PhHPO_4^-/NO_3^-$ (orange curve) antiport mechanisms. ***b)*** Schematic representation of Cl^-/NO_3^- or $PhHPO_4^-/NO_3^-$ antiport using SPBA assay.

As shown in **Fig. 20**, **TREN-Hex-U** receptors are capable of functioning as anion carriers, as evidenced by a clear decrease in fluorescence corresponding to chloride transport. However, their performance is poor: many other TREN-based carriers, such as **TREN-SF2**, can mediate chloride transport at lower concentrations than 1 mol%, and overall **TREN-Hex-U** exhibits lower transport efficiency. Transport of $PhHPO_4^-$ is even more challenging, with only a slight decrease in fluorescence observed, indicating a clearly inferior transport efficiency compared to other TREN-based carriers. [22] In **TREN-Hex-U**, increasing the number of hydrogen-bond donors (compared to tris ureas receptors as **TREN-SF2**) was therefore not effective in enhancing the transport rate.

Sulphate transport can be studied using SPBA assay, even if SO_4^{2-} does not quench SPBA fluorescence (**Tab. 3**), so we cannot directly monitor its concentration, but Cl^-/SO_4^{2-} and $PhHPO_4^-/SO_4^{2-}$ can be followed by monitoring the influx of Cl^- or $PhHPO_4^-$ in the SPBA assay.

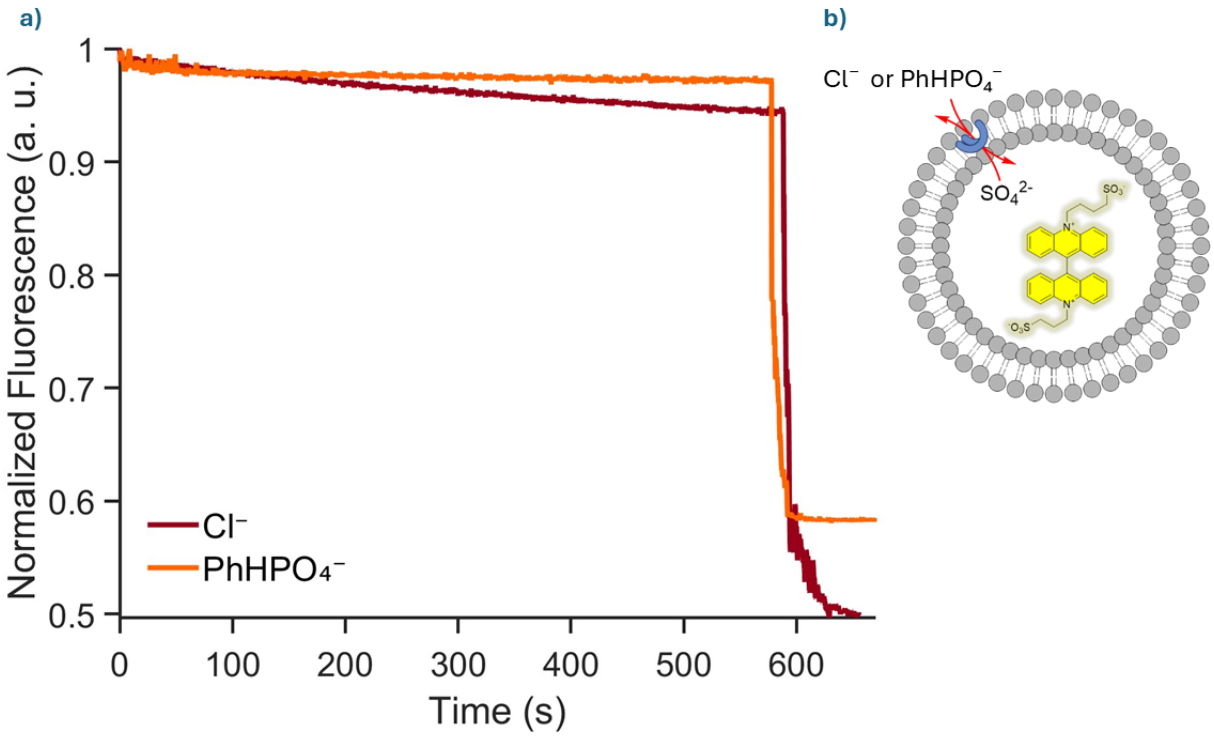

Figure 21: a) Transport activity of TREN-Hex-U (1 mol% carrier/lipid ratio) in SPBA assay monitoring Cl^-/SO_4^{2-} (brown curve) and $PhHPO_4^-/ SO_4^{2-}$ (orange curve) antiport mechanisms. ***b)*** Schematic representation of Cl^-/ SO_4^{2-} or $PhHPO_4^-/ SO_4^{2-}$ antiport using SPBA assay.

As shown in **Fig. 21**, almost no transport is observed. Unlike the Cl^-/NO_3^- antiport, **TREN-Hex-U** fails to mediate SO_4^{2-} transport, despite its known affinity for sulphate. This result highlights the difficulty in transporting strongly hydrated anions, which require more sophisticated receptor designs to be efficiently extracted from the aqueous phase.

Since TREN-Hex-U is a receptor that exhibits binding selectivity for sulphate over other anions, including NO_3^-, [35] we performed an experiment using the HPTS assay in which nitrate does not need to be transported. In this assay we monitored either Cl^-/OH^- antiport or Cl^-/H^+ uniport mechanisms.

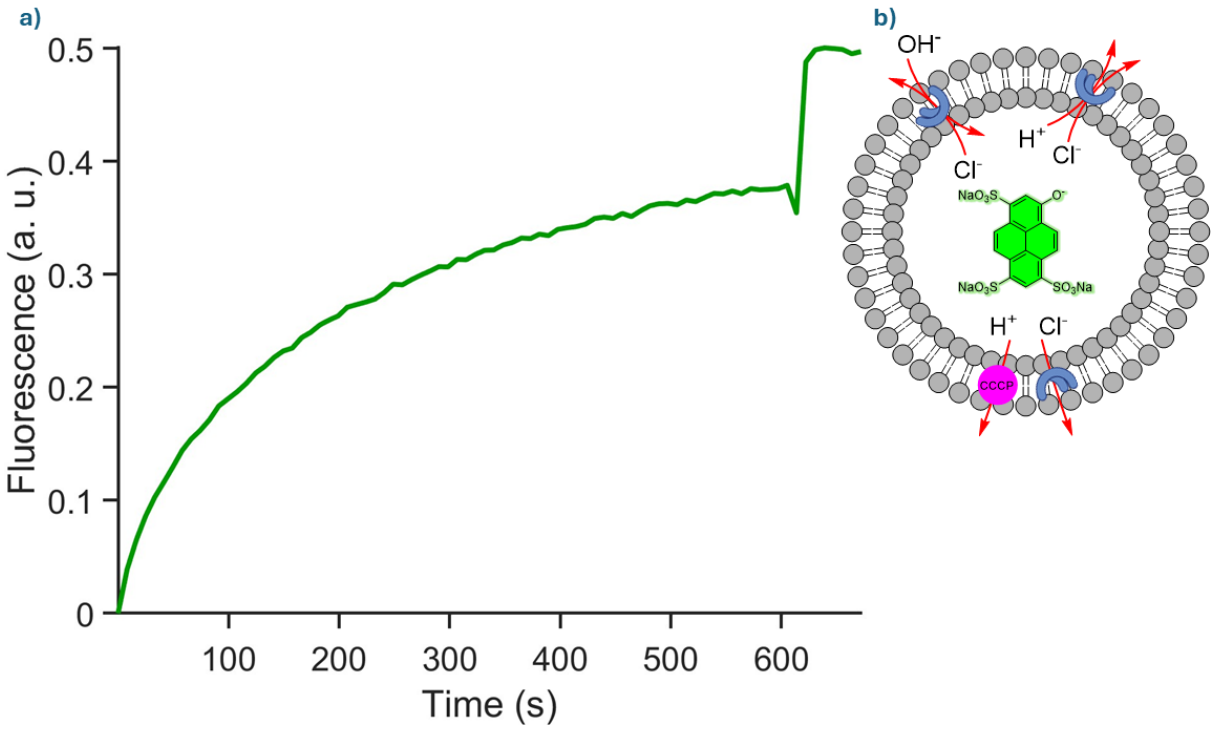

Figure 22: a) Transport activity of TREN-Hex-U (1 mol% carrier/lipid ratio) in HPTS assay monitoring Cl^-/OH^- antiport, Cl^-/H^+ symport mechanisms, Cl^-/H^+ symport mechanisms assisted by CCCP, ***b)*** Schematic representation of Cl^-/OH^- antiport or Cl^-/H^+ symport antiport using SPBA assay.

Although a direct comparison of chloride transport rates across different assays is not feasible, the experiments presented in **Fig. 20** and **Fig. 22** both show chloride transport and, in both cases, the internal and external environments of the liposomes do not immediately reach concentration equilibrium. These observations suggest no apparent limitation due to nitrate. Di-hydrogen phosphate transport was assessed via ^{31}P-NMR spectroscopy over 13 hours. Inorganic phosphate at pH 7 exists as a mixture of two species, HPO_4^{2-} and $H_2PO_4^-$ and $H_2PO_4^-$ is more easily transported across lipid membranes compared to HPO_4^{2-} due to the lower $\Delta H°_{hyd}$. [30] For this reason, the experiment was conducted at pH 5, where the protonated species ($H_2PO_4^-$) is predominant.

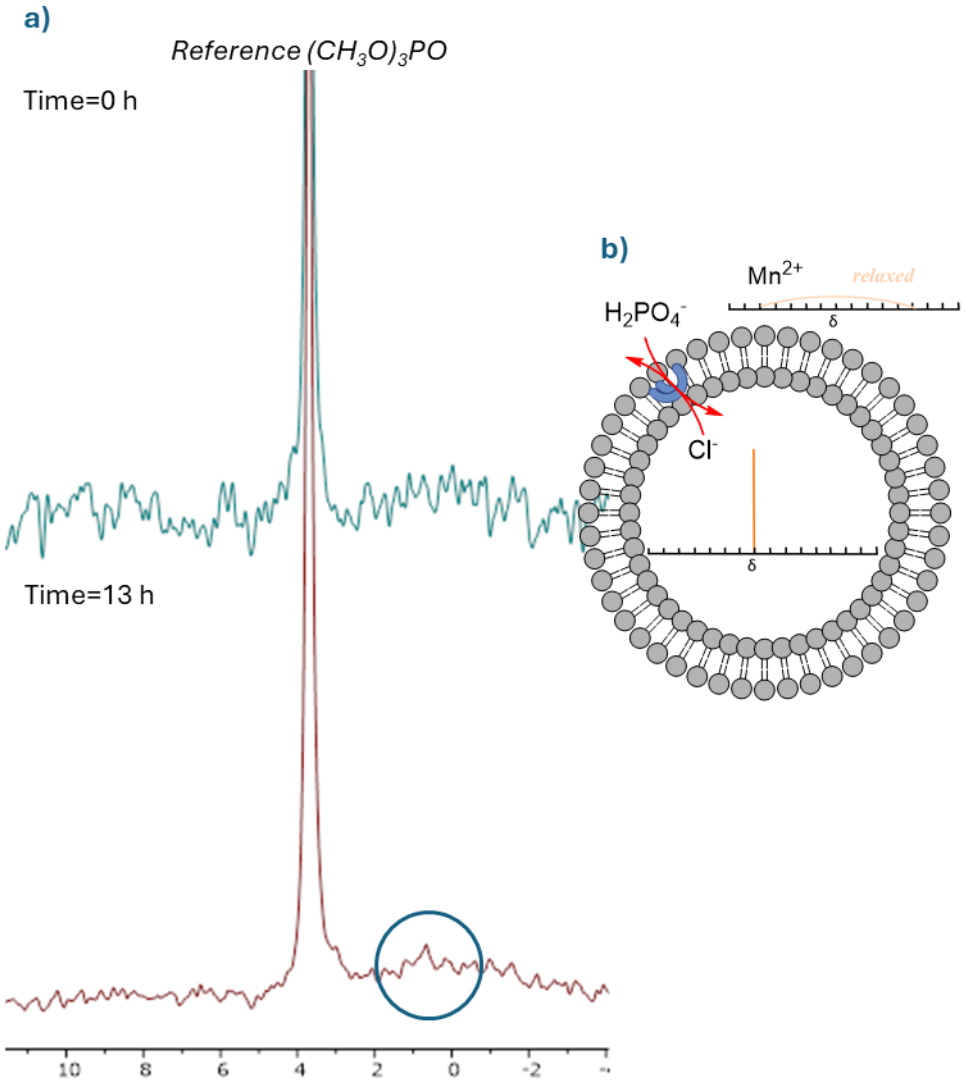

Figure 23: a) ^{31}P-NMR spectra recorded at time 0 (blue) and after 13 h (red) from the addition of NaH_2PO_4 with TREN-Hex-U as carrier (1 mol% carrier/lipid ratio), $H_2PO_4^-/Cl^-$ antiport mechanism. ***b)*** Schematic representation of the ^{31}P-NMR assay for $H_2PO_4^-$.

It is difficult to determine whether the observed peak (see blue mark) is due to actual transport or simply noise. If the carrier was capable of transporting inorganic phosphate efficiently, a distinct and clearly observable peak would be expected at in the spectra. appearing at around 1.2 ppm. [30] The inorganic phosphate transport is very difficult to achieve, and not many compounds are reported as inorganic phosphate carriers. [22]

3.3 TEP-SF2 and THP-SF2 synthesis

TEP-SF2 is a known compound, the synthesis of **TEP-SF2** starts from commercially available 1,3,5-tris(bromomethyl)-2,4,6-triethylbenzene. We explored different synthetic strategies to obtain the corresponding amine (**4**), going through the azide intermediate following the reported procedure (**Reaction Scheme 7**). [36] The azide intermediate was never purified and collected as a solid but was always kept in solution due to the potential explosiveness of azides.

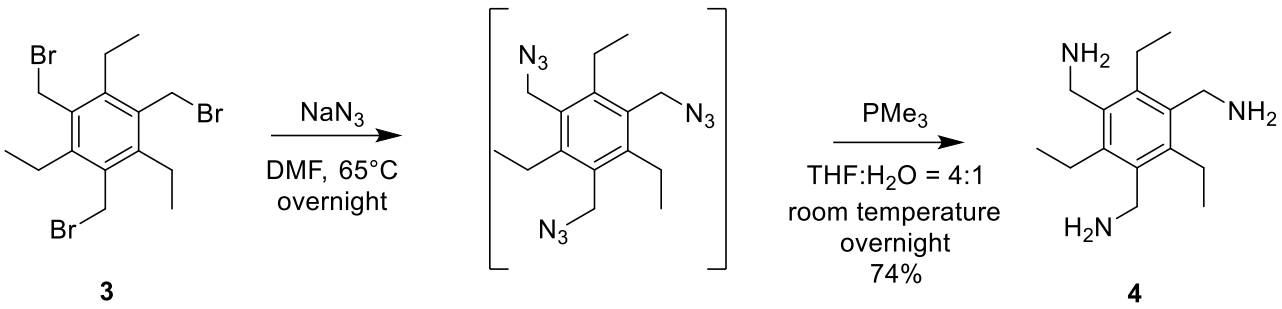

Reaction Scheme 5

The product was obtained containing trimethylphosphine oxide (O=PMe₃) as an impurity. The molar ratio between compound **4** (33%) and O=PMe₃ (67%), determined by ^{1}H-NMR. The need to remove N,N-dimethylformamide (DMF) and the amount of inert gas needed to remove the trimethylphosphine presented some practical issues for us, thus we decided to adopt a different procedure (**Reaction Scheme 8**) [42].

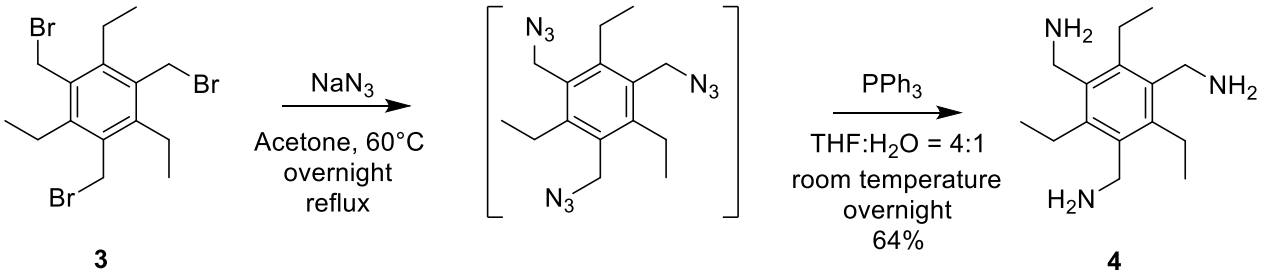

Reaction Scheme 6

While the new procedure addresses the previous limitations, the excess triphenylphosphine (PPh₃) could not be removed by evaporation under a stream of inert gas, unlike trimethylphosphine (PMe₃), which is more volatile. In this case the purity by molar ratio was compound **4** (9%) and O=PPh₃ (91%), also in this case was calculated by ^{1}H-NMR. As O=PMe₃ or O=PPh₃ had no influence in the next step (**reaction Scheme 7** and **11**), the amine **4** was used without further purification. The obtained amine **4** was reacted with the appropriate isothiocyanate to synthesize **TEP-SF2** (**Reaction Scheme 9**). The product was purified via flash column chromatography, which also allowed the removal of excess O=PPh₃.

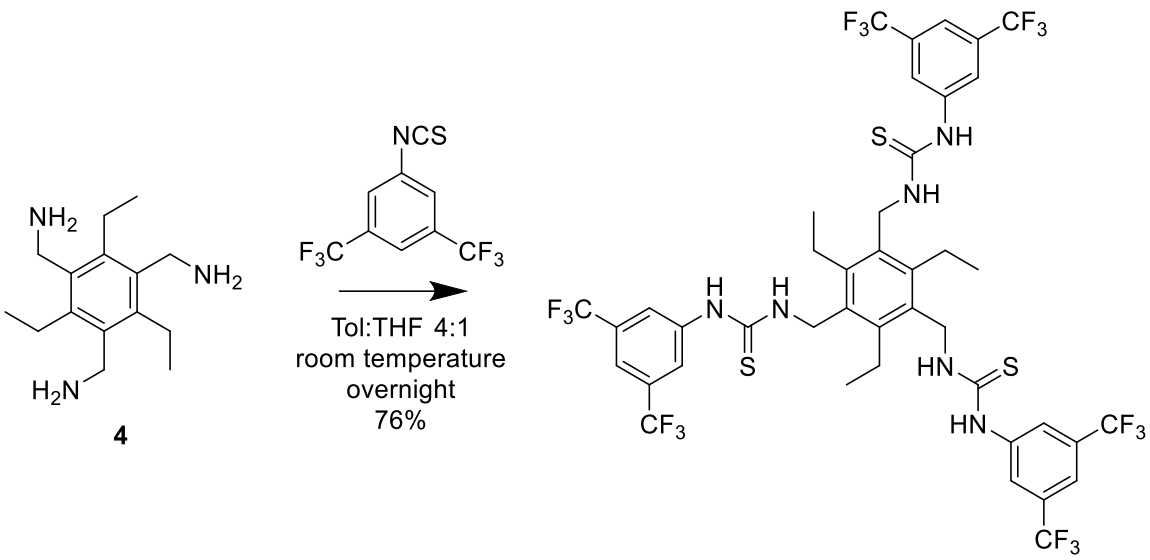

Reaction Scheme 7

To synthesize the analogous molecule lacking ethyl groups **THP-SF2**, compound **5** first reacted with sodium azide and then with PPh_3.

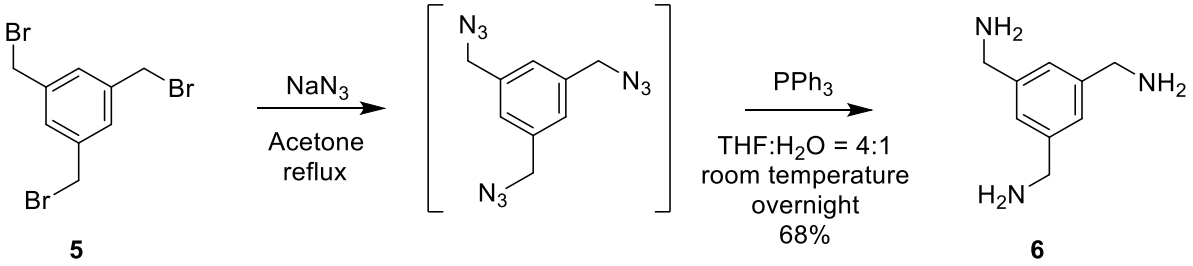

Reaction Scheme 8

In this case, the purity of compound **6** was 7% by molar ratio and 93% of $O=PPh_3$, as determined by ^{1}H-NMR, and it was used directly in the synthesis for the next step without further purification (**Reaction Scheme 10** and **12**). Compound **6** was reacted with 3,5-bis(trifluoromethyl)phenyl isothiocyanate to synthesize **THP-SF2** (**Reaction Scheme 12**). The product was purified by flash column chromatography to afford the pure compound in 37% yield.

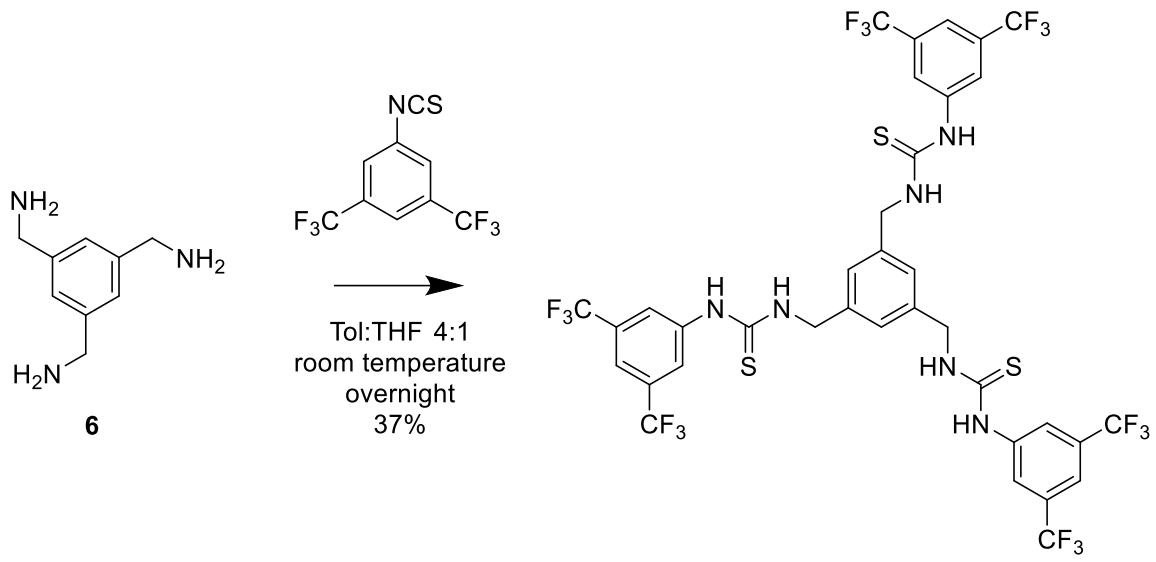

Reaction Scheme 9

3.4 TEP-SF2 and THP-SF2: Comparison of Cl⁻ Transport Activity

Anion transport capability of **TEP-SF2** was tested in the SPBA assay at a 1:100 **TEP-SF2** to lipid ratio in pre-incorporation (**Fig 24**). The exchange that we monitored was Cl^-/NO_3^- and $PhHPO_4^-/NO_3^-$ antiport.

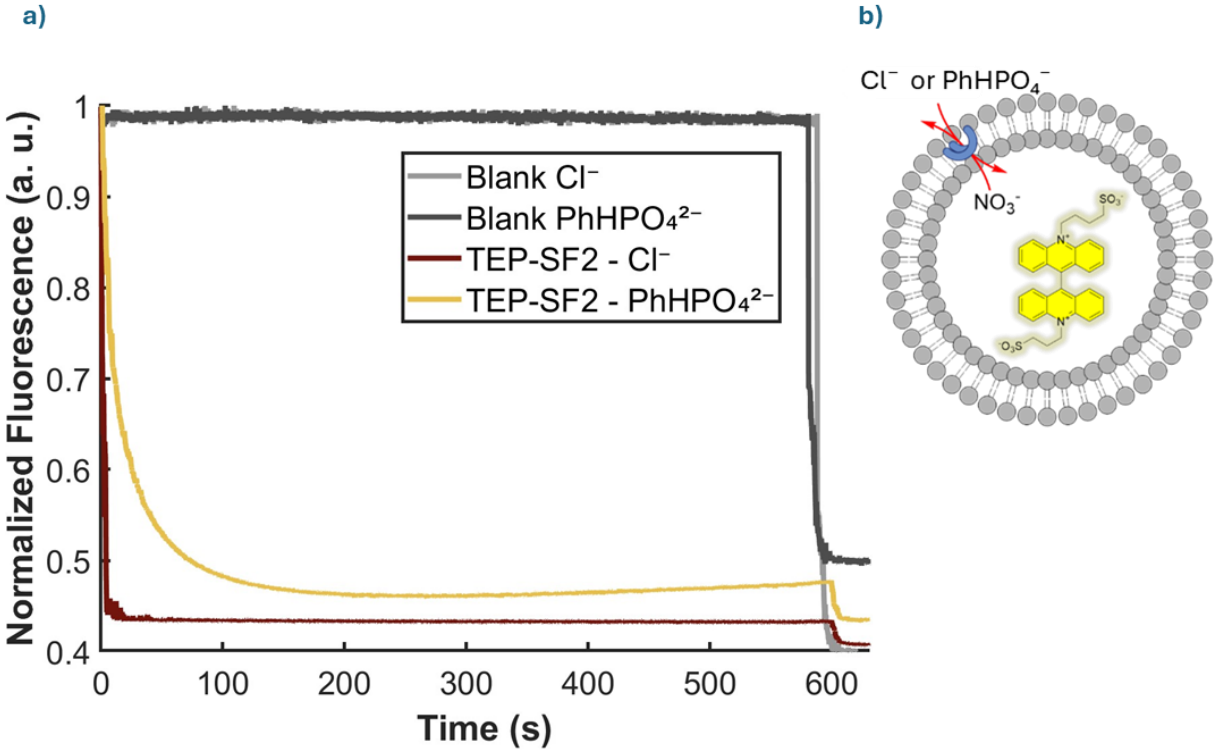

Figure 24: a) Transport activity of TEP-SF2 (1 mol% carrier/lipid ratio) in SPBA assay monitoring Cl^-/NO_3^- (dark red curve) and $PhHPO_4^-/ NO_3^-$ (yellow curve) antiport mechanisms. ***b)*** Schematic representation of Cl^-/NO_3^- or $PhHPO_4^-/NO_3^-$ antiport using SPBA assay.

The transport experiments reported in **Fig. 24** indicate that pre-incorporated **TEP-SF2**, at a 1 mol% ratio, transports Cl^- rapidly, reaching nearly immediately the equilibrium between internal and external concentration of chloride (dark red curve) and it shows fast transport also for $PhHPO_4^-$ (yellow curve).

To assess the post-insertion capability of **TEP-SF2** (**Fig. 25**), the compound was introduced into pre-formed liposomes at the same carrier-to-lipid ratio used in **Fig. 24**. Comparing the transport rates of pre-incorporated and post-inserted samples allowed evaluation of its ability to undergo post-insertion. **THP-SF2** was also tested in pre-incorporation and post-insertion, to evaluate the transport and deliverability.

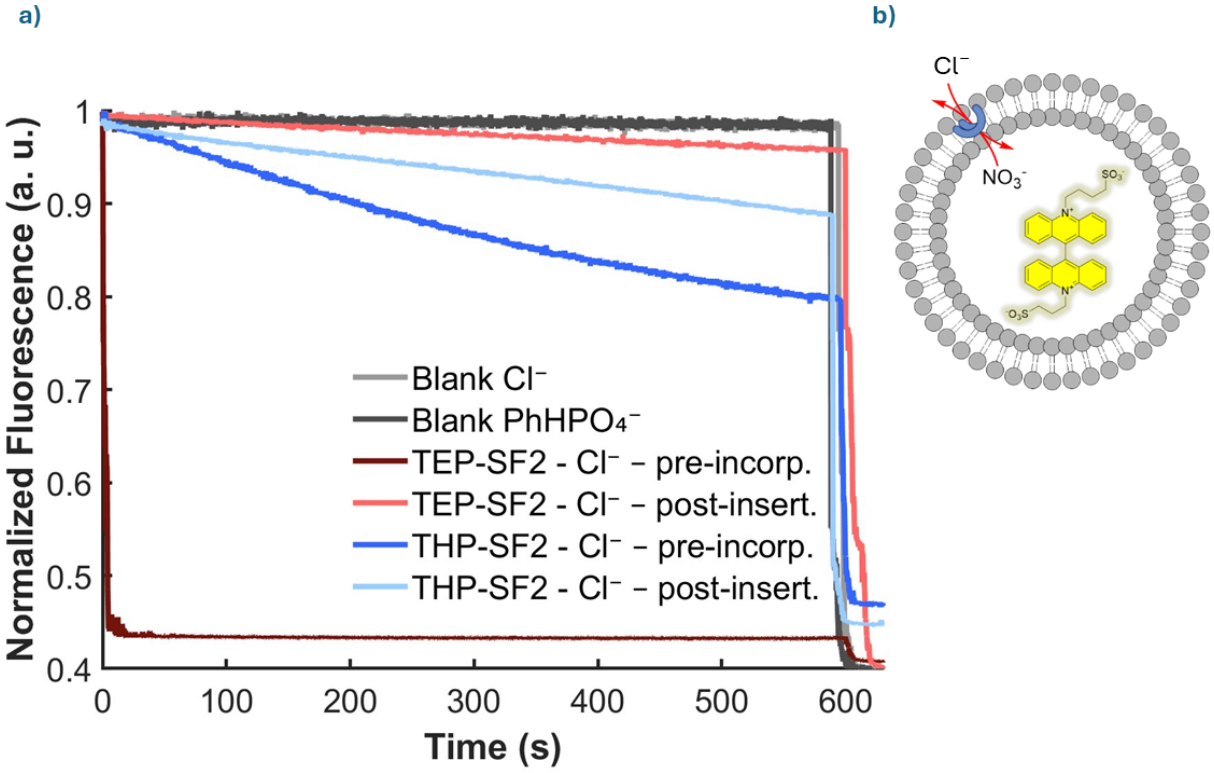

Figure 25: a) Transport activity of TEP-SF2 and THP-SF2 (1 mol% carrier/lipid ratio) in SPBA assay monitoring Cl^-/NO_3^- antiport mechanisms for TEP-SF2 pre-incorp. (dark red curve), TEP-SF2 post-insert. (light red curve), THP-SF2 pre-incorp. (blue curve), THP-SF2 post-insert. (light blue curve). ***b)*** Schematic representation of Cl^-/NO_3^- antiport using SPBA assay.

As shown in **Fig. 25**, pre-incorporated **TEP-SF2** ensures a very rapid chloride transport (dark red curve), whereas post-inserted **TEP-SF2** exhibits a drastic loss of activity (light red curve), highlighting its poor post-insertability. **THP-SF2**, on the other hand, is a less efficient carrier when pre-incorporated, clearly underperforming compared to **TEP-SF2** at 1 mol% ratio. However, its behaviour upon post-insertion reveals the opposite trend: due to its slightly higher hydrophilicity, **THP-SF2** can be effectively post-inserted, showing only a moderate decrease in activity and ultimately surpassing **TEP-SF2** in this context. This indicates that the removal of the ethyl substituents, while detrimental to intrinsic transport ability, provides a sufficient increase in hydrophilicity to enable post-insertion without a dramatic loss of performance.

In addition, both carriers were also tested as pre-incorporated at lower carrier-to-lipid ratios (1:10000). Even at this reduced concentration, **TEP-SF2** remains an efficient chloride carrier, whereas **THP-SF2** shows no evidence of transport. These results once again highlight the excellent performance of **TEP-SF2** as a chloride carrier, in sharp contrast with the poor efficiency of **THP-SF2** (**Fig. 26**).

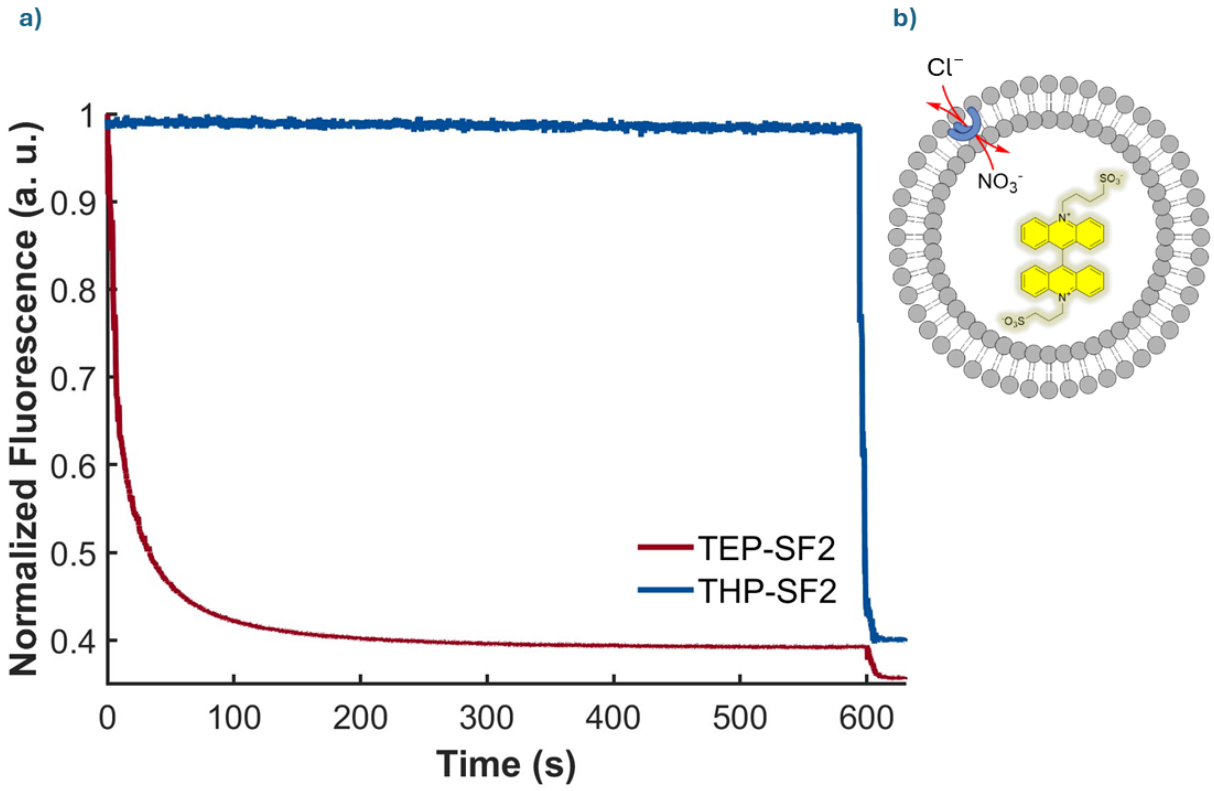

Figure 26: a) Transport activity of TEP-SF2 and THP-SF2 (1:10000 carrier/lipid ratio) in SPBA assay monitoring Cl^-/NO_3^- antiport for TEP-SF2 (red curve) and THP-SF2 (blue curve). ***b)*** Schematic representation of Cl^-/NO_3^- antiport using SPBA assay.

To investigate the reason for the drastic decrease in performance of **THP-SF2** as a chloride carrier, a ^{1}H-NMR titration was carried out to determine its binding constant with chloride. Since the K_a for the **TEP-SF2**/Cl^- complex is already reported to be 450 M^{-1} in DMSO-d_6 (with 0.5% of D_2O), [36] the experiment with **THP-SF2** was performed under the same conditions to enable direct comparison.

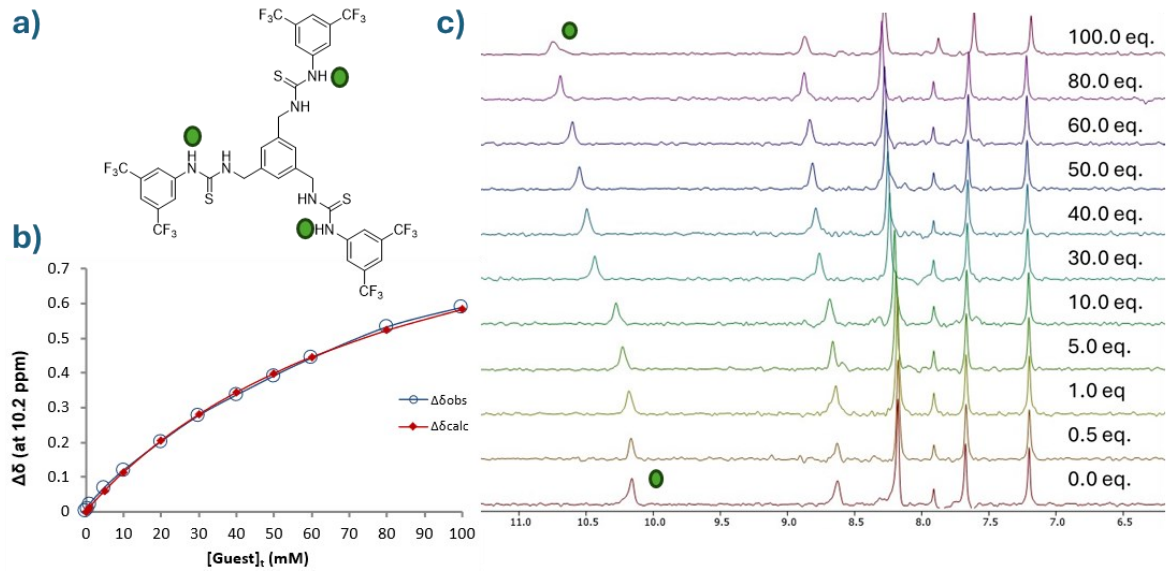

Figure 27: a) THP-SF2 structure, the green dots indicate the proton monitored. ***b)*** THP-SF2 binding curve obtained by fitting the shift of the signal at 10.2. ***c)*** ^{1}H-NMR (600MHz) titration of THP-SF2 (1mM) with TBACl (to 100.0 eq.) in DMSO-d_6 (with 0.5% of D_2O). The K_a value was obtained by fitting the shift indicated by green dots.

The obtained K_a value for **THP-SF2**, fitted for a 1:1 complex (**Fig. 27**), was calculated to be 11 M^{-1}, significantly lower than the previously reported K_a (**TEP-SF2**) = 450 M^{-1}. [36] This marked difference, nearly a 40-fold weaker chloride affinity, explaining the weak transport activity observed with **THP-SF2**. The absence of ethyl groups compromises the structural preorganization necessary for effective anion binding and transport.

3.5 TEP-ON and THP-ON: Comparison of Cl^- Transport Activity

We also synthesized two more compounds bearing TEP and THP scaffolds, as part of our initial attempt to develop hexa-urea receptors with an alternative scaffold to TREN. Tris-Ureas compounds **TEP-OP** and **THP-OP** were obtained starting from the previously described amines **5** and **7**, in both cases, the product was obtained as a yellow precipitate, and isolated by filtration.

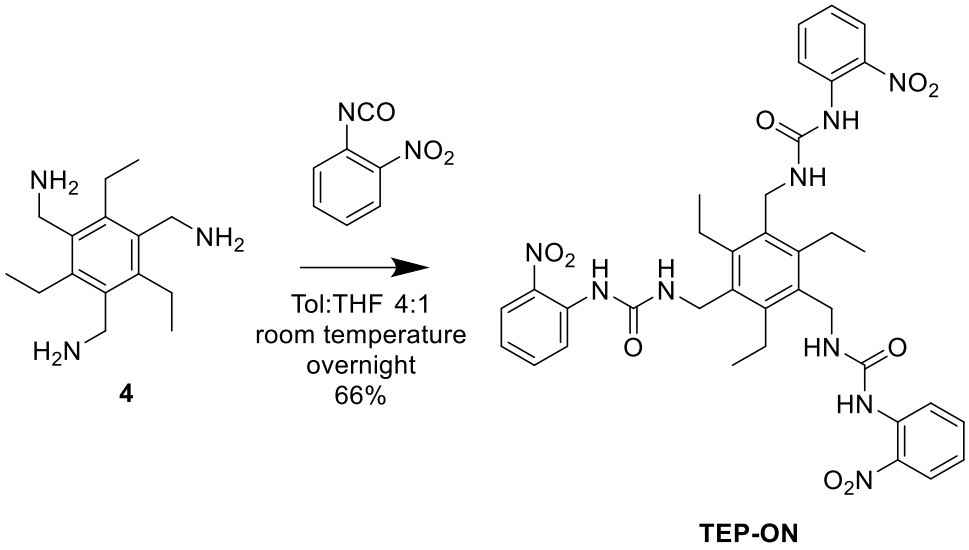

TEP-ON

Reaction Scheme 10

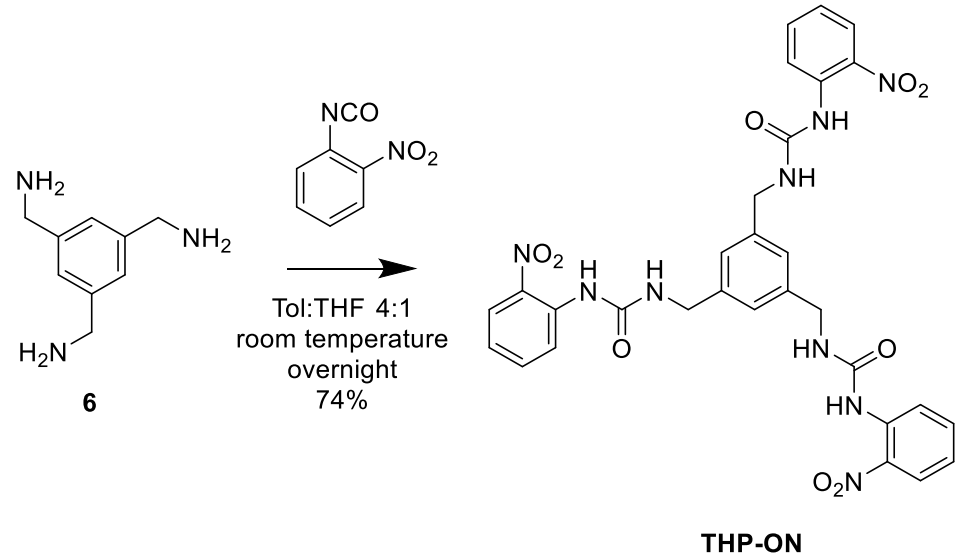

THP-ON

Reaction Scheme 11

To obtain the hexa-urea from TEP or THP scaffold, we attempted to reduce the nitro group to an amine, as previously done for the TREN-based **2**. However, none of the tested reducing agents (tin(II) chloride, iron powder, sodium dithionite) showed evidence of reduction. Nevertheless, other approaches may still be pursued to access TEP- or THP-based hexa-ureas, for example by using H_2 or N_2H_4 as reducing agent and Pd/C as catalyst.

TEP-ON and **THP-ON** were tested for Cl^- transport using the SPBA assay, offering a further comparison between TEP- and THP-derived receptors applied for anion transport and helping determine if the presence of ethyl groups again plays a critical role. Also, **TREN-ON** was tested for Cl^- transport using the SPBA assay, showing no transport activity (**Fig. ES22**).

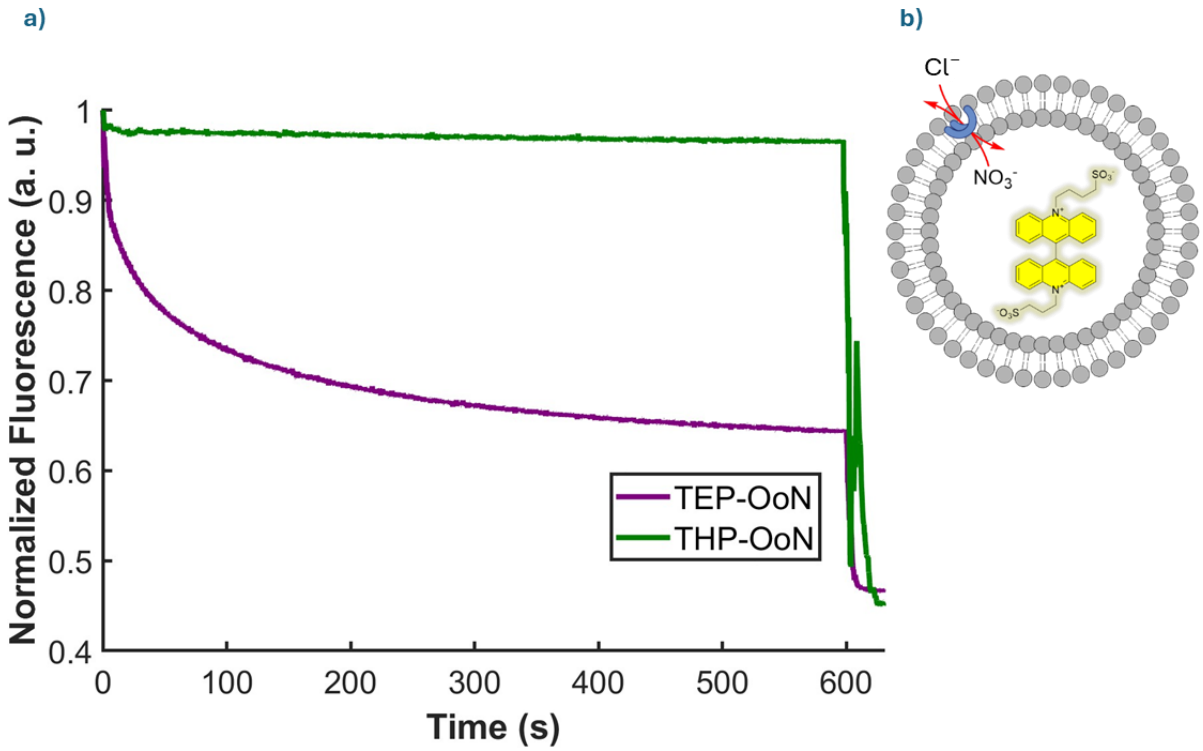

Figure 28: a) Transport activity of TEP-ON and THP-ON (1 mol% carrier/lipid ratio) in SPBA assay monitoring Cl^-/NO_3^- and $PhHPO_4^-/NO_3^-$ antiport mechanisms. ***b)*** Schematic representation of Cl^-/NO_3^- or $PhHPO_4^-/NO_3^-$ antiport using SPBA assay.

The chloride transport rates of **TEP-ON** and **THP-ON** (**Fig. 28**) exhibit a similar trend to the observed one for **TEP-SF2** and **THP-SF2** (**Fig. 25**). The receptor **TEP-ON** bearing ethyl groups acts as an active chloride carrier, while the compound **THP-ON** did not show any Cl^-/NO_3^- antiport transport activity. These results further demonstrate the critical role played by the ethyl groups in enabling tripodal phenylene-based receptors to interact effectively with anions and act as transmembrane carriers. The comparison between **TEP-SF2** and **TEP-ON** clearly shows that 3,5-bis(trifluoromethyl)phenyl is a highly effective electron-withdrawing group for transport applications and further supports the preference for thioureas over ureas.

4 Conclusion

In this thesis, tripodal receptors for anion transmembrane transport were synthesized (**Fig. 29**) with the aim of exploring new structural designs and evaluate their transport efficiency and deliverability.

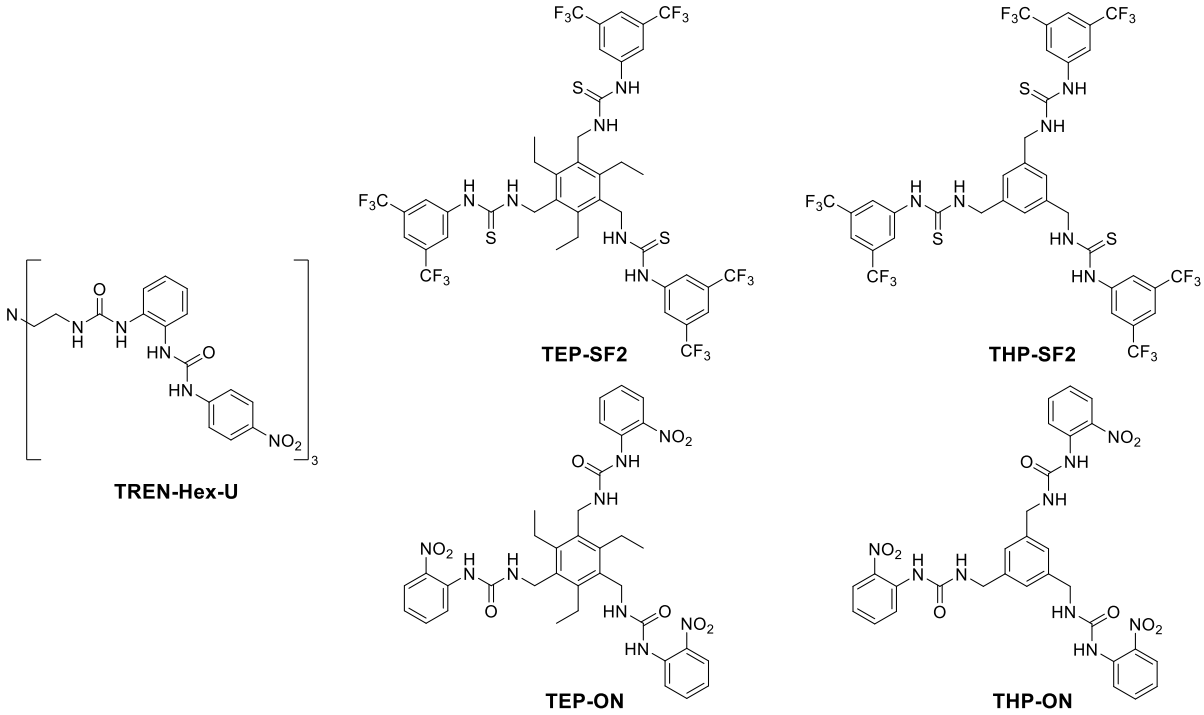

Figure 29: Receptor tested for anion carrier

In this work, a hexa-urea anion receptor featuring a TREN scaffold and *ortho*-nitro phenylene electron-withdrawing groups. Despite the potential for multiple hydrogen-bonding interactions offered by the **TREN-Hex-U** receptor, the compound did not demonstrate high transport efficiency. This limited performance can be generally explained by the presence of urea groups as binding sites, which may hinder the carrier's ability to traverse the lipid bilayer. Moreover, the presence of multiple binding sites increases the likelihood that unengaged functional groups interact with the polar head groups of the lipids, further reducing the transport rate. While it is capable of mediating chloride (Cl^-) transport, the observed transport rates are relatively mediocre, since even at high concentration (1:100 carrier to lipid ratio) it does not show fast transport. Its performance toward more challenging oxoanions is even more limited: phenylphosphate ($PhHPO_4^-$) is transported only to a minor extent, sulphate (SO_4^{2-}) transport is not observed, and dihydrogen phosphate ($H_2PO_4^-$) is practically not transported. Another limitation of the tested TREN hexa- ureas is the difficulty in generating structurally related analogues to improve performance: synthetic attempts bearing alternative electron-withdrawing groups were unsuccessful, while thiourea analogues face potential intramolecular side reactions that hinder their practical preparation. To overcome these challenges, hexa-ureas could be designed on alternative scaffolds like TEP, for example different reduction strategies to those used for **TEP-ON**, such as Pd/C reduction, may be

explored to enhance the transport properties of the receptor. **Table 7** summarizes the transport capabilities of TREN-Hex-U for the various anions tested.

Table 7

Synthetic anion carrier	**Investigated anion**			
TREN-Hex-U	Cl^-	$PhHPO_4^-$	SO_4^{2-}	$H_2PO_4^-$
Transport activity	Mediocre	Weak	None	Extremely weak/None

TEP-SF2 is a well-known synthetic anion carrier and ranks among the most effective tripodal receptors. Its calculated clogP value is relatively high, and comparison of transport experiments performed with pre-incorporation versus post-insertion clearly highlights a marked decrease in activity. These results demonstrate that the high lipophilicity of **TEP-SF2** prevents efficient post-insertion into liposomal membranes.

To reduce the clogP value, an analogue lacking the ethyl groups, **THP-SF2**, was synthesized and tested as a synthetic anion carrier. When pre-incorporated, **THP-SF2** was capable of functioning as a carrier. However, a direct comparison with pre-incorporated **TEP-SF2** highlights a substantial difference in performance; **THP-SF2** transports chloride significantly less efficiently, moreover, it does not work at lower concentration (1:10000 carrier to lipid ratio). Unlike **TEP-SF2**, **THP-SF2** can be delivered via post-insertion with only a modest reduction in transport rate. This makins it a comparatively better carrier than the post-inserted **TEP-SF2** setup (**Table 8**). To investigate the cause of its reduced activity compared to **TEP-SF2**, the binding constant K_a, between **THP-SF2** and chloride was determined. **THP-SF2** exhibits a markedly lower K_a for chloride compared to **TEP-SF2**, and this low binding affinity can account for its limited ability to act effectively as a synthetic anion carrier.

Table 8

Synthetic anion carrier	**Cl^- Transport activity (pre-incorporated)**	**Cl^- Transport activity (post inserted)**
TEP-SF2	Excellent	Extremely weak
THP-SF2	Weak	Weak

To harness the excellent anion transport properties of **TEP-SF2** while also ensuring its efficient delivery into liposomal membranes, alternative strategies are necessary. Approaches such as membrane fusion could allow incorporation of the carrier without relying on post-insertion,

thus overcoming limitations imposed by its high clogP value and preserving its superior transport performance.

The importance of ethyl groups was observed also for the **TEP-ON**/**THP-ON** pair. The TEP-based receptor acted as an active synthetic anion carrier, whereas the THP-based receptor proved inactive. These results further confirm that the presence of ethyl groups is necessary in both receptor pairs in order to function as synthetic anion carrier.

5 Experimental Section

5.1 General procedures for synthesis

All reagents and solvents were obtained from Sigma Aldrich, Fluorochem, Alfa Aesar and VWR, and were used without further purification. For the compounds evaluated in transport experiments, ^{1}H- and ^{13}C-NMR spectra were recorded on a 400MHz Jeol JNM-ECZ400R/S3 spectrometer, while ^{1}H-NMR spectra of the intermediates were recorded on a 300 MHz Bruker Avance 300 spectrometer. High-resolution mass spectra (HRMS) were obtained on an Agilent QTOF 6520 instrument using electrospray ionisation (ESI). Infrared (IR) measurements were recorded on a Shimadzu IRSpirit spectrometer equipped with the single-reflection ATR measurement attachment (QATR-S). Reaction progress was monitored by thin-layer chromatography (TLC) on silica gel 60 F254-coated aluminium sheets and visualised under UV irradiation at 254 nm. Purification, when required, was performed by column chromatography on silica gel (VWR Chemicals, particle size 35–70 µm).

5.2 Synthetic procedures

TREN-ON, *N,N',N''-tris[N'-(1-nitrophenyl)ureidoethyl]nitrilotriethane*

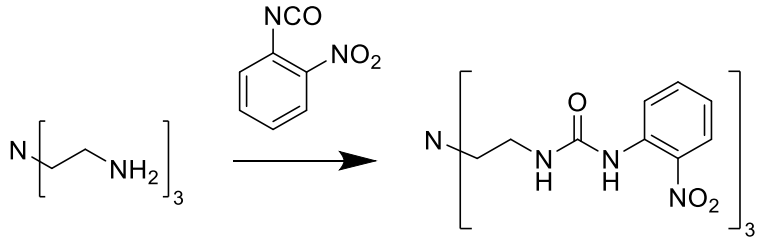

1 **TREN-ON**

In a round-bottom flask, a solution of *o*-nitrophenyl isocyanate (2.00 g, 12.19 mmol) in toluene (50 mL) was treated with a solution of compound **1** (608 µL, 4.06 mmol) in anhydrous tetrahydrofuran (THF, 10 mL). Upon addition, a yellow suspension formed immediately. The reaction mixture was stirred at room temperature for 4 h, after which the precipitate was collected by filtration and washed with toluene (10 mL) and diethyl ether (Et_2O, 10 mL). The product was obtained as a yellow solid (2.10 g, 3.81 mmol). Yield 94%.

^{1}H-NMR (400 MHz, DMSO-d_6) δ 9.34 (s, 3H, NHCH$_2$), 8.24 (dd, J = 8.6, 1.3 Hz, 3H, ArH), 8.00 (dd, J = 8.4, 1.7 Hz, 3H, ArH), 7.57 (ddd, J = 8.6, 7.2, 1.5 Hz, 3H, ArH), 7.49 (s, 3H, NHAr), 7.08 (ddd, J = 8.6, 7.2, 1.4 Hz, 3H, ArH), 3.25 – 3.16 (m, 6H, CH$_2$N), 2.63 (t, J = 7.0 Hz, 6H, CH$_2$N).

^{13}C-NMR (400 MHz, DMSO-d_6) δ 154.44 (CO), 136.36 (C), 135.55 (C), 133.07 (CH), 125.87 (CH), 122.61 (CH), 121.95 (CH), 37.96 (CH$_2$), 23.06 (CH$_2$).

IR (ν/cm $^{-1}$) 3391; 3270; 1670; 1541; 1273; 1379; 1335; 1121; 888; 680; 773.

HR-MS (ESI) to be acquired.

3, *N,N',N''-tris[N'-(1-aminophenyl)ureidoethyl]nitrilotriethane*

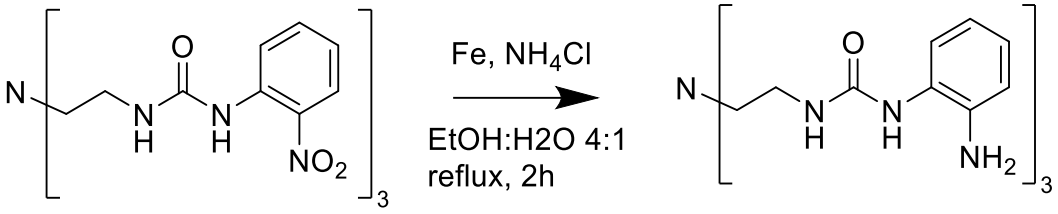

TREN-ON **3**

A mixture of **TREN-ON** (2.03 g, 3.13mmol), ammonium chloride (0.30 g, 5.54mmol) and iron fine powder (2.62mg, 46.95 mmol) are added to EtOH/H_2O = 4:1 (50 mL) in a round bottom flask, the suspension was refluxed at 95°C and stirred for 2h. After the reaction was completed, the suspension was filtered over Celite while hot, and the product was obtained by evaporating the solvent under reduced pressure, obtaining **3** as a pale-yellow solid (1.36 g, 2.59 mmol). Yield 83%.

^{1}H-NMR (300 MHz, DMSO-d_6) δ 7.71 (s, 3H, NHCH$_2$), 7.23 (dd, J = 7.9, 1.5 Hz, 3H, ArH), 6.78 (td, J = 7.5, 1.6 Hz, 3H, ArH), 6.67 (dd, J = 8.0, 1.7 Hz, 3H, ArH), 6.50 (td, J = 7.2, 1.7 Hz, 3H, ArH), 6.31 (s, 3H, NHAr), 4.70 (s, 6H, NH$_2$), 3.17 (dd, J = 5.5 Hz, 6H, CH$_2$NH), 2.56 (s, 6H, NCH$_2$CH$_2$).

TREN-Hex-U, *N,N',N''-tris[N'-(4-nitrophenyl)-N-(phenyl)bis(ureidoethyl)]nitrilotriethane*

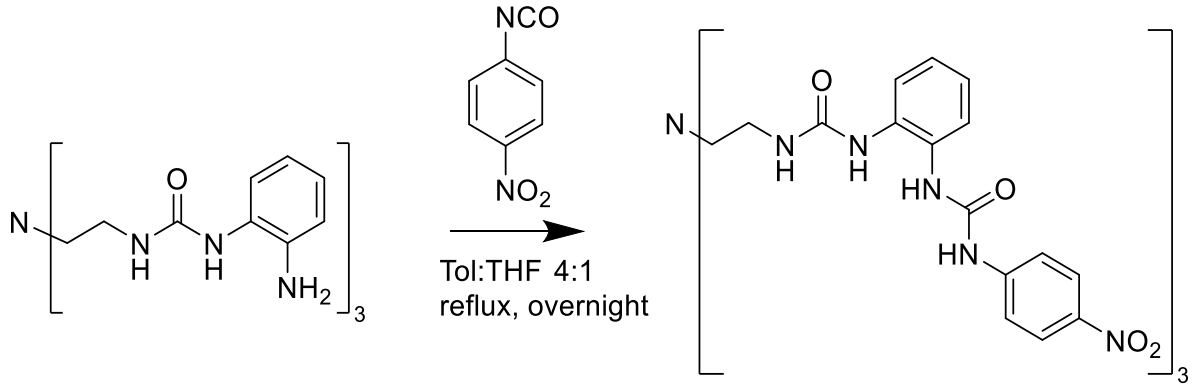

3 **TREN-Hex-U**

A solution of compound **3** (109.0 mg, 0.152 mmol) in toluene/anhydrous THF=4:1 (10mL) was treated with *p*-nitrophenyl isocyanate (100.0 mg, 0.61 mmol). The reaction mixture was refluxed at 90 °C for 18 h. The resulting precipitate was collected by filtration and washed with toluene (10 mL), Et_2O (10 mL). The crude product was further purified by flash column chromatography, using a eluent of increasing polarity combining: dichloromethane (DCM), acetone, and methanol (MeOH). The appropriate fractions were combined, and the solvent was removed under reduced pressure to afford **TREN-Hex-U** as a yellow solid (31.3 mg, 25.4 µmol). Yield 17%.

^{1}H-NMR (400 MHz, DMSO-d_6) δ 9.86 (s, 3H, NHAr), 8.26 (s, 3H, NHAr), 8.14 (d, J = 9.2 Hz, 6H, ArH), 8.01 (s, 3H, NHAr), 7.65(d, J = 9.3 Hz, 3H, ArH), 7.61 – 7.50 (m, 6H, ArH), 7.48 –

7.41 (m, 3H, Ar<u>H</u>), 7.07 – 6.98 (m, 6H, Ar<u>H</u>), 6.57 (s, 3H, N<u>H</u>CH_2), 3.19 (d, J = 7.0 Hz, 6H, $C\underline{H_2}CH_2NH$), 2.60 (t, J = 6.4 Hz, 6H, $NC\underline{H_2}CH_2$).

^{13}C-NMR (400 MHz, DMSO-d_6) δ 156.75 (<u>C</u>O), 153.09 (<u>C</u>O), 141.40 (<u>C</u>), 132.48 (<u>C</u>), 131.08 (<u>C</u>), 125.63 (<u>C</u>H), 124,95 (<u>C</u>H), 124.19 (<u>C</u>H), 117.86 (<u>C</u>H), 54.46 (<u>C</u>H_2), 38.36 (<u>C</u>H_2).

The IR spectrum of TREN-Hex-U was not recorded because not enough compound was left after testing.

HR-MS (ESI) to be acquired.

5, *(2,4,6-triethyl-1,3,5-trimethylamine)benzene*

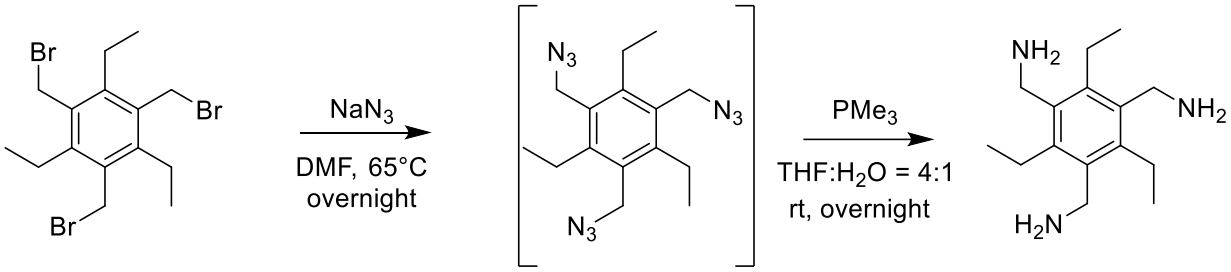

4 **5**

In a 50 mL round-bottom flask, **4** (700 mg, 1.58 mmol), sodium azide (512 mg, 7.9 mmol), and anhydrous DMF (20 mL) were combined and the mixture heated at 60 °C under stirring overnight.

To the mixture was then added EtOAc (30 mL) and washed with H_2O (3 x 20 mL). The organic phase was separated, dried over $MgSO_4$, filtered, and concentrated at to 4 mL after the addition of dry DMF (4 mL). The solution was transferred to a 250 mL round-bottom flask and combined with anhydrous, N_2-saturated THF (70 mL). A solution of PMe_3, 1 M in THF (9.48 mL, 9.48 mmol) was added, and the mixture was stirred for 40 min. N_2-saturated H_2O (16 mL) was then introduced, and the reaction was allowed to stir overnight. The solvent was removed by passing a gentle stream of Ar through the mixture. Compound **5** (585.6 mg, 1.16 mmol) was obtained as a white solid containing 67% of $O=PMe_3$ by molar ratio, as determined by ^{1}H-NMR. Compound was used without further purification. Yield 74%.

^{1}H-NMR (300 MHz, $CDCl_3$) δ 3.87 (s, 6H, N<u>H</u>$_2$), 2.82 (q, J = 7.5 Hz, 6H, C<u>H</u>$_2$), 1.43 (s, 6H, $C\underline{H_2}NH_2$), 1.23 (t, J = 7.5 Hz, 9H, <u>C</u>H_3). Trimethylphosphine oxide 1.52 (d, 2J(P-H)=12.5 Hz).

5 *(alternative synthesis)*

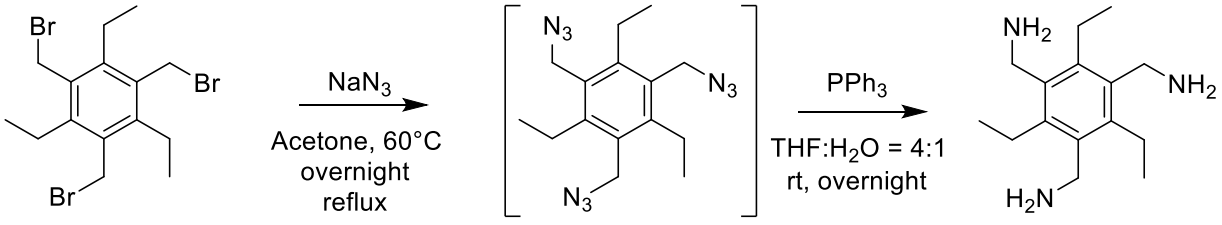

4 **5**

Compound **4** (0.500 g, 1.13 mmol) was dissolved in acetone (35 mL) and heated to reflux to ensure complete dissolution. Sodium azide (325 mg, 5.1 mmol) was then added, followed by the gradual addition of water (≈10 mL) until the solution became turbid. The reaction mixture was heated under reflux overnight. The solvent was removed under reduced pressure until approximately 4 mL remained. Ethyl acetate (EtOAc, 30 mL) was then added, and the mixture was washed with water. The organic layer was separated, dried over $MgSO_4$, and filtered. DMF (4 mL) was added to the filtrate, and the solution was again concentrated under reduced pressure to a final volume of 4 mL. The solution was transferred to a 250 mL round-bottom flask and combined with anhydrous, N_2-saturated THF (70 mL) and PPh3 (1.78 g, 7.79 mmol), and the mixture was stirred for 40 min. N_2-saturated H_2O (16 mL) was then introduced, and the reaction was allowed to stir overnight. The solvent was removed at reduced pressure. Compound **5** (1.94 g, 0.72mmol) was obtained as a white solid containing 98% of $O=PPh_3$ by molar ratio, as determined by ^{1}H-NMR. Compound was used without further purification. Yield 64%.

^{1}H-NMR (300 MHz, CD_3CN) δ 3.80 (s, 6H, $N\underline{H_2}$), 2.83 (q, *J* = 7.5 Hz, 6H, $C\underline{H_2}$), 1.43 (s, 6H, $C\underline{H_2}NH_2$), 1.17 (t, *J* = 7.5 Hz, 9H, $C\underline{H_3}$). Triphenylphosphine oxide 7.71-7.20 (m).

TEP-SF2, *cis,cis-1,3,5-tris[N'-(3,5-bis(trifluoromethyl)phenyl)thioureidomethyl]-2,4,6-triethylbenzene*

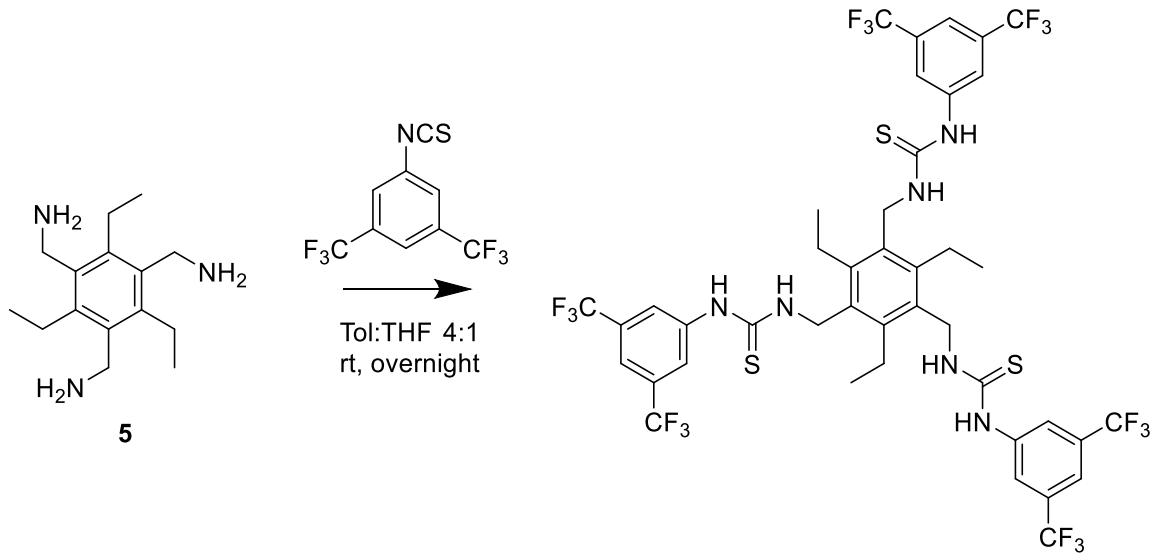

A solution of compound **5** (171 mg, 687 µmol) in anhydrous THF (5 mL) was prepared, and 3,5-*bis*(trifluoromethyl)phenyl isothiocyanate (370 µL, 4.50 mmol) was added dropwise. The reaction mixture was stirred at room temperature for 18 h. Upon completion, the solvent was removed under reduced pressure. The crude product was purified by flash column chromatography using dry loading: the solid was dissolved in approximately 2 mL of MeOH, celite was added, and the solvent was evaporated. Chromatography was then performed with a gradient elution from MeOH:DCM = 0:1 to MeOH:DCM = 1:9, affording the pure product **TEP-SF2** (166 mg, 156 µmol). Yield 76%.

^{1}H-NMR (400 MHz, ACETONE-d_6) δ 9.31 (s, 3H, NHAr), 8.36 (s, 6H, ArH), 7.69 (s, 3H, ArH), 7.44 (s, 3H, $NHCH_2$), 4.86 (d, *J* = 4.3 Hz, 6H, CH_2NH), 2.84 (q, *J* = 7.6 Hz, 6H, CH_2), 1.22 (t, *J* = 7.5 Hz, 9H, CH_3).

^{13}C-NMR (400 MHz, ACETONE-d_6) δ 144.99 (CS), 142.13 (C), 132.05 (C), 130.97 (CH_2), 124.90 (C), 122.20 (CH), 116.71 (CH),42.96 (CH_2NH), 23.15 (CH_2CH_3), 15.96 (CH_3).

IR (ν/cm $^{-1}$) 3245; 2972; 1497; 1276; 1181; 1119; 950; 885; 681.

HR-MS (ESI) to be acquired.

7, *1,3,5-tris(aminomethyl)benzene*

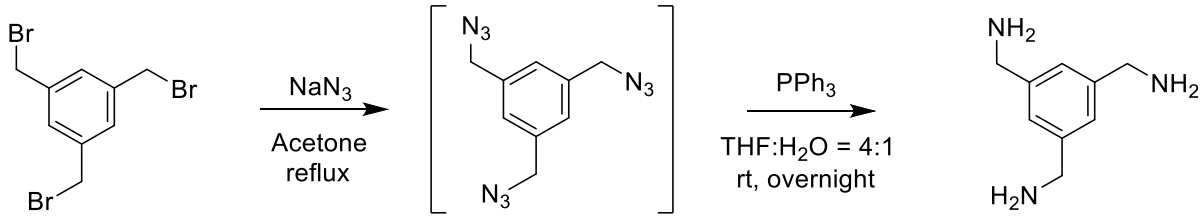

6 **7**

To a solution of **6** (500mg, 1.40 mmol) in acetone (35 mL), sodium azide was added (410 mg, 6.30 mmol), followed by the gradual addition of water (≈10 mL) until the solution became turbid. The reaction mixture was heated under reflux overnight. The solvent was removed under reduced pressure until approximately 4 mL remained. EtOAc (30 mL) was then added, and the mixture was washed with water. The organic layer was separated, dried over $MgSO_4$, and filtered. DMF (4 mL) was added to the filtrate, and the solution was again concentrated under reduced pressure to a final volume of 4 mL. Completion of the reaction was confirmed by ^{1}H-NMR of a crude aliquot from the reaction mixture.

The solution was transferred to a 250 mL round-bottom flask and combined with anhydrous, N_2-saturated THF (70 mL) and PPh3 (2.13g, 6,78 mmol), and the mixture was stirred for 40 min. N_2-saturated H_2O (16 mL) was then introduced, and the reaction was stirred overnight. The solvent was removed at reduced pressure. 3,63 g of Compound 5 was obtained as a white solid containing 93% of $O=PPh_3$ by molar ratio, as determined by ^{1}H-NMR. Compound was used without further purification. Yield 68%.

^{1}H-NMR (300 MHz, CD_3CN) δ 7.37 – 7.27 (m, 3H, ArH), 4.44 (s, 6H, CH_2N).

THP-SF2, *cis,cis-1,3,5-tris[N'-(3,5-bis(trifluoromethyl)phenyl)thioureidomethyl] benzene*

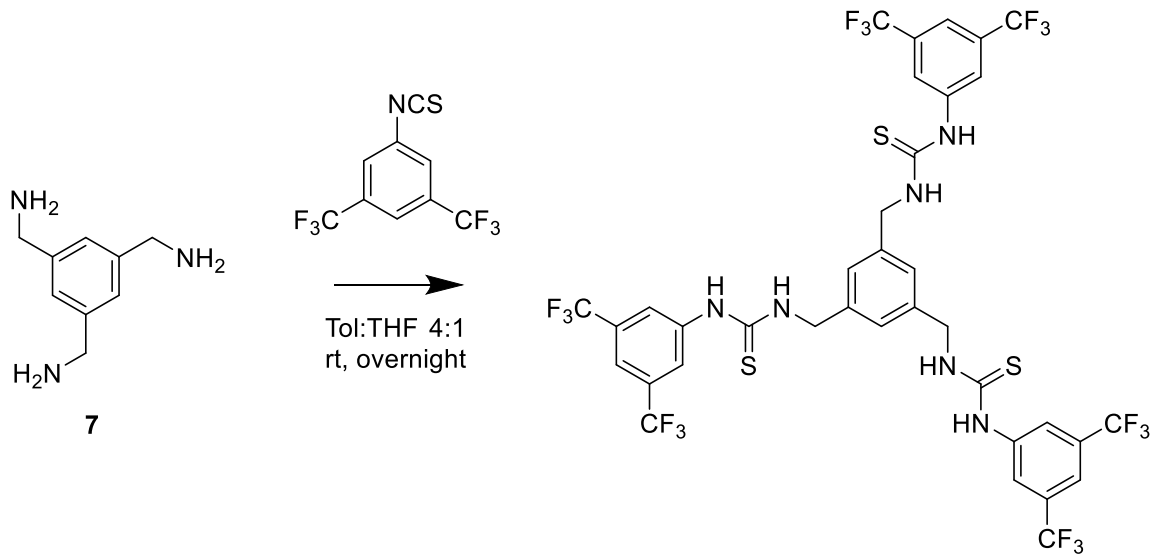

7 **THP-SF2**

A solution of compound **7** (400mg, 1,93.66 µmol) in anhydrous THF (5 mL) was prepared, and 3,5-*bis*(trifluoromethyl)phenyl isothiocyanate (370 µL, 4,50 mmol) was added dropwise. The reaction mixture was stirred at room temperature for 18 h. Upon completion, the solvent was removed under reduced pressure. The crude product was purified by flash column chromatography using dry loading: the solid was dissolved in approximately 2 mL of MeOH, celite was added, and the solvent was evaporated. Chromatography was then performed with a gradient elution from MeOH:DCM = 0:1 to MeOH:DCM = 2:8, affording the pure product **THP-SF2** (69.06 mg, 71.64 µmol). Yield 37%.

^{1}H-NMR (400 MHz, Acetone-d_6) δ 9.52 (s, 3H, NHAr), 8.37 – 8.30 (m, 6H, ArH), 8.13 (t, J = 5.5 Hz, 3H, ArH), 7.70 (s, 3H, ArH), 7.37 (s, 3H, NHCH$_2$), 4.90 (d, J = 5.4 Hz, 6H, NCH$_2$Ar).

IR (ν/cm $^{-1}$) 3222, 3045, 2932, 1541, 1379, 1274 1169, 1125, 888, 680.

HR-MS (ESI) m/z calculated for [M+Na]$^+$ 1026.0858, found 1026.0858.

TEP-ON, *cis,cis-1,3,5-tris[N'-(2-nitrophenyl)ureidomethyl]-2,4,6-triethylbenzene*

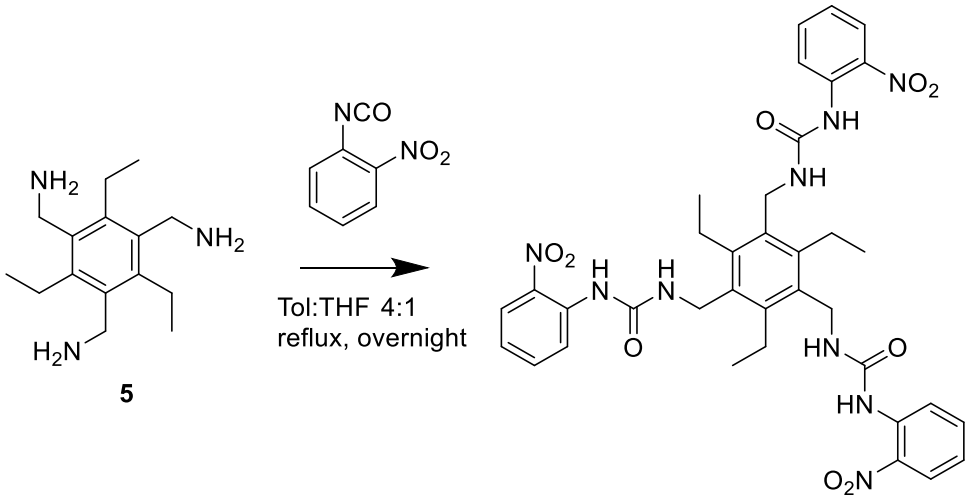

5

TEP-ON

In a round-bottom flask, to a solution of *o*-nitrophenyl isocyanate (310mg, 1.89 mmol) in toluene (40 mL) was added a solution of compound **5** (1.50 g, 541.29 µmol) in anhydrous THF (10 mL). The reaction mixture was stirred at room temperature for 4 h, during this period, a yellow suspension is formed, the precipitate was isolated by filtration and washed with toluene (10 mL), THF (10 mL) and Acetone (10 mL). The product **TEP-ON** was obtained as a yellow solid (264.66 mg, 357.25 µmol). Yield 66%.

^{1}H-NMR (400 MHz, DMSO-d_6) δ 9.35 (s, 3H, NHAr), 8.41 (d, J = 7.6 Hz, 3H, ArH), 8.05 (d, J = 10.1 Hz, 3H, ArH), 7.71 – 7.61 (m, 6H, ArH + NHCH$_2$), 7.12 (t, J = 7.8 Hz, 3H, ArH), 4.40 (d, J = 4.9 Hz, 6H, NHCH$_2$), 2.80 (q, J = 7.6 Hz, 6H, CH$_2$CH$_3$), 1.18 (t, J = 7.4 Hz, 9H, CH$_3$).

^{13}C-NMR (400 MHz, DMSO-d_6) δ 154.39 (CO), 137.25 (C), 136.32 (C), 135.55 (C), 133.07 (CH), 125.87 (CH), 122.61(CH), 121.95 (CH), 37.95 (CH$_2$N), 23.06 (CH$_2$CH$_3$), 16.81 (CH$_3$).

IR (ν/cm $^{-1}$) 3317, 2968, 2157, 1647, 1479, 1336, 1253, 1148, 730

HR-MS (ESI) to be acquired.

THP-ON, *cis,cis-1,3,5-tris[N'-(2-nitrophenyl)ureidomethyl]benzene*

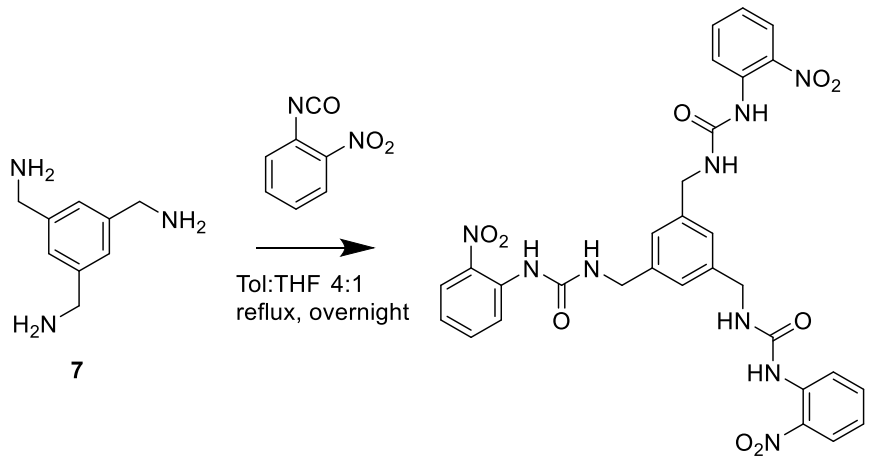

7

THP-ON

In a round-bottom flask, to a solution of *o*-nitrophenyl isocyanate (310mg, 1.89 mmol) in toluene (40 mL) was added a solution of compound **7** (1.72 g, 968.29 µmol) in anhydrous THF (10 mL), addition, a yellow suspension formed immediately The reaction mixture was stirred at room temperature for 4 h, during this period, a yellow suspension is formed, the precipitate was isolated by filtration and washed with toluene (10 mL), THF (10 mL) and Acetone (10 mL). The product **THP-ON** was obtained as a yellow solid (264.66 mg, 357.25 µmol). Yield 74%.

^{1}H-NMR (400 MHz, DMSO-d_6) δ 9.44 (s, 3H, NHAr), 8.32 (dd, J = 8.7, 1.4 Hz, 3H, ArH), 8.06 (d, J = 6.0 Hz, 3H, NHCH2), 8.03 (dd, J = 8.4, 1.5 Hz, 3H, ArH), 7.59 (ddd, J = 8.6, 7.1, 1.5 Hz, 3H, ArH), 7.17 (s, 3H, ArH), 7.10 (ddd, J = 8.4, 7.2, 1.4 Hz, 3H, ArH), 4.31 (d, J = 5.8 Hz, 6H, CH2N).

^{13}C-NMR (400 MHz, DMSO-d_6) δ 154.81 (CO), 137.30 (CH), 136.37 (CH), 135.46 (CH), 125.83 (CH), 122.49 (CH), 121.94 (CH), 43.43 (CH_2N).

IR (ν/cm $^{-1}$) 3311, 1655,1584, 1499, 1336, 1281, 1254, 1148, 734.

HR-MS (ESI) m/z calculated for $[M+Na]^+$ 636.2002, found 636.2043

5.3 Characterization

(5.3.1) TREN-ON, *characterization*

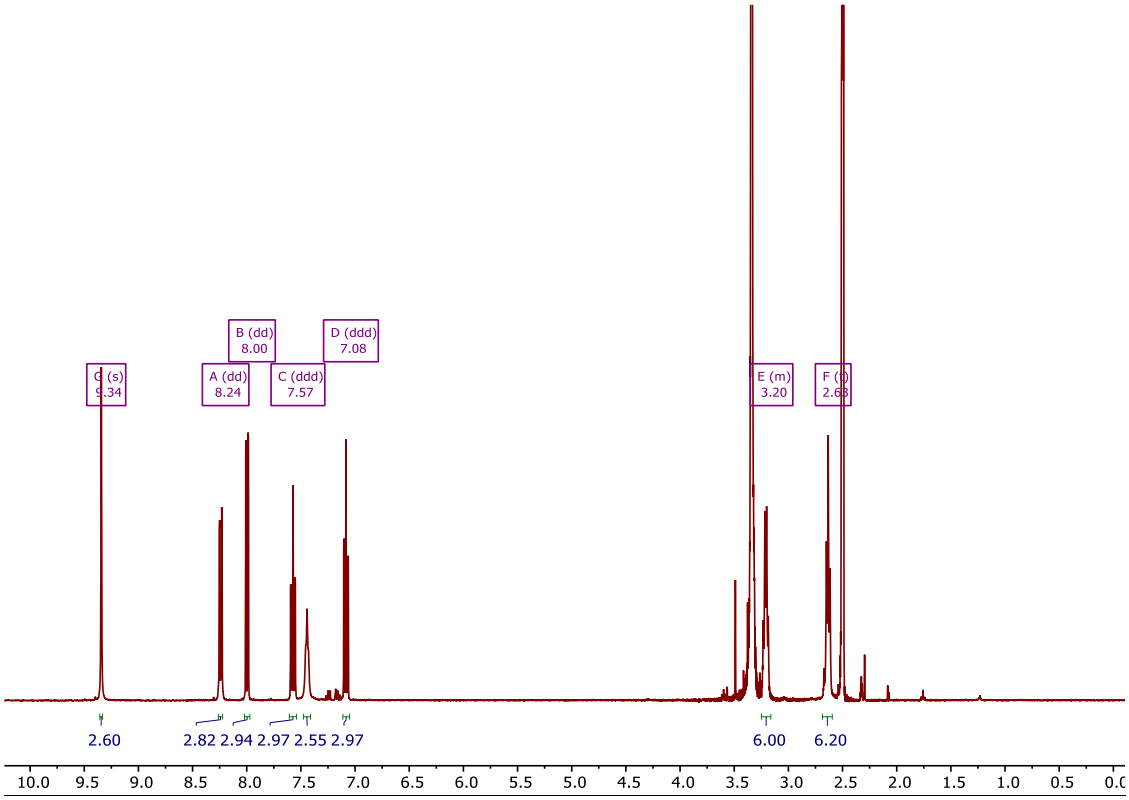

Figure ES1: TREN-ON ^{1}H-NMR (400 MHz, DMSO-d_6)

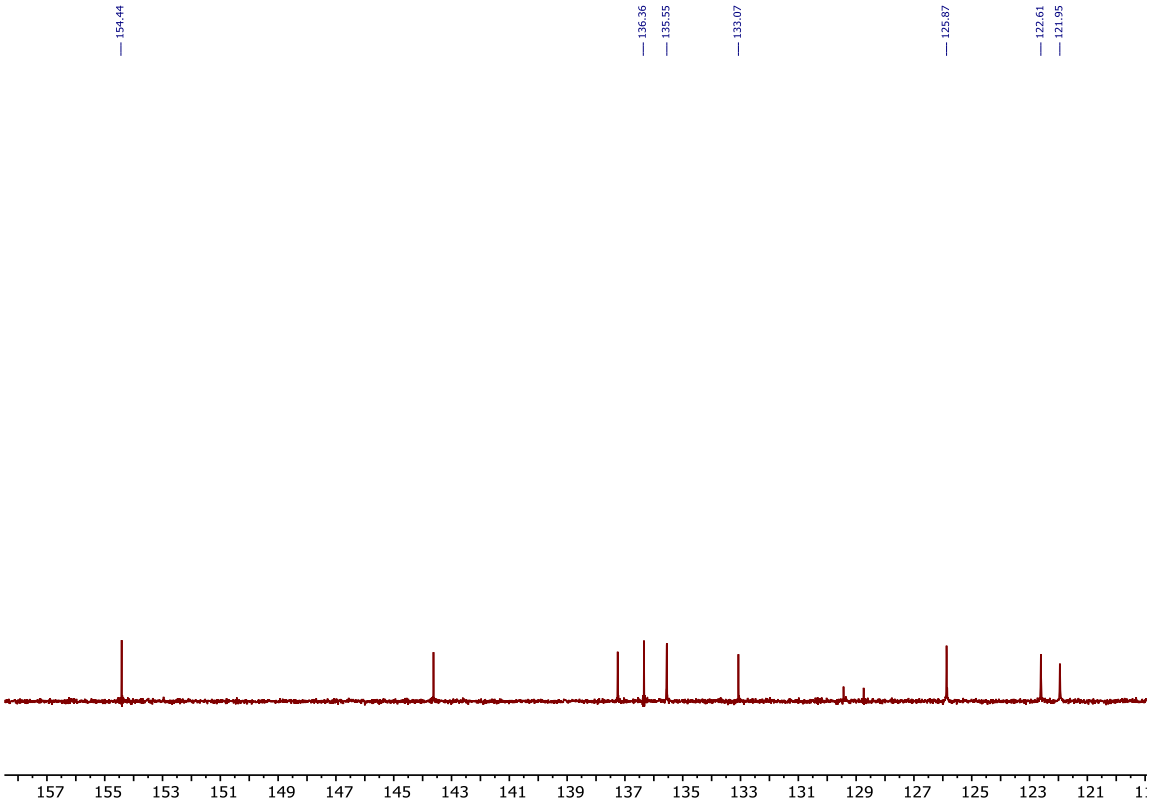

Figure ES2: TREN-ON ^{13}C-NMR (400 MHz, DMSO-d_6)

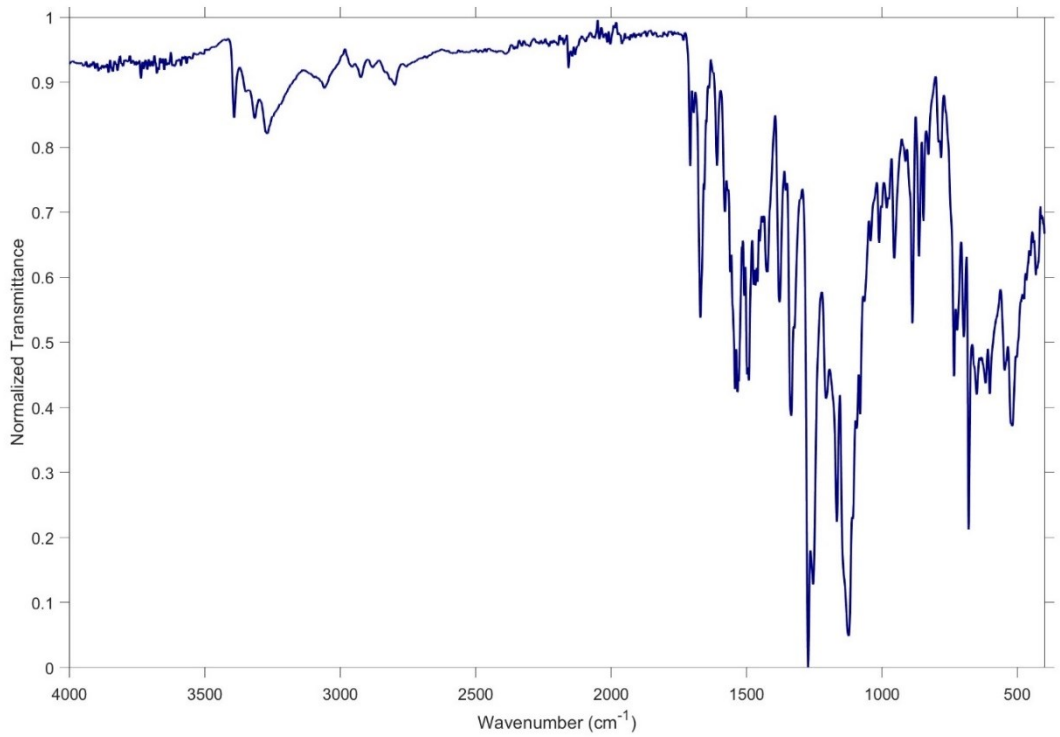

Figure ES3: TREN-ON IR spectra

(5.3.2) 3, *characterization*

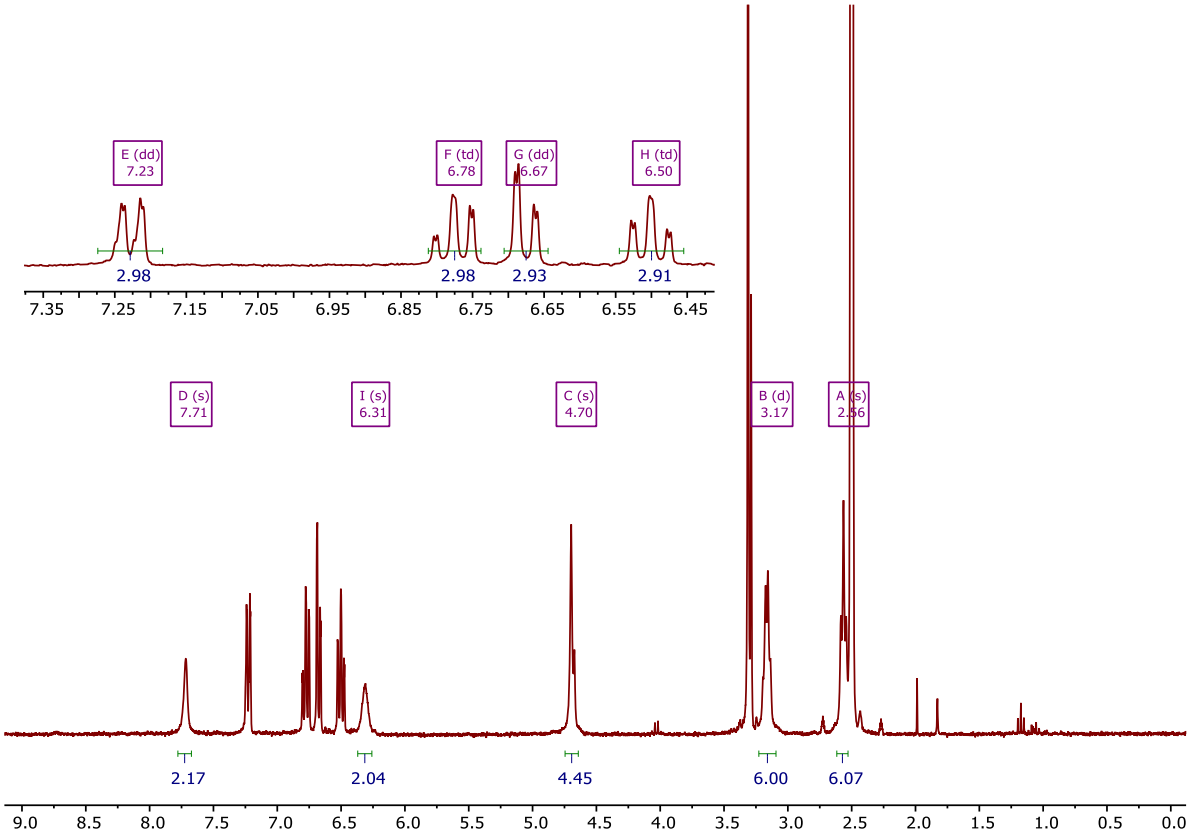

Figure ES4: ^{1}H-NMR (400 MHz, DMSO-d_6)

(5.3.3) TREN-Hex-U, *characterization*

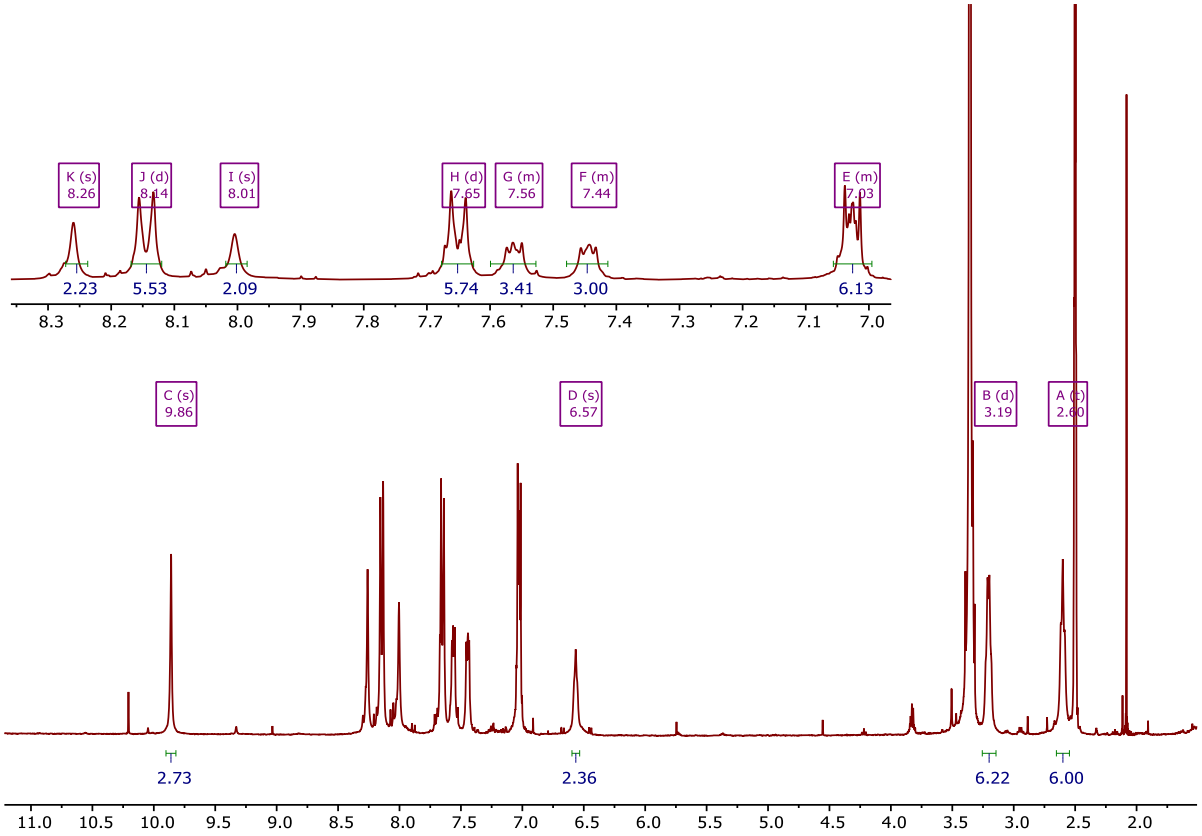

Figure ES5: TREN-Hex-U ^{1}H-NMR (400 MHz, DMSO-d_6)

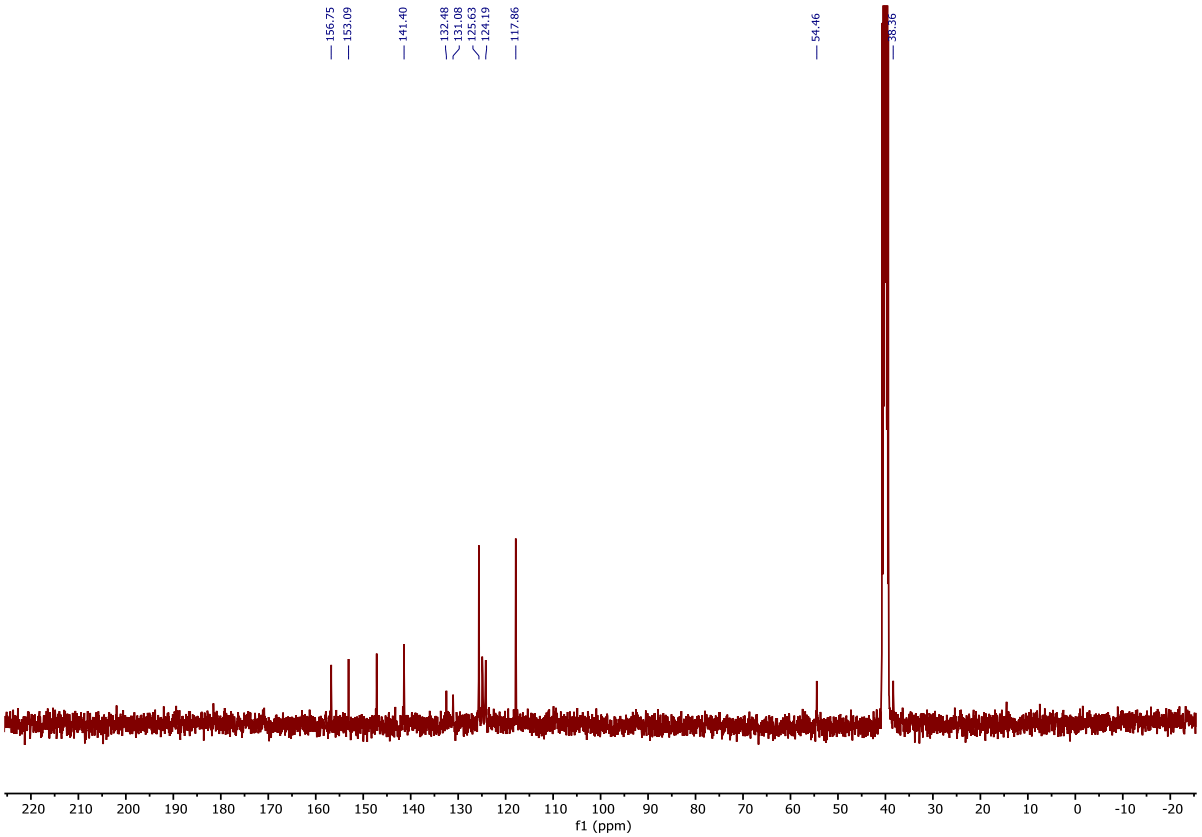

Figure ES6: TREN-Hex-U ^{13}C-NMR (400 MHz, DMSO-d_6)

(5.3.4) 5, *characterization*

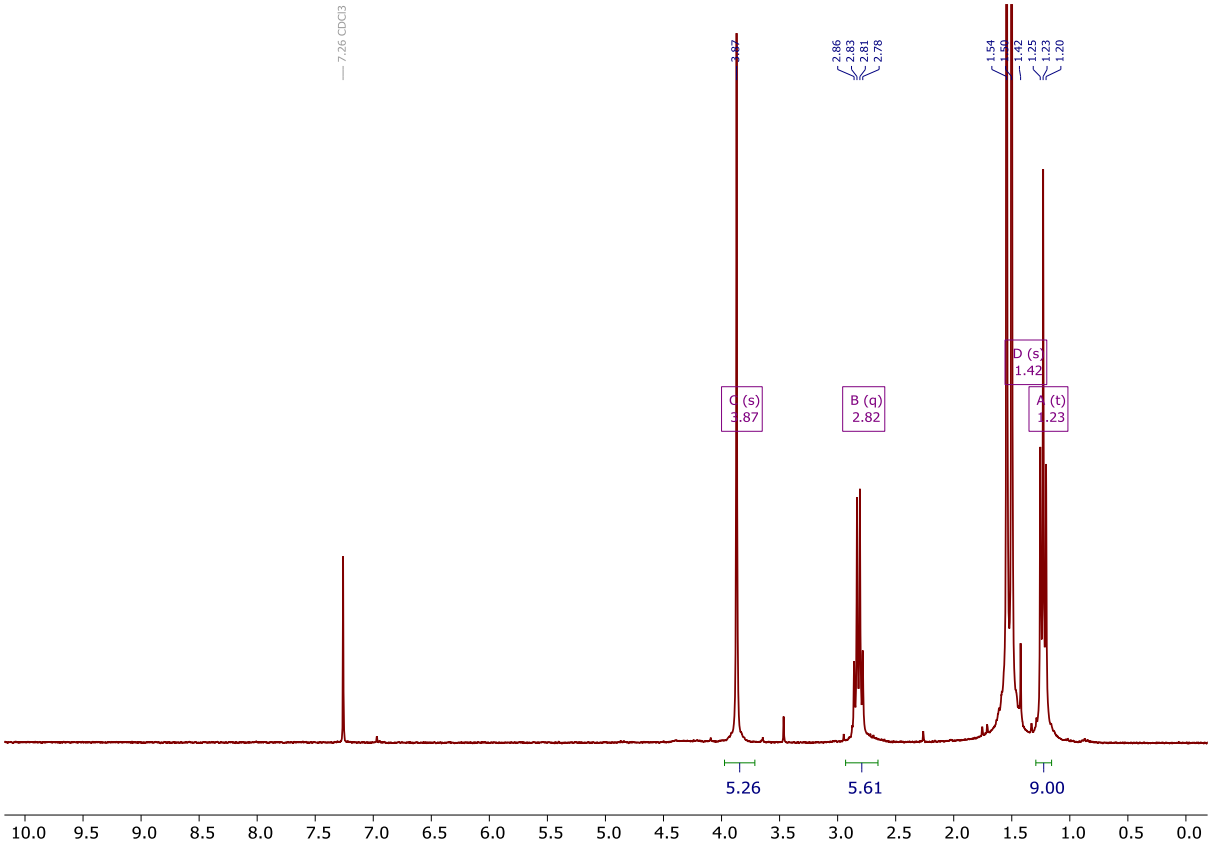

Figure ES7: ^{1}H-NMR (300 MHz, CD_3CN) δ 3.80 (s, 1H), reaction with PMe_3

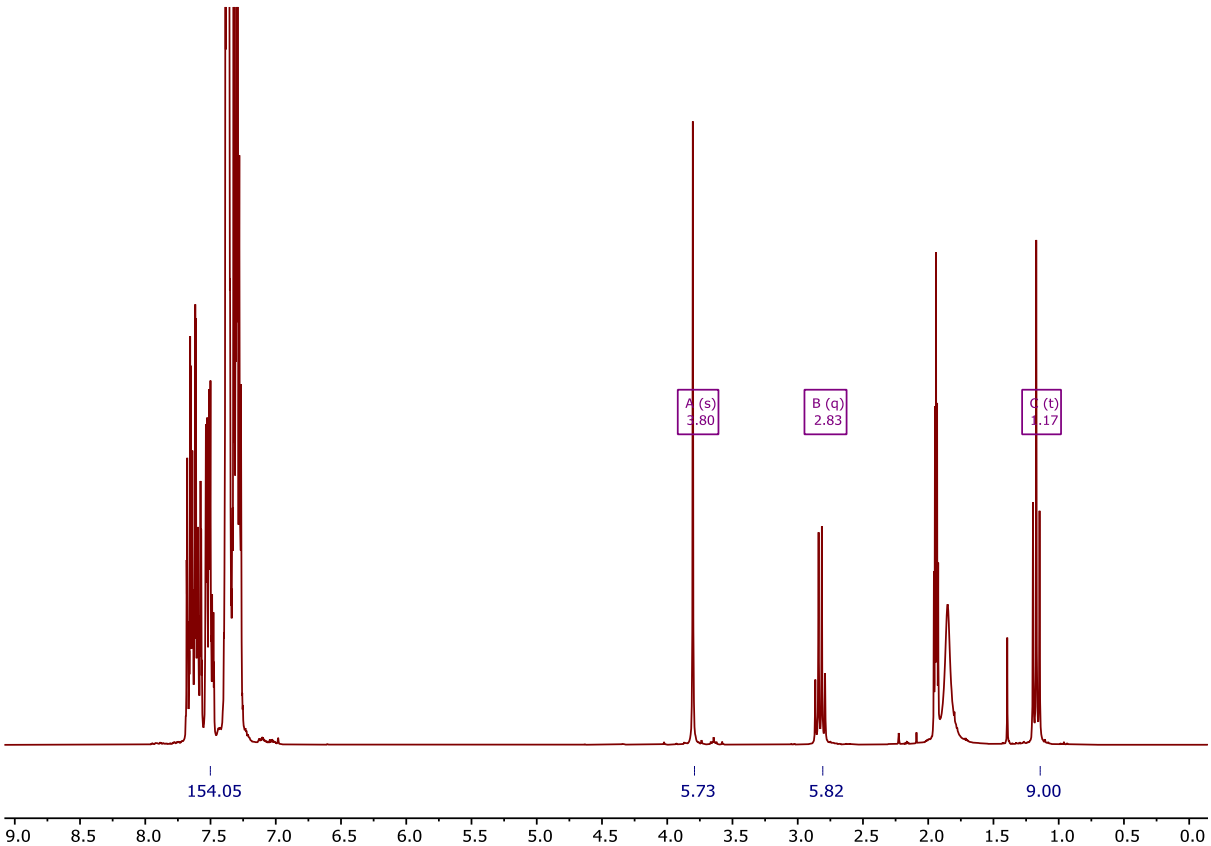

Figure ES8: ^{1}H-NMR (300 MHz, CD_3CN) δ 3.80 (s, 1H), reaction with PPh_3

(5.3.5) TEP-SF2, *characterization*

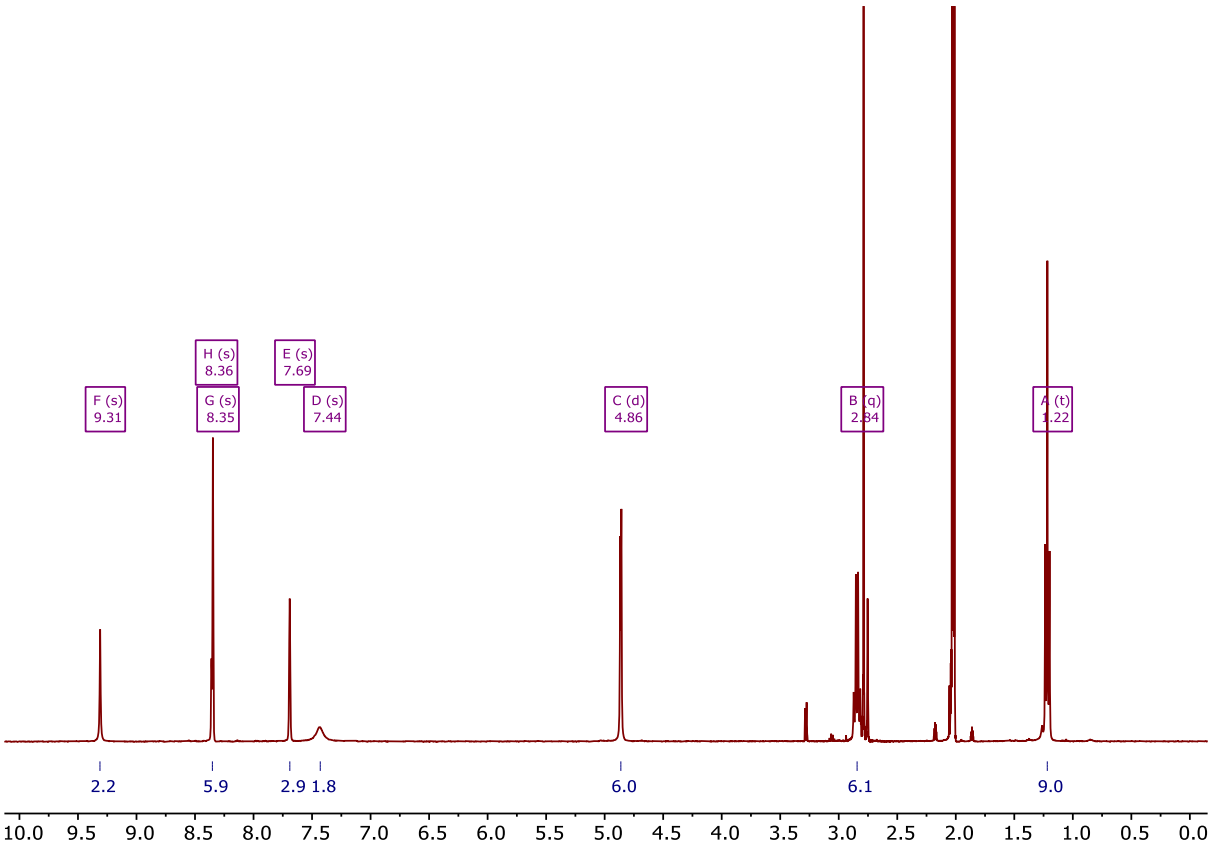

Figure ES9: TEP-SF2 ^{1}H-NMR (400 MHz, ACETONE-d_6)

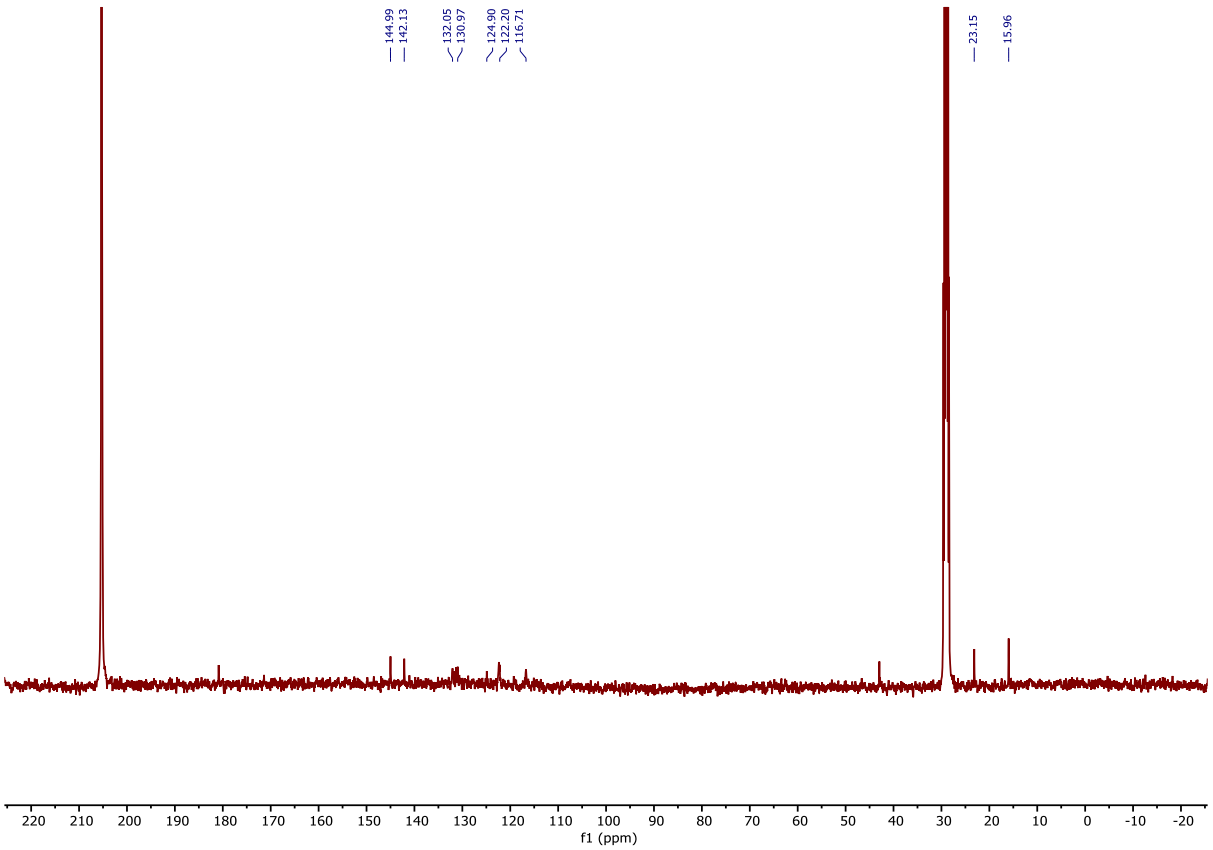

Figure ES10: TEP-SF2 ^{13}C-NMR (400 MHz, ACETONE-d_6)

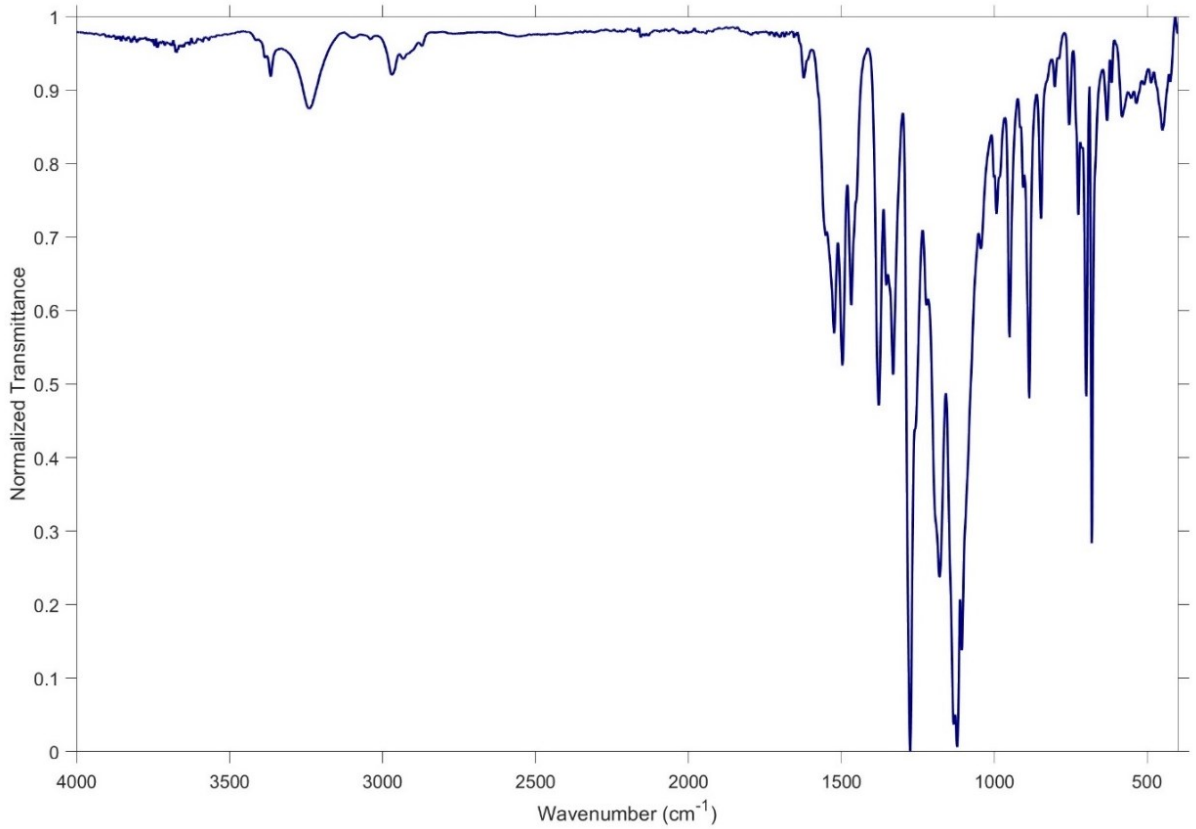

Figure ES11: TEP-SF2 IR spectra

(5.3.6) 7, *characterization*

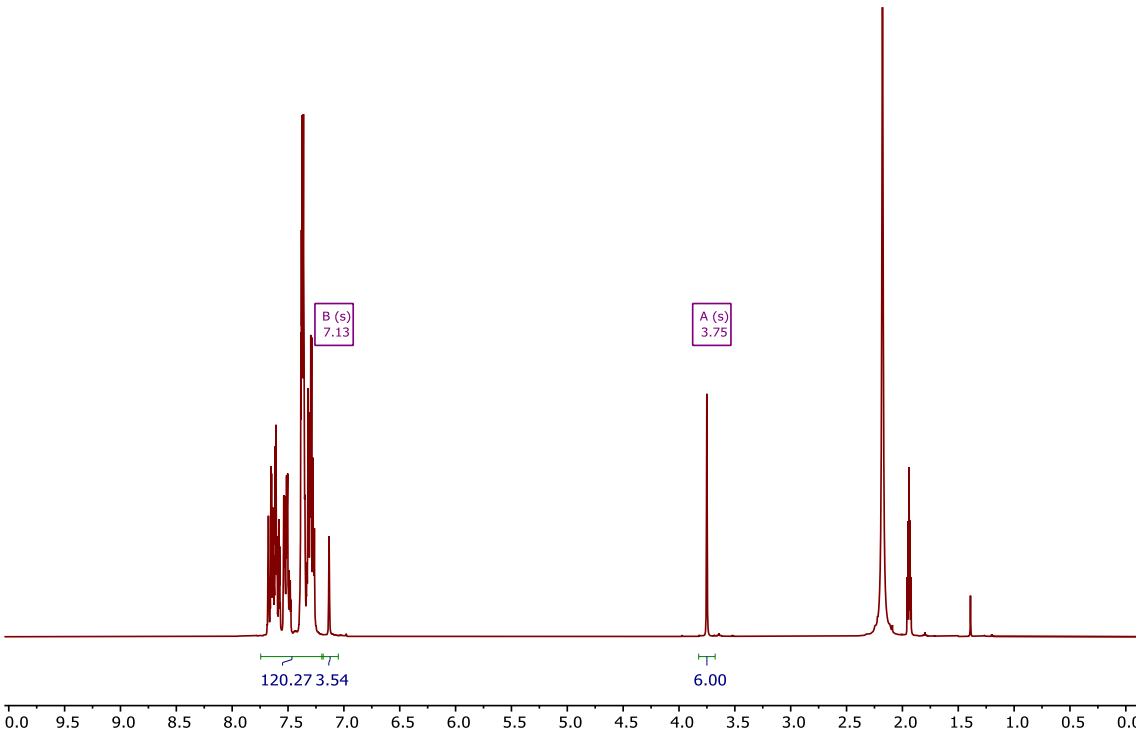

Figure ES12: ^{1}H-NMR (300 MHz, CD_3CN)

(5.3.7) THP-SF2, *characterization*

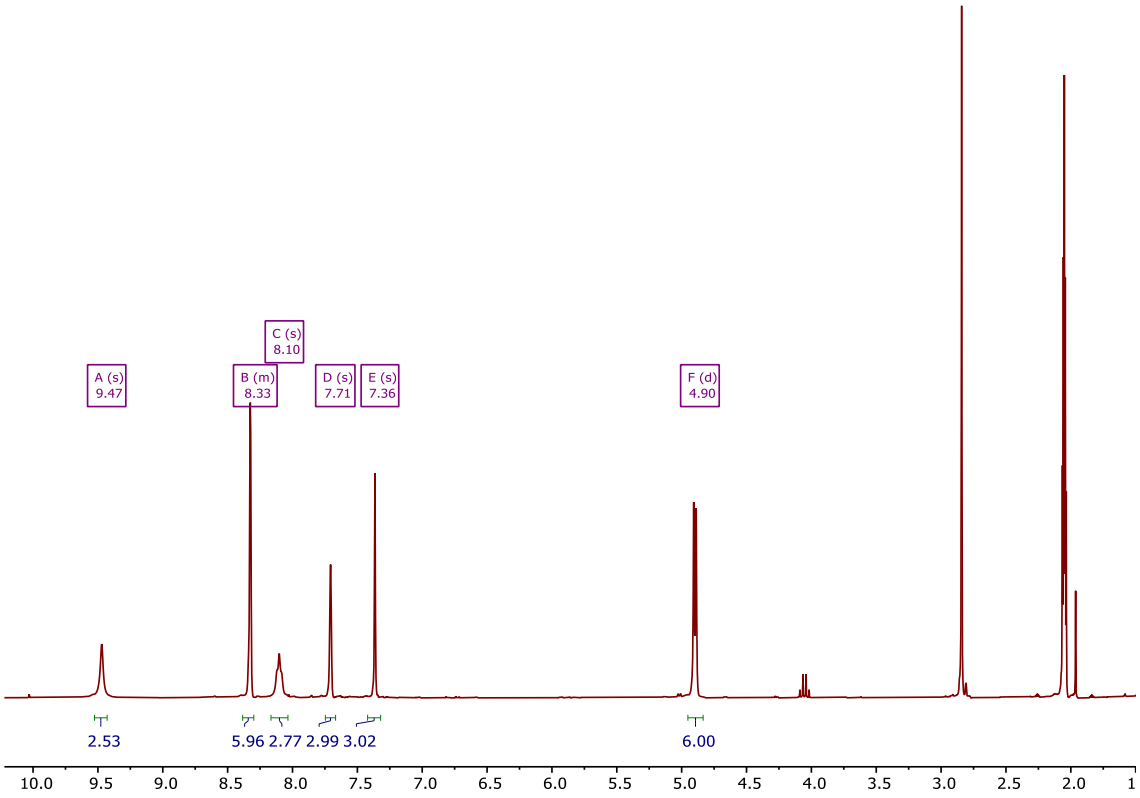

Figure ES13: THP-SF2 ^{1}H-NMR (400 MHz, ACETONE-d_6)

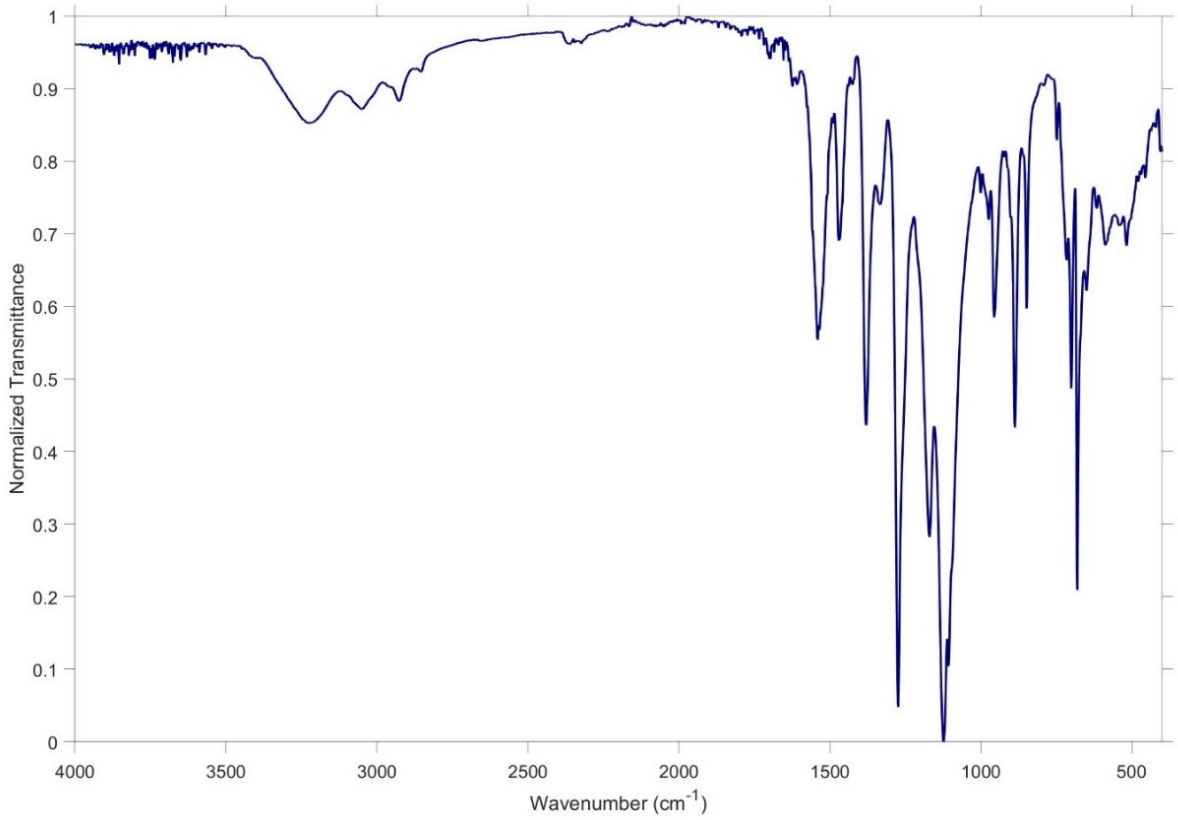

Figure ES14*:* THP-SF2 IR spectra

*(5.3.8) **TEP-ON,** characterization*

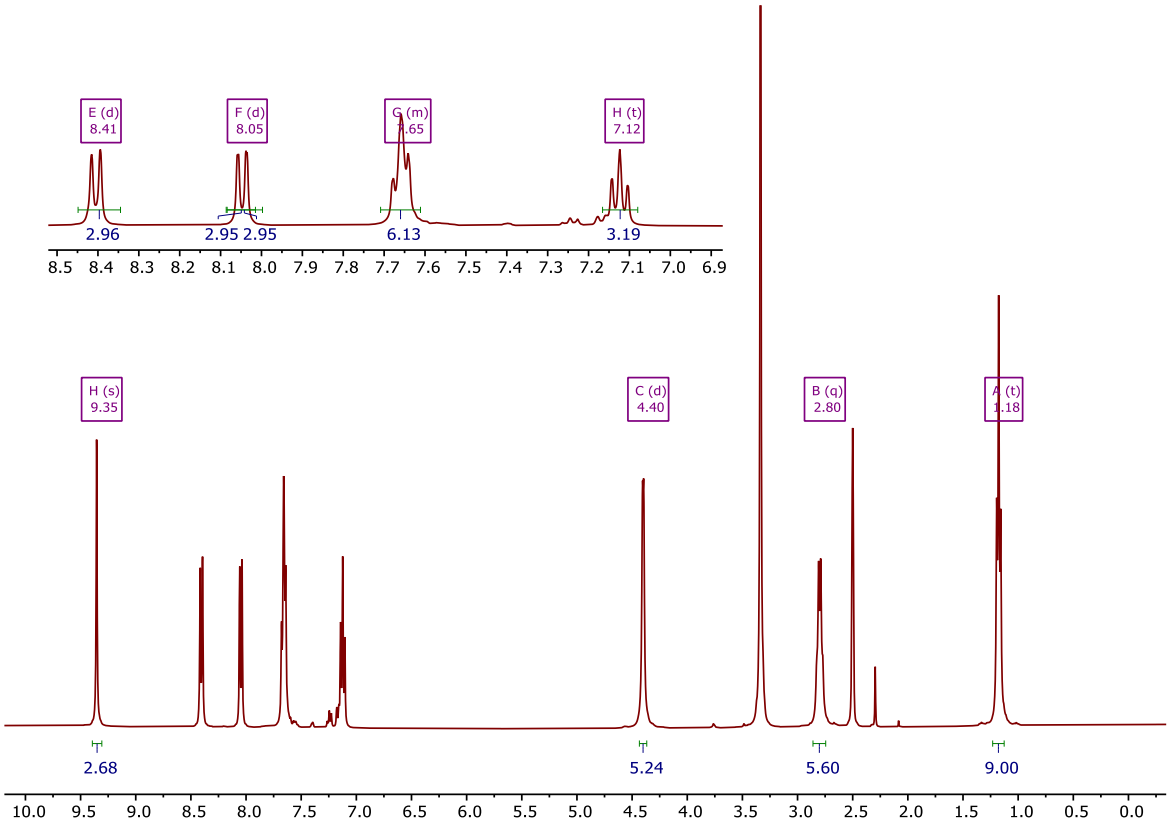

Figure ES15: TEP-ON ^{1}H-NMR (400 MHz, DMSO-d_6)

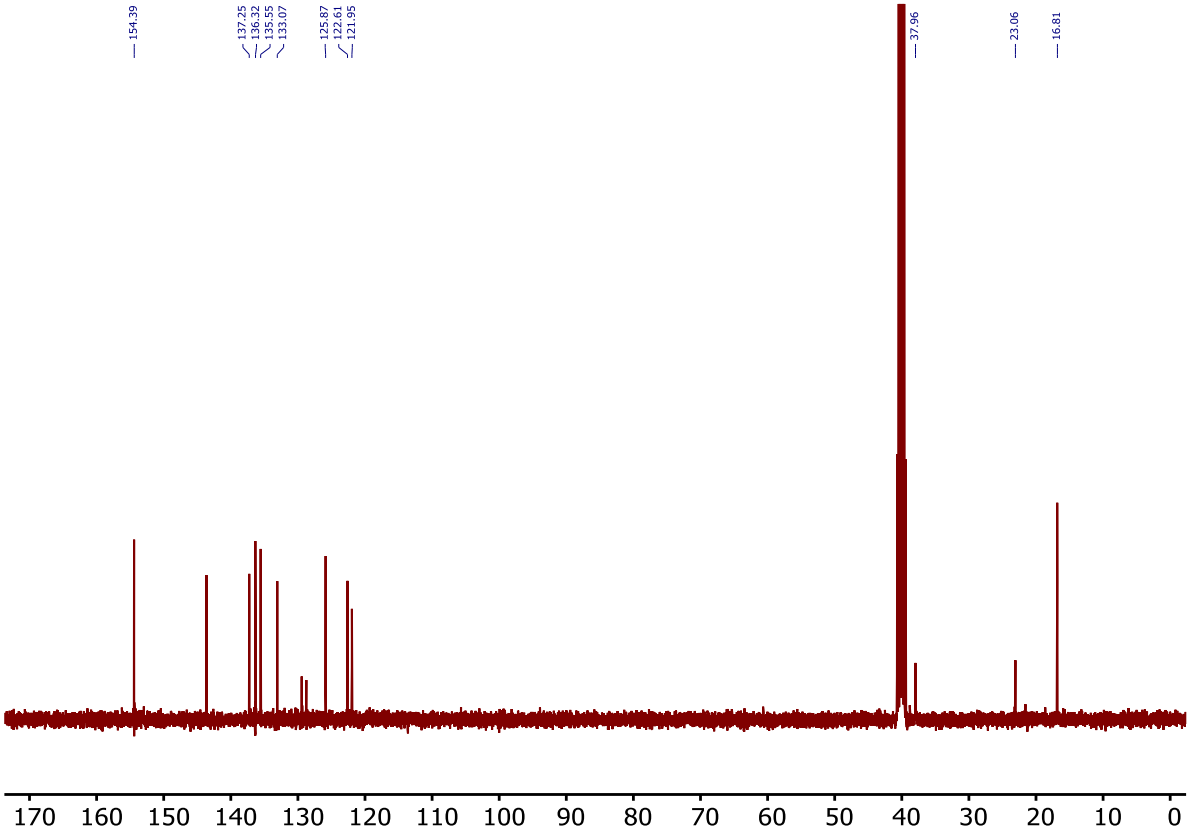

Figure ES16: TEP-ON ^{13}C-NMR (400 MHz, DMSO-d_6)

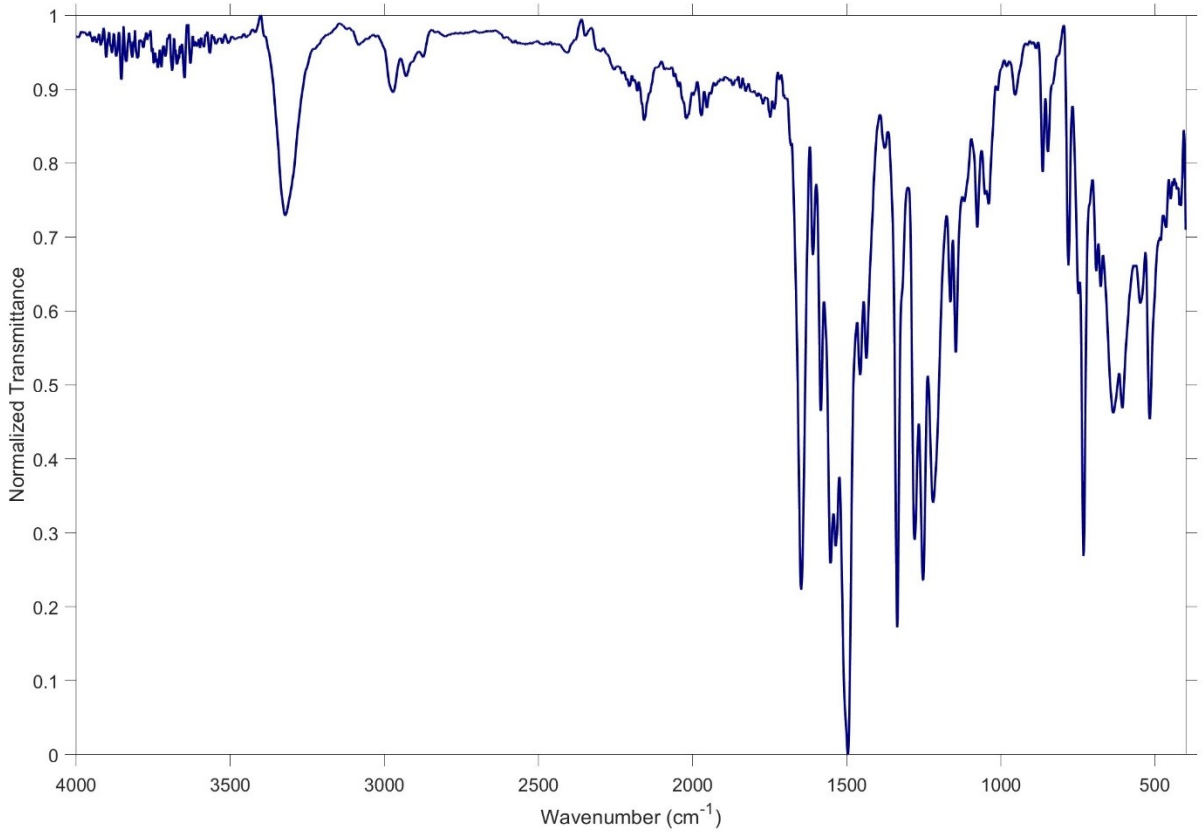

Figure ES17: TEP-ON IR spectra

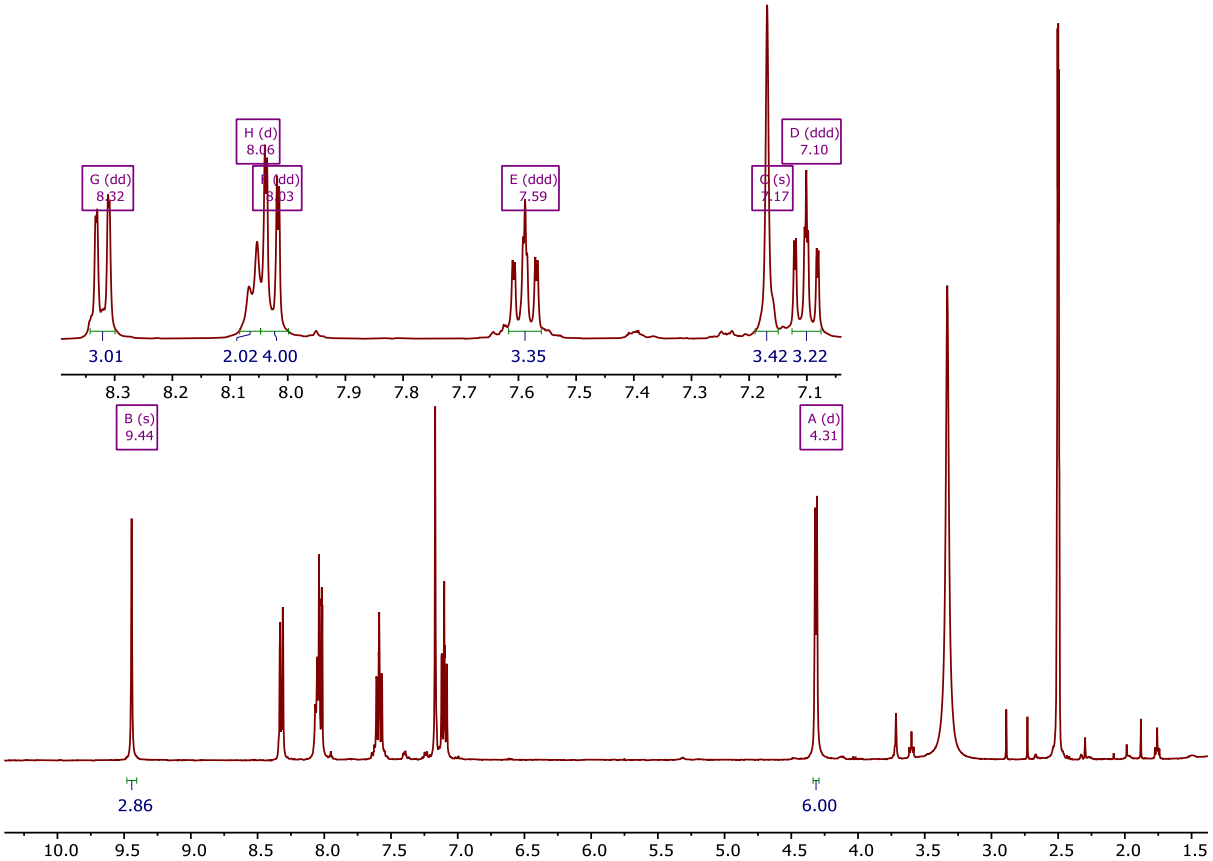

Figure ES18: THP-ON ^{1}H-NMR (400 MHz, DMSO-d_6)

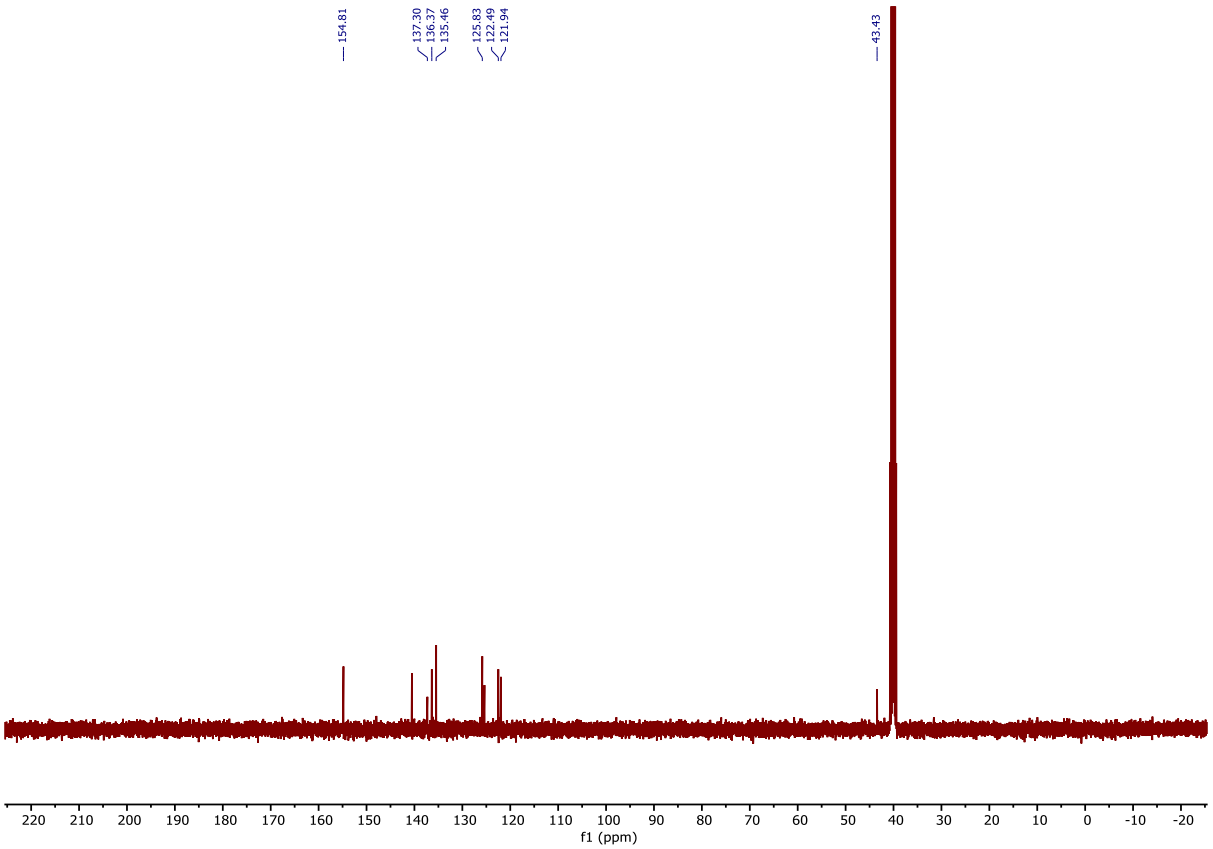

Figure ES19: THP-ON ^{13}C-NMR (400 MHz, DMSO-d_6)

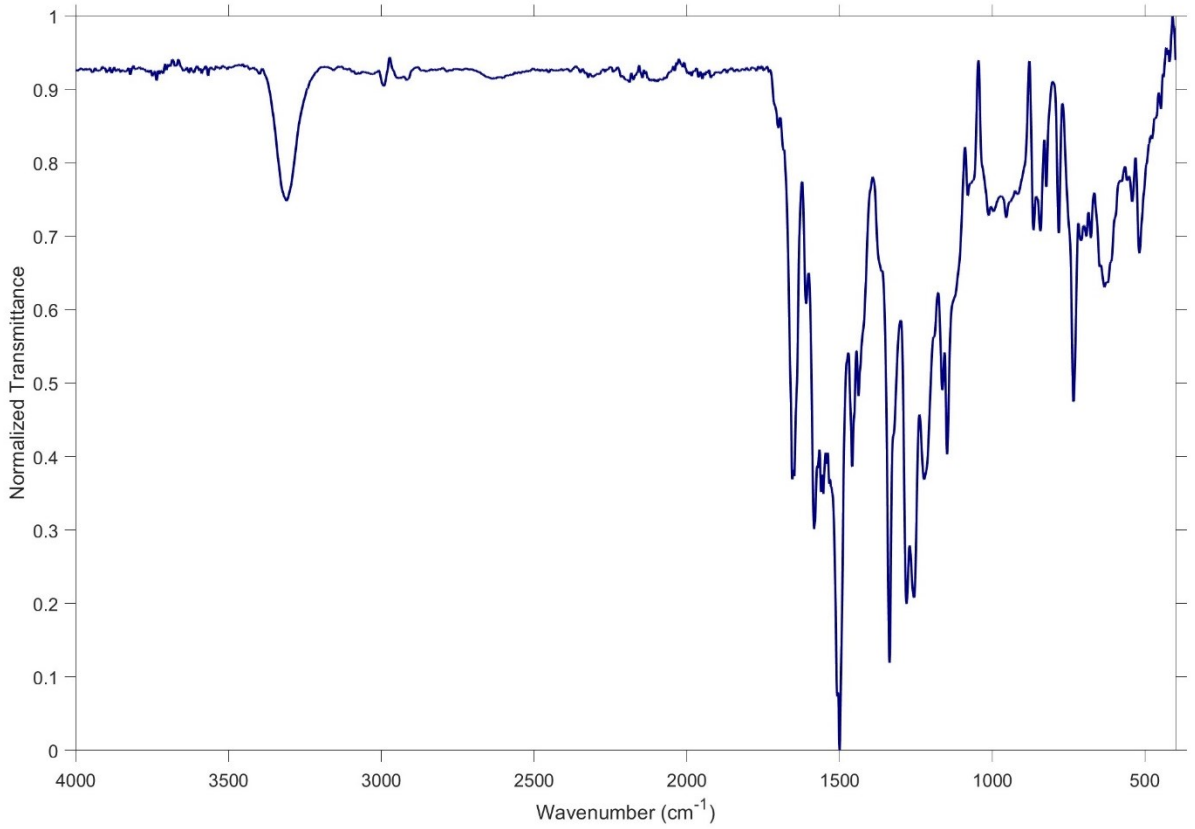

Figure ES20: THP-ON IR spectra

5.4 Liposomes Preparation for the Transport Studies

1-Palmitoyl-2-oleoyl-sn-glycero-3-phosphocholine (POPC) was purchased from Sigma Aldrich. A stock solution of POPC was prepared in deacidified chloroform ($CHCl_3$) and stored in a freezer. Volumes were calculated to obtain a final lipid concentration of 0.4 mM for HPTS assay, 0.1 mM for SPBA assay and 50 mM for ^{31}P-NMR assay. Depending on the experiment and the assay the right amount of Lipid solution is poured to a 5mL round bottom flask and combined with the synthetic anion carrier solution to achieve the desired ratio, this step is not performed for post-insertion experiments. The solvent is evaporated under a flow of nitrogen and dried under vacuum for at least 1 h to obtain a lipid film. Buffer solutions were prepared in water that was deionized with a Millipore filtration system. Depending on the method used, the lipid films were hydrated with:

-SPBA: 500 µL of an aqueous solution of SPBA (0.8 mM) in $NaNO_3$ (225 mM) or Na_2SO_4 (112 mM) and HEPES (10 mM) buffered at pH 7.

-HPTS assay: 500 µL of an aqueous solution of HPTS (1 mM) in $NMDGH^+Cl^-$ (100 mM) and HEPES (10 mM) buffered at pH 6.8. The buffer solution was prepared by mixing a 1.0 M solution of N-methyl-D-glucamine (NMDG) with the appropriate amounts of HCl, HEPES, and water to reach the desired concentrations and pH.

-^{31}P-NMR: 500 µL of an aqueous solution (H_2O) of NaCl (400 mM) and MES (5 mM) buffered at pH 5.

The hydrated lipid films were sonicated for ca. 30 s and stirred for 1 hour, at room temperature to create a heterogeneous mixture of vesicles. The suspension was subjected to 10 freeze thawing cycles to generate unilamellar vesicles, diluted to 1 mL with the same salt solution previously employed for the hydration of the lipid film (without the fluorescent probe in case of fluorescence spectroscopy-based assays) and extruded 29 times through a polycarbonate membrane (200 nm pore size). In the case of ^{31}P-NMR assay, no further steps were required in the preparation of the LUVs. In the case of fluorescence spectroscopy-based assays, the large unilamellar vesicles (LUVs) suspension was eluted through a size exclusion column (Sephadex G-25) using the external salt solution as eluent to remove the external fluorescent probe. The resulting suspension was further diluted with the same salt solution to obtain the desired final lipids concentration.

5.5 SPBA assay general Procedure

The liposome solution was prepared following the reported procedure (*5.4*). Fluorescence measurements were carried out on a Fluoromax-4 spectrometer using a quartz cuvette equipped with a stir bar. The cuvette holder temperature was controlled at 25 °C using a water bath and allowed to stabilize for at least 3 minutes before each experiment. For post-insertion measurements, transporters were added as 5 µL of a 2.4 µM solution in DMF. The fluorescence intensity of SPBA (excitation at 435 nm, emission at 505 nm) was monitored over 11 min. Pulses were generated by dissolving the corresponding salts in the external solution: a 75 µL aliquot of NaCl or Na_2PhPO_4 (1 M, final external anion concentration 25 mM) was added approximately 30 seconds after the start of the experiment, and fluorescence was recorded

for an additional 10 minutes. Finally, vesicles were lysed by adding 50 µL of Triton X-100 (5 wt% in water), and measurements continued for about 30 s.

5.6 Data treatment for SPBA assay transport experiments

Each experiment was repeated at least three times. For receptors that did not show evidence of transport, the measurements were repeated just twice, while the blank experiment was carried out only once. For each averaged dataset, the raw fluorescence data (**Fig ES21**) were processed by removing the 30 seconds preceding the pulse and the sharp decrease in fluorescence immediately following the pulse, after which the remaining signal was normalized. This decrease in fluorescence is attributed to residual external probe not removed during the size-exclusion chromatography step.

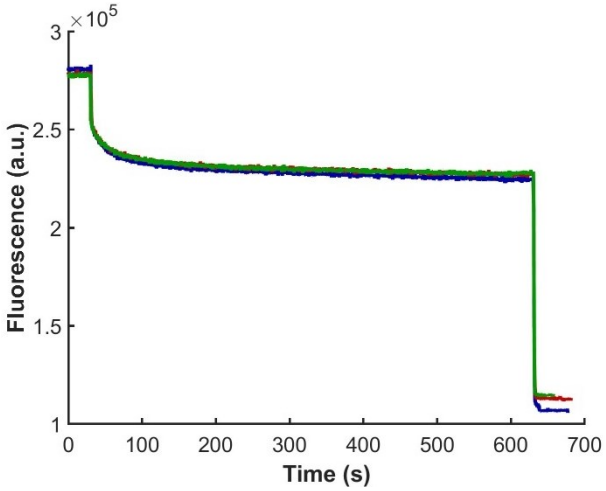

Figure ES1: Example of a transport curve

5.7 Transport experiment: SPBA assay

(5.7.1) TREN-ON, *SPBA transport experiments*

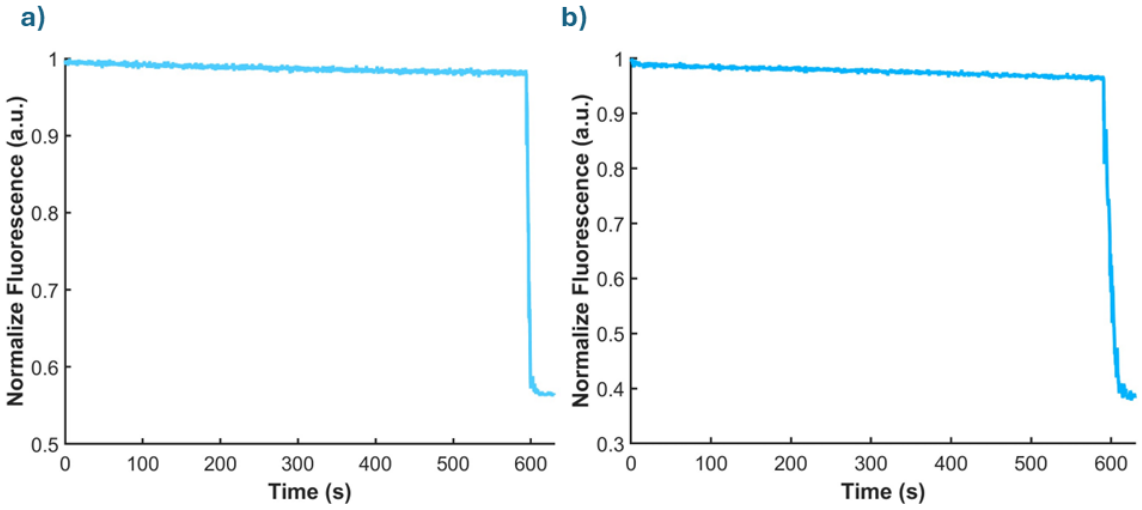

Figure ES2a: Normalized fluorescence curves of **TREN-ON** in SPBA assay. SPBA (0.8 mM) in LUVs (100% POPC, 0.4 mM total lipid), Buffer: 225 mM $NaNO_3$, 25 mM HEPES pH 7. Pulse: 25 mM NaCl. TREN-ON **pre-incorporated**, carrier/lipid ratio: **1 mol%** .

Figure ES22b: Normalized fluorescence curves of **TREN-ON** in SPBA assay. SPBA (0.8 mM) in LUVs (100% POPC, 0.4 mM total lipid), Buffer: 225 mM $NaNO_3$, 25 mM HEPES pH 7. Pulse: 25 mM NaCl or Na_2PhPO4. TREN-ON **post-inserted**, carrier/lipid ratio: **1 mol%**.

(5.7.2) TREN-Hex-U, *SPBA transport experiments*

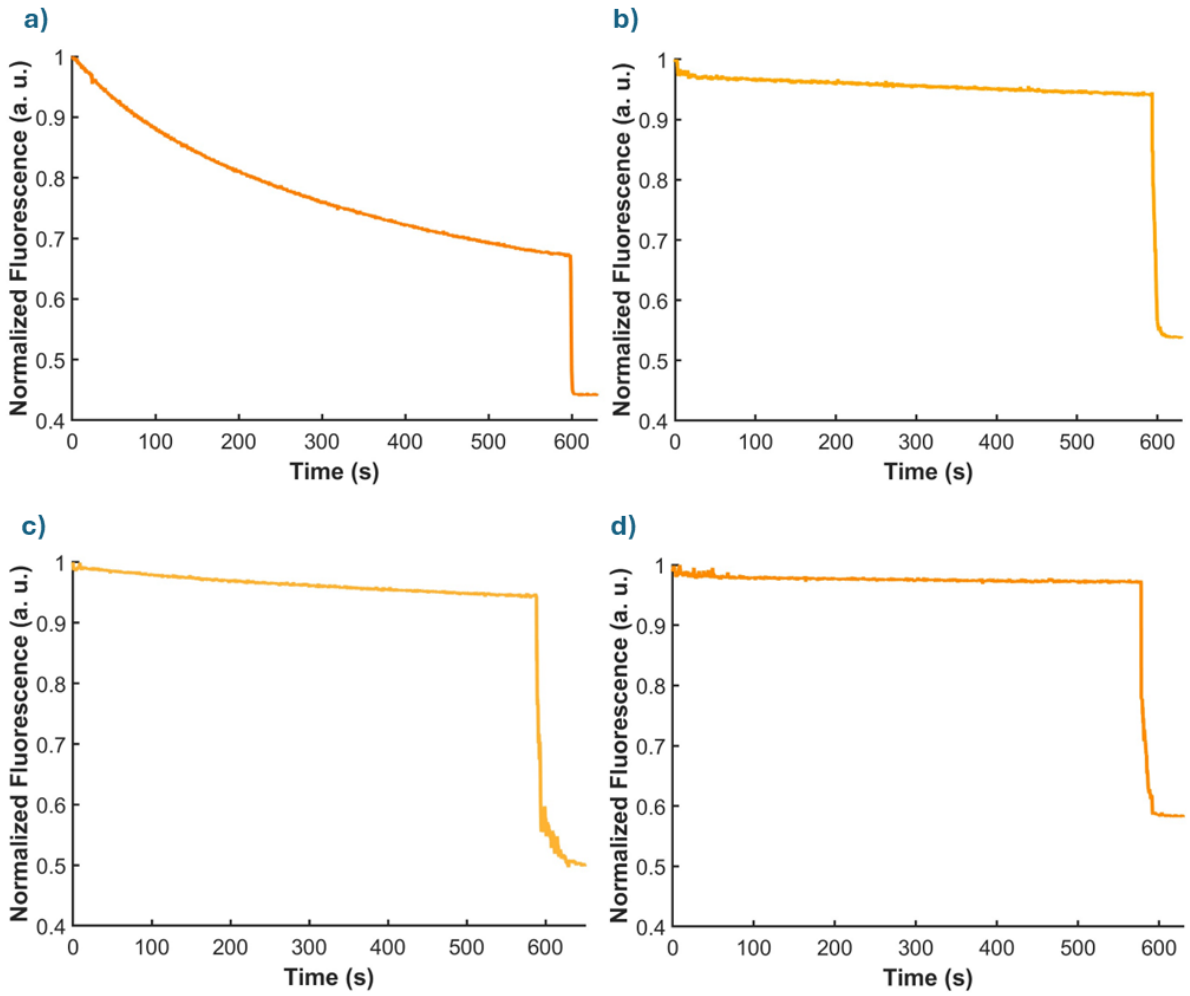

Figure ES3a: Normalized fluorescence curves of **TREN-Hex-U** in SPBA assay. SPBA (0.8 mM) in LUVs (100% POPC, 0.4 mM total lipid), Buffer: 225 mM $NaNO_3$, 25 mM HEPES pH 7. Pulse: 25 mM NaCl. TREN-Hex-U **pre-incorporated**, carrier/lipid ratio: **1 mol%**.
Figure ES23b: Normalized fluorescence curves of **TREN-ON** in SPBA assay. SPBA (0.8 mM) in LUVs (100% POPC, 0.4 mM total lipid), Buffer: 225 mM $NaNO_3$, 25 mM HEPES pH 7. Pulse: 25 mM Na_2PhPO4. TREN-Hex-U **pre-incorporated**, carrier/lipid ratio: **1 mol%**.
Figure ES23c: Normalized fluorescence curves of **TREN-Hex-U** in SPBA assay. SPBA (0.8 mM) in LUVs (100% POPC, 0.4 mM total lipid), Buffer: 112 mM Na_2SO_4, pH 7. Pulse: 25 mM NaCl. TREN-Hex-U **pre-incorporated**, carrier/lipid ratio: **1 mol%**.
Figure ES23c: Normalized fluorescence curves of **TREN-Hex-U** in SPBA assay. SPBA (0.8 mM) in LUVs (100% POPC, 0.4 mM total lipid), Buffer: 112 mM Na_2SO_4, pH 7. Pulse: 25 mM Na_2PhPO4. TREN-Hex-U **pre-incorporated**, carrier/lipid ratio: **1 mol%**.

(5.7.3) TEP-SF2, *SPBA transport experiments*

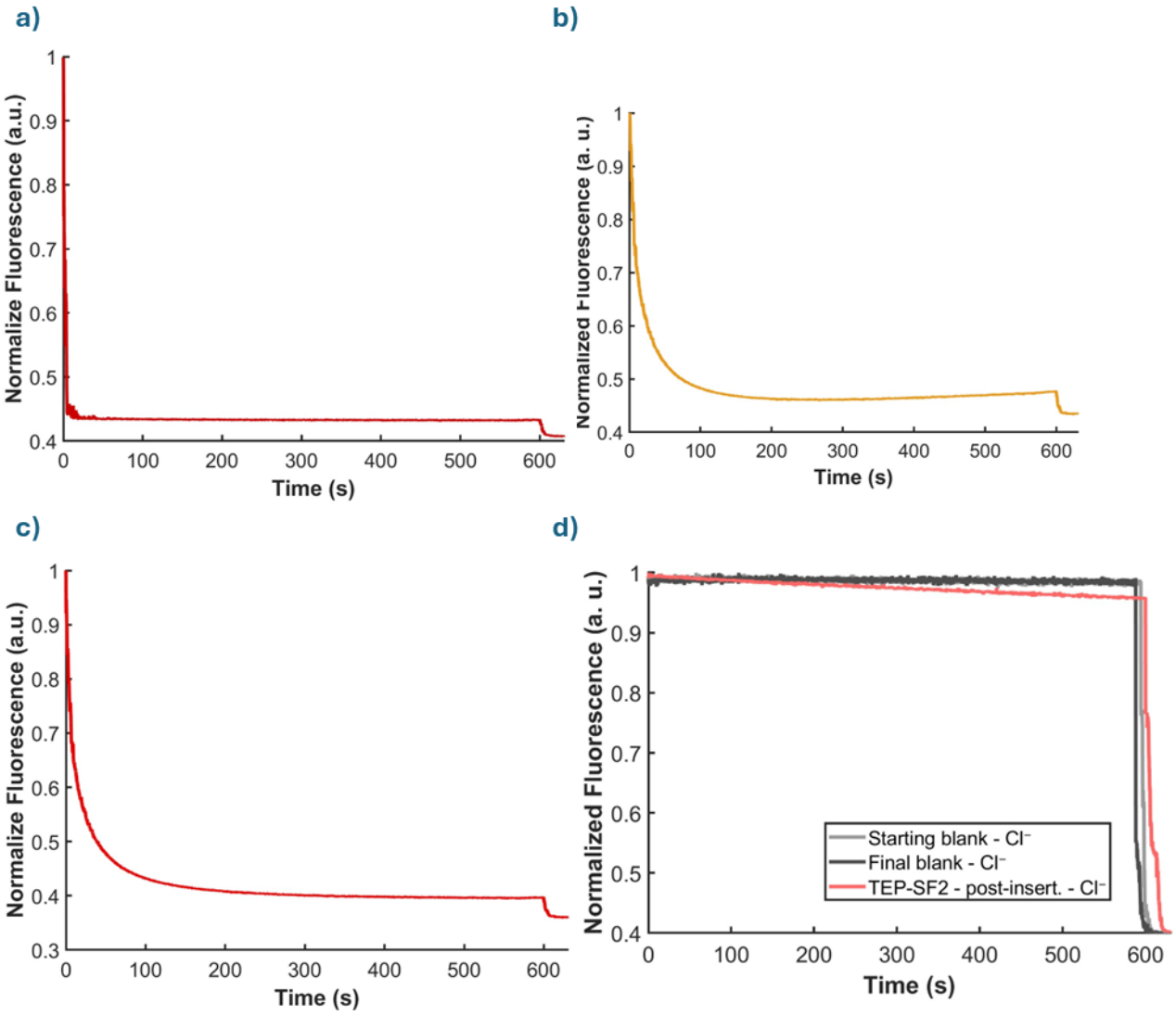

Figure ES4a: Normalized fluorescence curves of **TEP-SF2** in SPBA assay. SPBA (0.8 mM) in LUVs (100% POPC, 0.4 mM total lipid), Buffer: 225 mM $NaNO_3$, 25 mM HEPES pH 7. Pulse: 25 mM NaCl. TEP-SF2 **pre-incorporated**, carrier/lipid ratio: **1 mol%**.
Figure ES24b: Normalized fluorescence curves of **TEP-SF2** in SPBA assay. SPBA (0.8 mM) in LUVs (100% POPC, 0.4 mM total lipid), Buffer: 225 mM $NaNO_3$, 25 mM HEPES pH 7. Pulse: 25 mM Na_2PhPO4. TEP-SF2 **pre-incorporated**, carrier/lipid ratio: **1 mol%**.
Figure ES24c: Normalized fluorescence curves of **TEP-SF2** in SPBA assay. SPBA (0.8 mM) in LUVs (100% POPC, 0.4 mM total lipid), Buffer: 225 mM $NaNO_3$, 25 mM HEPES pH 7. Pulse: 25 mM NaCl, TEP-SF2 **pre-incorporated**, carrier/lipid = **1:10000**.
Figure ES24d: Normalized fluorescence curves of **TEP-SF2** in SPBA assay. SPBA (0.8 mM) in LUVs (100% POPC, 0.4 mM total lipid), Buffer: 225 mM $NaNO_3$, 25 mM HEPES pH 7. Pulse: 25 mM NaCl. TEP-SF2 **post-inserted**, carrier/lipid ratio: **1 mol%**.

(5.7.4) THP-SF2, *SPBA transport experiments*

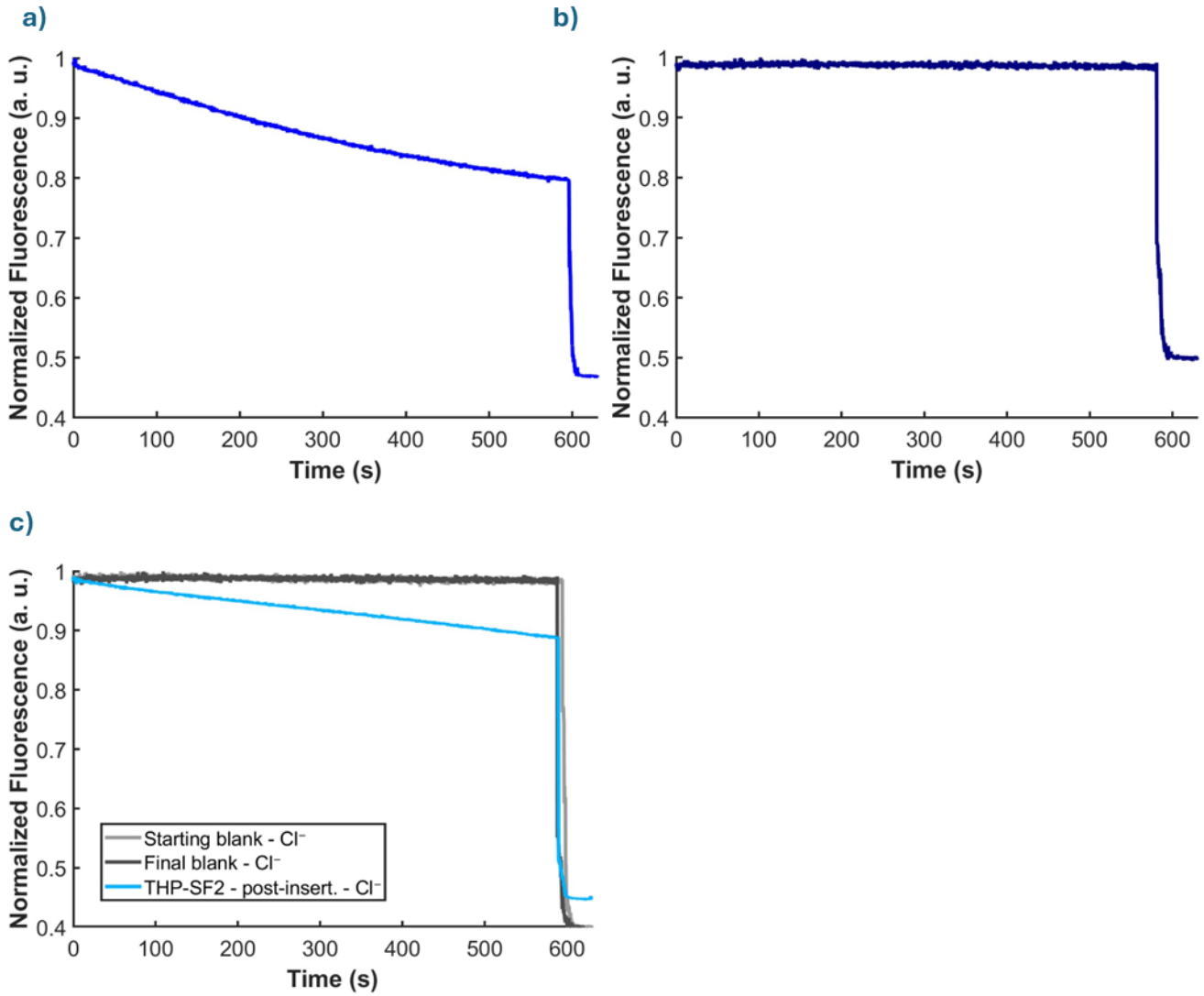

Figure ES5a: Normalized fluorescence curves of **THP-SF2** in SPBA assay. SPBA (0.8 mM) in LUVs (100% POPC, 0.4 mM total lipid), Buffer: 225 mM $NaNO_3$, 25 mM HEPES pH 7. Pulse: 25 mM NaCl. THP-SF2 **pre-incorporated**, carrier/lipid ratio: **1 mol%**.
Figure ES25b: Normalized fluorescence curves of **THP-SF2** in SPBA assay. SPBA (0.8 mM) in LUVs (100% POPC, 0.4 mM total lipid), Buffer: 225 mM $NaNO_3$, 25 mM HEPES pH 7. Pulse: 25 mM NaCl, THP-SF2 **pre-incorporated**, carrier/lipid = **1:10000**.
Figure ES25c: Normalized fluorescence curves of **THP-SF2** in SPBA assay. SPBA (0.8 mM) in LUVs (100% POPC, 0.4 mM total lipid), Buffer: 225 mM $NaNO_3$, 25 mM HEPES pH 7. Pulse: 25 mM NaCl. THP-SF2 **post-inserted**, carrier/lipid ratio: **1 mol%**.

(5.7.5) TEP-ON, SPBA transport experiments

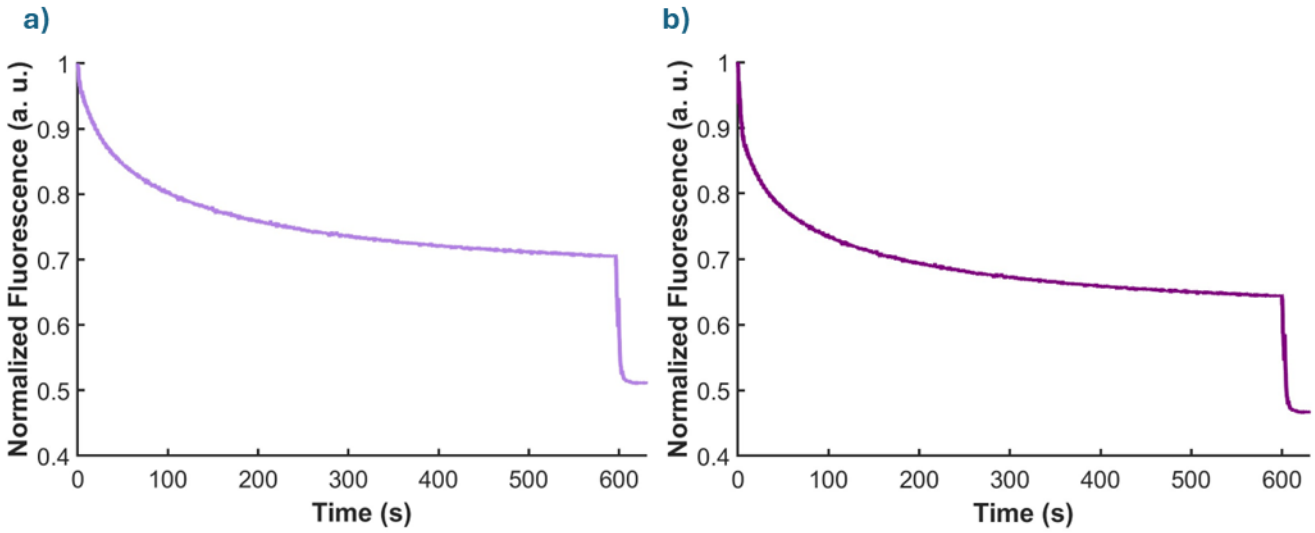

Figure ES6a: Normalized fluorescence curves of **TEP-ON** in SPBA assay. SPBA (0.8 mM) in LUVs (100% POPC, 0.4 mM total lipid), Buffer: 225 mM $NaNO_3$, 25 mM HEPES pH 7. Pulse: 25 mM NaCl. TEP-ON **pre-incorporated**, carrier/lipid ratio: **1 mol%**.
Figure ES26b: Normalized fluorescence curves of **TEP-ON** in SPBA assay. SPBA (0.8 mM) in LUVs (100% POPC, 0.4 mM total lipid), Buffer: 225 mM $NaNO_3$, 25 mM HEPES pH 7. Pulse: 25 mM NaCl. TEP-ON **post-inserted**, carrier/lipid ratio: **1 mol%**.

(5.7.6) THP-ON, *SPBA transport experiments*

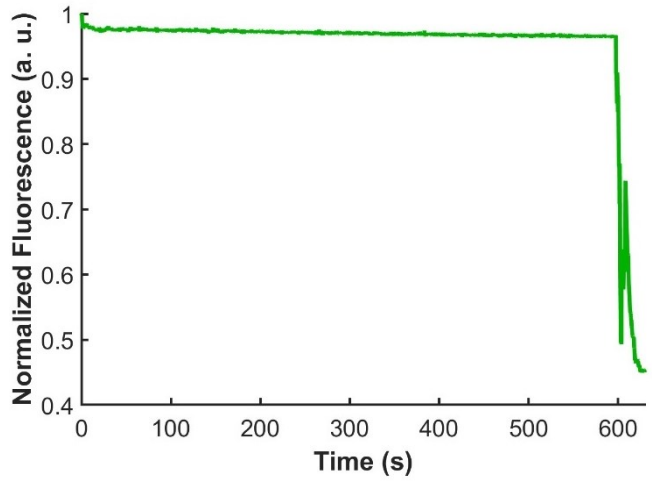

Figure ES7: Normalized fluorescence curves of **THP-ON** in SPBA assay. SPBA (0.8 mM) in LUVs (100% POPC, 0.4 mM total lipid), Buffer: 225 mM $NaNO_3$, 25 mM HEPES pH 7. Pulse: 25 mM NaCl. THP-ON **pre-incorporated**, carrier/lipid ratio: **1 mol%**.

5.8 Transport experiment: HPTS assay

Liposome solutions were prepared following the reported procedure (5.4). Quartz cuvettes containing 3.00 mL of LUV suspension with encapsulated HPTS dye (1 mM) were placed in the sample compartment of an Agilent Cary Eclipse fluorescence spectrometer equipped with a xenon flash lamp and magnetic stirrer. Samples were excited at 403 and 455 nm (slit width: 5 nm), and the emission intensity was monitored at 511 nm (slit width: 5 nm) over time. Three transport experiments were performed in parallel. Prior to the measurement, CCCP in MeOH

was added to reach a CCCP:lipid ratio of 0.1 mol%. After 30 s of recording, a base pulse of NMDG (5 mM) in water was added to establish a pH gradient between the interior (pH 6.8) and exterior (pH 7.8) of the liposomes. Fluorescence ratios were recorded for 10 min, after which the vesicles were lysed by addition of Triton X-100 (50 µL, 5 wt% in water). Measurements were continued for an additional 30 s. Also, for HPTS transport curves, the initial jump is cut.

5.9 Transport experiment: ^{31}P-NMR assay

Liposomes were prepared following the reported procedure (*5.2*). ^{31}P-NMR spectra were recorded at 243 MHz on a 14.1 T Jeol JNM-ECZ600R/S3 spectrometer with a 5 mm Royal Probe. A coaxial insert containing trimethyl phosphate in D_2O (50 mM) was used as reference and the chemical shift of its ^{31}P-NMR signal was set at 3.7 ppm (H_3PO_4=0 ppm). 400 µL of liposomes were placed in an NMR tube with a coaxial insert containing trimethyl phosphate in D_2O (50 mM), used as chemical shift reference (3.70 ppm) and a first ^{31}P-NMR was recorded. No ^{31}P-NMR signal was observed for the POPC lipid headgroups, due to the large size of the liposomes. 45 µL of a phosphate solution (1 M) prepared in the buffer used for the preparation of the liposomes was added to the liposomes sample to obtain a 100 mM phosphate extra-vesicular pulse. After 1 h, $MnSO_4$ (1 µL, 1 M in H_2O) was added to reach a final concentration of 2 mM, ensuring relaxation of the extravesicular phosphate. Transport was monitored over 13 h.

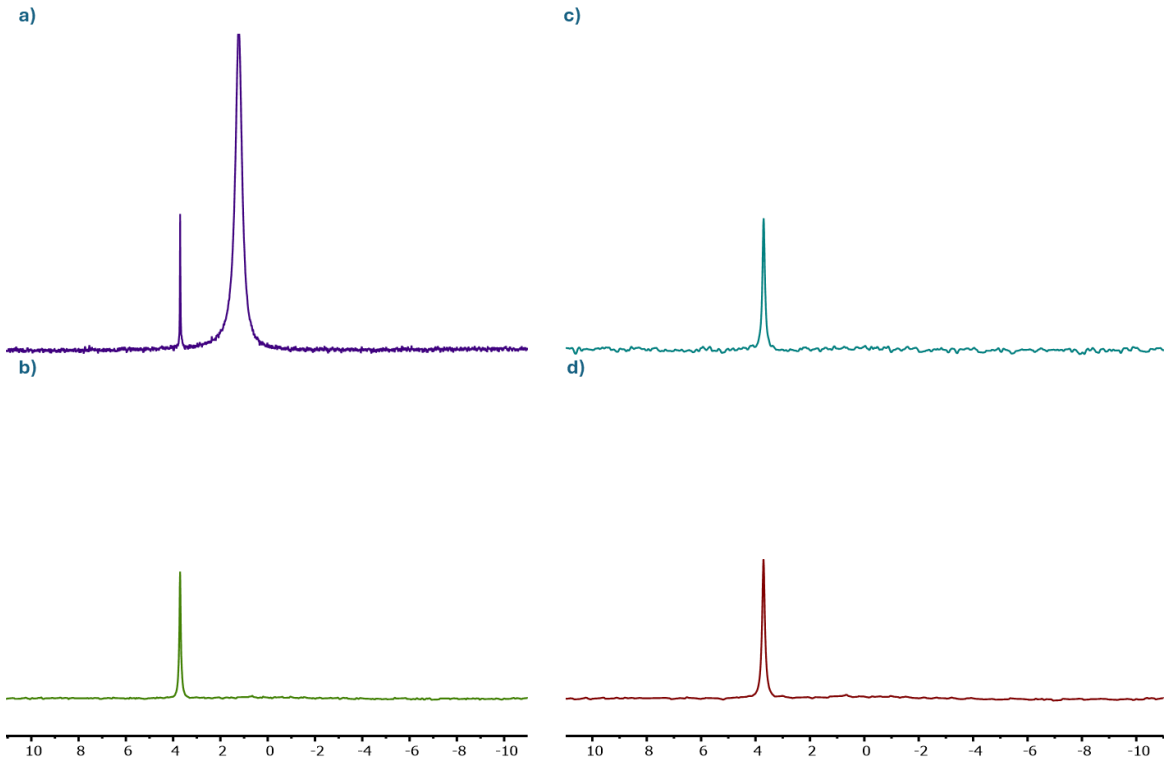

Figure ES8a: ^{31}P-NMR of TREN-Hex-U at pH 5 in NaCl buffer in H_2O after addition of NaH_2PO_4.
Figure ES9b: ^{31}P-NMR of TREN-Hex-U after 1h, after adding MnSO4 (2mM).
Figure ES10c: ^{31}P-NMR of TREN-Hex-U recorded after 2h.
Figure ES11d: ^{31}P-NMR of TREN-Hex-U recorded after 13h.

5.10 THP-SF2 titration

The binding constants with chloride for **THP-SF2** was assessed using ^{1}H-NMR titration using n-TBACl in DMSO-d_6/H_2O (200:1). Titration was carried out at 298K on a JEOL JNM-ECZ600R/S3 spectrometer. The salt was dried under high vacuum overnight to remove residual solvents or water before preparing the solutions. The host concentration used was 1 mM and aliquots of a 50 mM guest solution were added incrementally up to 100 eq. Due to the fast exchange regime observed for the binding of **THP-SF2** with chloride, the downfield shift of the resonance at 10.2 ppm was monitored.

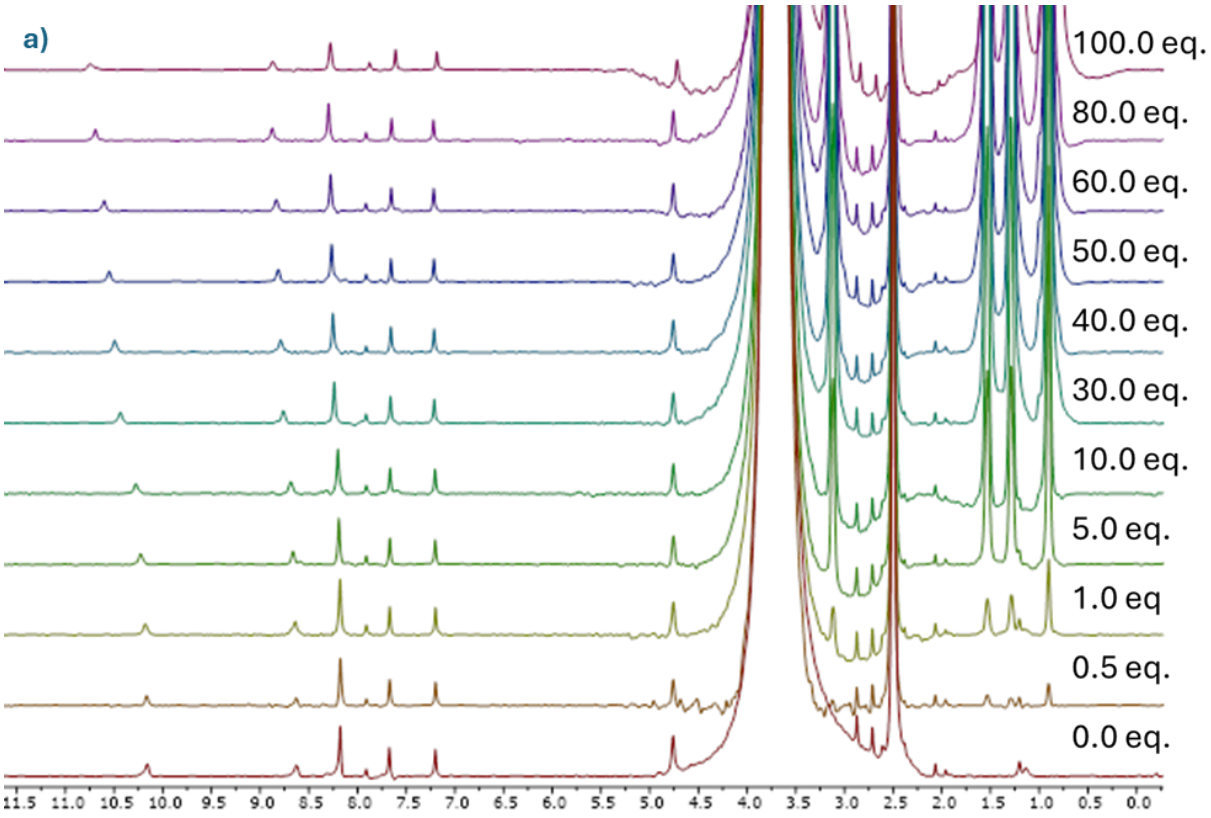

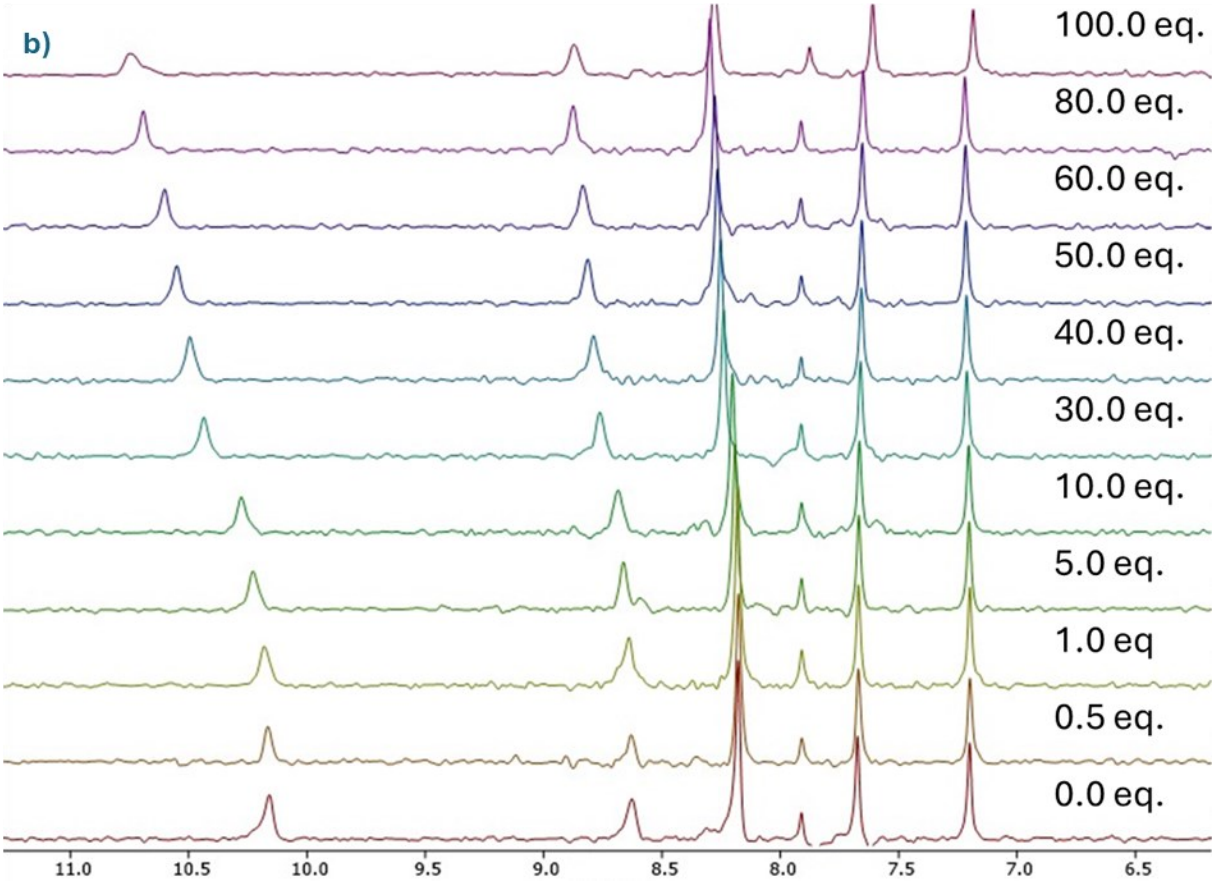

Figure ES12a: ^{1}H-NMR (400 MHz) titration spectra of compound 1 (1 mM) with TBACl (to 100 eq.) in DMSO-d_6 (D_2O content 0.5%).
Figure ES32b: zoom-in of Figure ES32a.

Table ES1

Guest concentration / M	Thioureas proton δ /ppm
0.00	10.1589
5.00E-04	10.1656
1.00E-03	10.18
5.00E-03	10.2278
1.00E-02	10.2771
2.00E-02	10.3604
3.00E-02	10.4355
4.00E-02	10.4947
5.00E-02	10.5499
6.00E-02	10.6012
8.00E-02	10.6914
1.00E-01	10.7483

To determine the association constant (K_a) for a 1:1 binding model, the following equations were applied:

$$K_a = \frac{[HG]}{[H][G]} \qquad (7)$$

$$[H]_0 = [H] + [HG] \quad (8)$$

$$[G]_0 = [G] + [HG] \quad (9)$$

$$K_a = \frac{[HG]}{([H]_0+[HG])([G]_0+[HG])} \quad (10)$$

$$[HG] = \frac{1}{2}\{\left([H]_0 + [G]_0\frac{1}{K_a}\right) - \sqrt{([H]_0 + [G]_0 + \frac{1}{K_a})^2 - 4[H]_0[G]_0}\} \quad (11)$$

In ^{1}H-NMR titration the shift of the signal is to the HG specie concentration in solution:

$$\Delta\delta = \delta_{\Delta HG}\frac{[HG]}{[H]_0} \quad (12)$$

K_a and $\delta_{\Delta HG}$ are not known values, but they can be derived through non-linear regression fitting of the chemical shift data obtained from the ^{1}H-NMR titration.

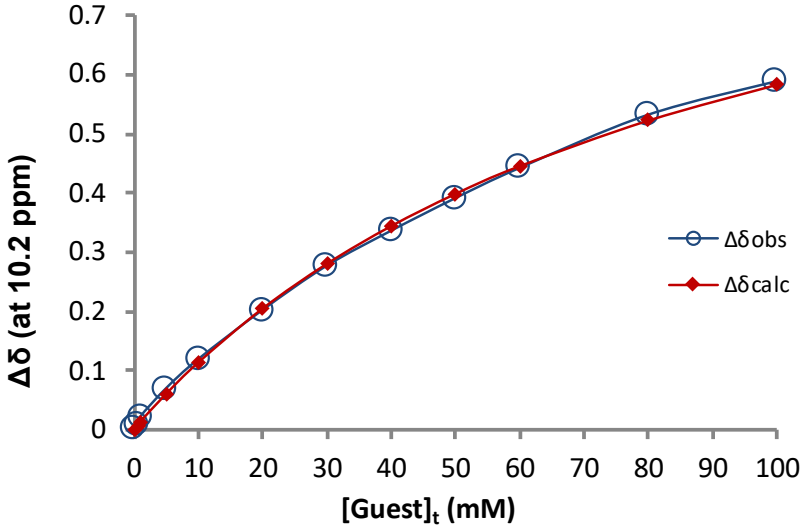

Figure ES13: Observed (blue) and calculated (red) binding curves from the UV-Vis titration of THP-SF2 through additions of TBACl solution in DMSO-d_6 (with 0.5% D_2O) to get an increasing concentration of the salt.

The value obtained from the non-linear regression fitting of the ^{1}H-NMR titration data is K_a=**11** M^{-1}.

6 List of abbreviations and symbols

ACN (CD_3CN) –Acetonitrile/deuterated acetonitrile

CCCP – Carbonyl cyanide m-chlorophenyl hydrazone

$CHCl_3$ – Chloroform

clogP – Logarithm of the octanol–water partition coefficient

D_2O – Deuterated water

DCM – Dichloromethane

DMF - N,N-Dimethylformamide

DMSO (DMSO-d_6)– Dimethyl sulfoxide (deuterated)

eq. – Equivalents

ESI – Electrospray Ionization

Et_2O – Diethyl ether

EtOH – Ethanol

G - Guest

GUVs – Giant unilamellar vesicles

H - Host

HEPES – 4-(2-hydroxyethyl)-1-piperazineethanesulfonic acid

HG – Host-guest complex

HRMS – High-Resolution Mass Spectrometry

HPTS – 8-Hydroxypyrene-1,3,6-trisulfonic acid

IR – Infrared spectroscopy

ISE – Ion Selective Electrode

K_a – Association constant

K_{SV} – Stern–Volmer constant

LUVs – Large Unilamellar Vesicles

MeOH – Methanol

MES – 2-(N-morpholino)ethanesulfonic acid

m/z – Mass to charge ratio

NMDG – N-Methyl-D-glucamine

NMR (^{1}H, ^{13}C, ^{31}P, ^{33}S, ^{35}Cl) – Nuclear Magnetic Resonance (proton, carbon, phosphorus, sulfur, chlorine)

ON – *Ortho*-nitrophenyl

Pd/C – Palladium on carbon

$PhHPO_4^-$ – Phenyl phosphate

$Ph_2PO_4^-$ – Diphenyl phosphate

POPC – 1-Palmitoyl-2-oleoyl-sn-glycero-3-phosphocholine (lipid)

PMe_3 – Trimethylphosphine

PPh_3 – Triphenylphosphine

QTOF - Quadrupole Time-Of-Flight

$-SF_2$ – Bis(trifluoromethyl)phenyl thiourea fragment

SPBA – Bis(3-sulfopropyl)-9,9’-biacridine

TBACl – Tetrabutylammonium chloride

TEP- – 1,3,Triethylphenylene scaffold

THF – Tetrahydrofuran

THP- – Trihydrophenylene scaffold

TLC – Thin Layer Chromatography

Tol – Toluene

UV-Vis – Ultraviolet–Visible spectroscopy

wt% - weight percentage

ΔH°hyd - standard enthalpy of hydration

$\boldsymbol{\Delta\delta}$ - chemical shift difference

$\boldsymbol{\delta_{\Delta HG}}$ - chemical shift difference of the host–guest complex

$\boldsymbol{\lambda_{exc}}$ - excitation wavelength

7 References

(1) Https://Www.Brainkart.Com/Article/Constituents-of-Extracellular-and-Intracellular-Fluids_19371/.

(2) Https://Byjus.Com/Biology/Transport-across-Cell-Membrane/.

(3) Kim, J. B. Channelopathies. *Korean J. Pediatr.* **2014**, 57 (1), 1–18. Https://Doi.Org/10.3345/Kjp.2014.57.1.1.

(4) Puljak, L.; Kilic, G. Emerging Roles of Chloride Channels in Human Diseases. *Biochim. Biophys. Acta, Mol. Basis Dis.* **2006**, 1762 (4), 404–413. Https://Doi.Org/10.1016/j.Bbadis.2005.12.008.

(5) Cystic Fibrosis Canada. Canadian Cystic Fibrosis Patient Data Registry Report 2007; Cystic Fibrosis Canada: **2007**.

(6) Yang, J.; Yu, G.; Sessler, J. L.; Shin, I.; Gale, P. A.; Huang, F. Artificial Transmembrane Ion Transporters as Potential Therapeutics. *Chem* **2021**, 7 (12), 3256–3291. Https://Doi.Org/10.1016/j.Chempr.2021.10.028.

(7) Feo, E.; Gale, P. A. Therapeutic Synthetic Anion Transporters. *Curr. Opin. Chem. Biol.* **2024**, 83, 102535. Https://Doi.Org/10.1016/j.Cbpa.2024.102535.

(8) Saggiomo, V.; Otto, S.; Marques, I.; Félix, V.; Torroba, T.; Quesada, R. The Role of Lipophilicity in Transmembrane Anion Transport. *Chem. Commun.* **2012**, 48 (43), 5274–5276. Https://Doi.Org/10.1039/C2CC31825C.

(9) Sessler, J. L.; Eller, L. R.; Cho, W.-S.; Nicolaou, S.; Aguilar, A.; Lee, J. T.; Lynch, V. M.; Magda, D. J. Synthesis, Anion-Binding Properties, and In Vitro Anticancer Activity of Prodigiosin Analogues. *Angew. Chem., Int. Ed.* **2005**, 44 (37), 5989–5992. Https://Doi.Org/10.1002/Anie.200501740.

(10) Koulov, A. V.; Lambert, T. N.; Shukla, R.; Jain, M.; Boon, J. M.; Smith, B. D.; Li, H.; Sheppard, D. N.; Joos, J.-B.; Clare, J. P.; Davis, A. P. Chloride Transport Across Vesicle and Cell Membranes by Steroid-Based Receptors. *Angew. Chem., Int. Ed.* **2003**, 42 (40), 4931–4933. Https://Doi.Org/10.1002/Anie.200351957.

(11) McCready, J. W.; Lee, J. S. S. H.; Brown, W. M. An Estimate of the Human Lens Epithelial Cell Size In Vivo. *Exp. Eye Res.* **1983**, 37 (2), 311–316. Https://Doi.Org/10.1016/0014-4835(83)90052-0.

(12) Chvojka, M.; Singh, A.; Cataldo, A.; Torres-Huerta, A.; Konopka, M.; Šindelář, V.; Valkenier, H. The Lucigenin Assay: Measuring Anion Transport in Lipid Vesicles. *Anal. Sens.* **2023**, 4 (2), E202300044. Https://Doi.Org/10.1002/Anse.202300044.

(13) Van Swaay, D.; de Mello, A. Microfluidic Methods for Forming Liposomes. *Lab Chip* **2013**, 13 (5), 752–767. Https://Doi.Org/10.1039/C2LC41121K.

(14) Chvojka, M.; Šindelář, V.; Valkenier, H. Substituent Effects of Fluorinated Bambusurils on Their Anion Transport. *Org. Biomol. Chem.* **2025**, 23 (12), 2772–2782. Https://Doi.Org/10.1039/D5ob00400d.

(15) Valkenier, H.; Judd, L. W.; Li, H.; Hussain, S.; Sheppard, D. N.; Davis, A. P. Preorganized Bis-Thioureas as Powerful Anion Carriers: Chloride Transport by Single Molecules in Large Unilamellar Vesicles. *J. Am. Chem. Soc.* **2014**, 136 (35), 12507–12512. Https://Doi.Org/10.1021/Ja507551z.

(16) Li, H.; Valkenier, H.; Judd, L. W.; Brotherhood, P. R.; Hussain, S.; Cooper, J. A.; Jurček, O.; Sparkes, H. A.; Sheppard, D. N.; Davis, A. P. Efficient, Non-Toxic Anion Transport by Synthetic Carriers in Cells and Epithelia. *Nat. Chem.* **2016**, 8 (1), 24–32. Https://Doi.Org/10.1038/Nchem.2384.

(17) Martínez-Crespo, L.; Sun-Wang, J. L.; Ferreira, P.; Mirabella, C. F. M.; Aragay, G.; Ballester, P. Influence of the Insertion Method of Aryl-Extended Calix[4]Pyrroles into Liposomal Membranes on Their Properties as Anion Carriers. *Chem. – Eur. J.* **2019**, 25 (12), 3026–3034. Https://Doi.Org/10.1002/Chem.201806169.

(18) López Mora, N.; Bahreman, A.; Valkenier, H.; Li, H.; Sharp, T. H.; Sheppard, D. N.; Davis, A. P.; Kros, A. Targeted Anion Transporter Delivery by Coiled-Coil Driven Membrane Fusion. *Chem. Sci.* **2016**, 7 (3), 2349–2356. Https://Doi.Org/10.1039/C5SC04282H.

(19) Shannon, R. D. Revised Effective Ionic Radii and Systematic Studies of Interatomic Distances in Halides and Chalcogenides. *Acta Crystallogr.*, Sect. A: Cryst. Phys., Diffr., Theor. Gen. Crystallogr. **1976**, 32 (5), 751–767. Https://Doi.Org/10.1107/S0567739476001551.

(20) Norvaisa, K.; Torres-Huerta, A.; Valkenier, H. Synthetic Transporters for Oxoanions. *Curr. Opin. Chem. Biol.* **2024**, 74, 102290. Https://Doi.Org/10.1016/j.Cbpa.2023.102290.

(21) Marcus, Y. The Thermodynamics of Solvation of Ions. Part 2.—The Enthalpy of Hydration at 298.15 K. *J. Chem. Soc.*, Faraday Trans. 1 **1987**, (2), 339–348. Https://Doi.Org/10.1039/F19878300339.

(22) Torres-Huerta, A.; Norvaisa, K.; Cataldo, A.; Tits, P.-O.; Panda, P. R.; Dias, C. M.; Davis, A. P.; Bodman, S. E.; Butler, S. J.; Valkenier, H. Structural Requirements of Synthetic Anionophores for Inorganic Phosphate and Phosphate Esters. *Chem. Eur. J.* **2025**, 3 (2), E202400076. Https://Doi.Org/10.1002/Ceur.202400076.

(23) Bodman, S. E.; Breen, C.; Plasser, F.; Butler, S. J. Impact of Varying the Phenylboronic Acid Position in Macrocyclic Eu(III) Complexes on the Recognition of Adenosine Monophosphate. *Org. Chem. Front.* **2022**, 9 (20), 5494–5504. Https://Doi.Org/10.1039/D2qo01067d.

(24) Werner, T.; Fähnrich, K.; Huber, C.; Wolfbeis, O. S. Anion-Induced Fluorescence Quenching of a New Zwitterionic Biacridine Derivative. Photochem. *Photobiol.* **1999**, 70 (4), 585–589. Https://Doi.Org/10.1111/j.1751-1097.1999.Tb08255.x.

(25) McNally, B. A.; Koulov, A. V.; Smith, B. D.; Joos, J.-B.; Davis, A. P. A Fluorescent Assay for Chloride Transport: Identification of a Synthetic Anionophore with Improved Activity. *Chem. Commun.* **2005**, (8), 1087–1089. Https://Doi.Org/10.1039/B414589E.

(26) Gilchrist, A. M.; Wang, P.; Carreira-Barral, I.; Alonso-Carrillo, D.; Wu, X.; Quesada, R.; Gale, P. A. Supramolecular Methods: The 8-Hydroxypyrene-1,3,6-Trisulfonic Acid (HPTS) Transport Assay. *Supramol. Chem.* **2021**, 33 (7), 325–344. Https://Doi.Org/10.1080/10610278.2021.1999956.

(27) Scarciglia, A.; Di Gregorio, E.; Aime, S.; Ferrauto, G. Effects of Cations on HPTS Fluorescence and Quantification of Free Gadolinium Ions in Solution; Assessment of Intracellular Release of Gd^{3+} from Gd-Based MRI Contrast Agents. *Molecules* **2022**, 27 (8), 2490–2505. Https://Doi.Org/10.3390/Molecules27082490.

(28) Busschaert, N.; Jolliffe, K.; Plavec, J.; Gale, P. A. Synthetic Transporters for Sulfate: A New Method for the Direct Detection of Lipid Bilayer Sulfate Transport. *Chem. Sci.* **2014**, 5 (3), 1118–1127. Https://Doi.Org/10.1039/C3sc52006d.

(29) Martínez-Crespo, L.; Valkenier, H. Transmembrane Transport of Bicarbonate by Anion Receptors. *ChemPlusChem* **2022**, 87 (1), E202200266. Https://Doi.Org/10.1002/Cplu.202200266.

(30) Cataldo, A.; Norvaisa, K.; Halgreen, L.; Bodman, S. E.; Bartik, K.; Butler, S. J.; Valkenier, H. Transmembrane Transport of Inorganic Phosphate by a Strapped Calix[4]Pyrrole. *J. Am. Chem. Soc.* **2023**, 145 (30), 16310–16314. Https://Doi.Org/10.1021/Jacs.3c04631.

(31) De Kruijff, B.; Cullis, P. R.; Verkleij, A. J.; Hope, M. J.; Van Echteld, C. J. A.; Taraschi, T. F. Lipid Polymorphism and the Functional Roles of Lipids in Biological Membranes. In The Enzymes of Biological Membranes; *Springer* **1981**; Pp 131–204. Https://Doi.Org/10.1007/978-1-4684-4598-5_4.

(32) Kuswandi, B.; Nuriman; Verboom, W.; Reinhoudt, D. N. Tripodal Receptors for Cation and Anion Sensors. *Sensors* **2006**, 6 (8), 978–1017. Https://Doi.Org/10.3390/S6080978.

(33) Marques, I.; Martinez-Crespo, L.; Vítor, F.; Valkenier, H. Hydrazones in Anion Transporters: The Detrimental Effect of a Second Binding Site. *Org. Biomol. Chem.* **2021**, 19 (1), 1–10. Https://Doi.Org/10.1039/D1ob01279g.

(34) Gale, P. A.; Valkenier, H.; Sheppard, D. N.; Davis, A. P. Tripodal Transmembrane Transporters for Bicarbonate. *Chem. Commun.* **2010**, 46 (34), 6252–6254. Https://Doi.Org/10.1039/C0cc01684e.

(35) Jia C, Wu B, Li S, Huang X, Zhao Q, Li Q-S, and Yang X-J. Highly Efficient Extraction of Sulfate Ions with a Tripodal Hexaurea Receptor. *Angew. Chem. Int. Ed.* 50(2):486–490, **2011**. DOI: 10.1002/Anie.201004461.

(36) Valkenier, H.; Dias, C. M.; Porter Goff, K. L.; Jurček, O.; Puttreddy, R.; Rissanen, K.; Davis, A. P. Sterically Geared Tris-Thioureas; Transmembrane Chloride Transporters with Unusual Activity and Accessibility. *Chem. Commun.* **2015**, 51 (75), 14235–14238. Https://Doi.Org/10.1039/C5cc05737j.

(37) Wang, X.; Hof, F. (How) Does 1,3,5-Triethylbenzene Scaffolding Work? Analyzing the Abilities of 1,3,5-Triethylbenzene- and 1,3,5-Trimethylbenzene-Based Scaffolds to Preorganize the Binding Elements of Supramolecular Hosts and to Improve Binding of Targets. Beilstein *J. Org. Chem.* **2012**, 8, 1–10. Https://Doi.Org/10.3762/Bjoc.8.1.

(38) Rosien, J.-R.; Seichter, W.; Mazik, M. Trimethoxybenzene- and trimethylbenzene-based compounds bearing imidazole, indole and pyrrole groups as recognition units: synthesis and evaluation of the binding properties towards carbohydrates. *Org. Biomol. Chem.* **2013**, 11 (38), 6569–6579. https://doi.org/10.1039/c3ob41540f

(39) Li, H.; Valkenier, H.; Thorne, A. G.; Dias, C. M.; Cooper, J. A.; Kieffer, M.; Busschaert, N.; Gale, P. A.; Sheppard, D. N.; Davis, A. P. Anion Carriers as Potential Treatments for Cystic Fibrosis: Transport in Cystic Fibrosis Cells, and Additivity to Channel-Targeting Drugs. *Chem. Sci.* **2019**, 10 (42), 9663–9672. Https://Doi.Org/10.1039/C9SC04242C.

(40) Yamanaka, M.; Nakagawa, T.; Aoyama, R.; Nakamura, T. Synthesis and Estimation of Gelation Ability of C3-Symmetry Tris-Urea Compounds. *Tetrahedron* **2008**, 64 (51), 11558–11567. Https://Doi.Org/10.1016/j.Tet.2008.10.036.

(41) Xu, Y.; Hao, S.-Y.; Zhang, X.-J.; Li, W.-B.; Qiao, X.-P.; Wang, Z.-X.; Chen, S.-W. Discovery of Novel 2,4-Disubstituted Pyrimidines as Aurora Kinase Inhibitors. *Bioorg. Med. Chem. Lett.* **2020**, 30 (3), 1268–1273. Https://Doi.Org/10.1016/j.Bmcl.2020.01.015.

(42) Kilway, K. V.; Siegel, J. S. Control of Functional Group Proximity and Direction by Conformational Networks: Synthesis and Stereodynamics of Persubstituted Arenes. *Tetrahedron* **2001**, 57 (17), 3615–3627. Https://Doi.Org/10.1016/S0040-4020(01)00248-4.